RSC Advances

REVIEW

View Article Online
View Journal | View Issue

Cite this: *RSC Adv.*, 2025, **15**, 40998

Current progress of 1,2,3-triazole hybrids as EGFR inhibitors for cancer therapy – a literature review

Hussam Elddin Nabeih Khasawneh,[a] Hesham M. Hassan,[b] Amal Ali Alharbi,[c] Wesam Taher Almagharbeh,[d] Raed Fanoukh Aboqader Al-Aouadi,[e] Kirandeep Kaur,[f] Ramya Maranan,[g] Hadeer M. Farhan, *[h] Hamada Hashem,[i] Mariam M. Hassan,[i] Stefan Bräse[j] and Ahmed Al-Emam[bk]

Epidermal growth factor receptor (EGFR) is a validated oncogenic driver in numerous solid tumors, and resistance to first- and second-generation tyrosine kinase inhibitors continues to limit clinical outcomes. In recent years, 1,2,3-triazole scaffolds have been extensively hybridized with diverse heterocycles to enhance potency, selectivity, and pharmacokinetic properties against wild-type and mutant EGFR. This review systematically classifies over 130 triazole-based EGFR inhibitors according to their co-scaffold architectures—including quinazoline, chromene/coumarin, pyridine/pyrimidine, quinoline, benzimidazole, indole, oxindole/isatin, imidazole, oxadiazole, thiadiazine, and natural-product-inspired hybrids—and analyzes structure–activity relationships (SAR), key hinge-binding interactions, docking and molecular dynamics insights, and ADMET profiles. For each class, we highlight lead compounds that achieved sub-nanomolar to low-micromolar EGFR inhibition, delineate substituent effects on kinase affinity and cellular antiproliferative activity, and discuss strategies to overcome common resistance mutations (*e.g.*, L858R, T790M, C797S). Computational studies are integrated to reveal binding modes within the ATP-cleft and allosteric pockets, supporting the rational design of next-generation inhibitors. Finally, we identify current challenges—such as off-target toxicity and limited aqueous solubility—and propose future directions for optimizing triazole hybrids toward clinical translation. This scaffold-centric perspective aims to guide medicinal chemists in designing innovative triazole-based EGFR inhibitors with improved efficacy and safety profiles.

Received 30th May 2025
Accepted 2nd October 2025

DOI: 10.1039/d5ra03819g

rsc.li/rsc-advances

1. Introduction

Cancer remains one of the leading causes of mortality worldwide, with incidence rates projected to continue rising.[1] A major hallmark of many cancers is the dysregulation of growth signaling pathways, among which the epidermal growth factor receptor (EGFR) pathway is especially prominent.[2] EGFR is a transmembrane receptor tyrosine kinase of the ErbB/HER family that, upon activation by ligand binding, triggers downstream signaling cascades (RAS–RAF–MEK–ERK, PI3K–AKT–mTOR, *etc.*) that promote cell proliferation and survival.[3] Overexpression or mutation of EGFR is observed in various malignancies, notably non-small cell lung cancer (NSCLC),[4] breast cancer,[5] and head and neck cancers,[6] and is correlated with aggressive tumor behavior and poor prognosis.[7] In particular, activating mutations in the EGFR kinase domain (such as L858R[8] and exon 19 deletions[9]) drive a subset of NSCLCs, making EGFR a well-validated therapeutic target in oncology.

Therapeutic targeting of EGFR has led to the development of several generations of EGFR tyrosine kinase inhibitors (TKIs)[10] that have transformed the management of EGFR-mutant lung

[a]*Chemical Engineering Department, Al-Huson University College, Al-Balqa' Applied University, P.O. Box 19117, Al-Salt, Jordan*
[b]*Department of Pathology, College of Medicine, King Khalid University, P.O. Box 62529, Asir 61421, Saudi Arabia*
[c]*Department of Nursing Leadership and Education, Faculty of Nursing, University of Tabuk, Tabuk, Saudi Arabia*
[d]*Medical and Surgical Nursing Department, Faculty of Nursing, University of Tabuk, Tabuk, Saudi Arabia*
[e]*College of Medicine, Al-Ayen Iraqi University, AUIQ, An Nasiriyah, Iraq*
[f]*Department of Chemistry, Maharaja Ranjit Singh Punjab Technical University, Bathinda 151001, Punjab, India*
[g]*Department of Research and Innovation, Saveetha School of Engineering, SIMATS, Chennai, Tamil Nadu-602105, India*
[h]*Department of Pharmacology & Toxicology, Faculty of Pharmacy, Deraya University, Minia, Egypt. E-mail: hadeer.farhan@deraya.edu.eg*
[i]*Department of Pharmaceutical Chemistry, Faculty of Pharmacy, Sohag University, Sohag 82524, Egypt*
[j]*Institute of Biological and Chemical Systems—Functional Molecular Systems (IBCS-FMS), Karlsruhe Institute of Technology (KIT), Kaiserstrasse 12, 76131 Karlsruhe, Germany*
[k]*Department of Forensic Medicine and Clinical Toxicology, Mansoura University, Mansoura, Egypt*

cancer. First-generation reversible EGFR TKIs (*e.g.*, gefitinib and erlotinib) and second-generation irreversible TKIs (*e.g.*, afatinib) showed initial efficacy. Still, they were limited by the emergence of resistance,[11,12] most commonly the gatekeeper T790M mutation in EGFR.[13,14] Third-generation TKIs such as osimertinib were designed to target the T790M mutant receptor covalently and have become standard of care.[15] Yet, additional resistance mechanisms (*e.g.*, C797S mutation, MET amplification) still arise.[16] Hence, there is ongoing demand for novel EGFR inhibitors to overcome resistance and provide broader anticancer efficacy. One approach has been the design of hybrid molecules[17–19] or new scaffolds that can concurrently modulate multiple signaling pathways or bind mutant EGFR variants, thereby improving therapeutic outcomes and possibly delaying resistance. In this context, the 1,2,3-triazole heterocycle has gained attention as a valuable building block in anticancer drug design, including EGFR-targeted agents.

1,2,3-Triazoles are five-membered aromatic rings containing three nitrogen atoms.[20] They typically exist as 1,4-disubstituted triazoles when synthesized *via* the Huisgen azide–alkyne click cycloaddition (often catalyzed by Cu(I)).[21] This facile "click chemistry" route allows rapid assembly of diverse triazole-containing compounds in high yield, making the triazole an attractive linker or core structure in medicinal chemistry.[22] The triazole ring is remarkably stable under physiological and chemical conditions, resistant to hydrolysis, oxidation, and reduction, ensuring that it can survive *in vivo* metabolism and harsh chemical steps.[23] Moreover, 1,2,3-triazoles are considered bioisosteres of amide bonds and other functional groups, meaning they can often mimic the H-bonding and spatial arrangement of such groups when bound to biological targets, but with improved metabolic stability.[24] The triazole ring is polar and can engage in multiple non-covalent interactions: it can serve as a hydrogen bond acceptor (through the nitrogen atoms) and, when appropriately protonated or substituted, even as a weak hydrogen bond donor.[25] These features enable 1,2,3-triazoles to form key interactions in enzyme binding sites, contributing to high-affinity binding. Indeed, triazole-containing compounds display a broad spectrum of bioactivities (antimicrobial,[26] antiviral,[27] antiparasitic,[28] anticonvulsant,[29] and anticancer[30,31]), and several triazole-derived drugs are clinically used (*e.g.*, antibacterial tazobactam[32]).

2. EGFR biology and therapeutic targeting

EGFR (ErbB1/HER1) is a 170-kDa transmembrane glycoprotein composed of an extracellular ligand-binding domain, a single-pass helical transmembrane segment, and an intracellular tyrosine kinase domain.[33] EGFR is activated by ligand binding and subsequent receptor homodimerization or heterodimerization,[34] leading to autophosphorylation of tyrosine residues and recruitment of adaptor proteins such as Shc and

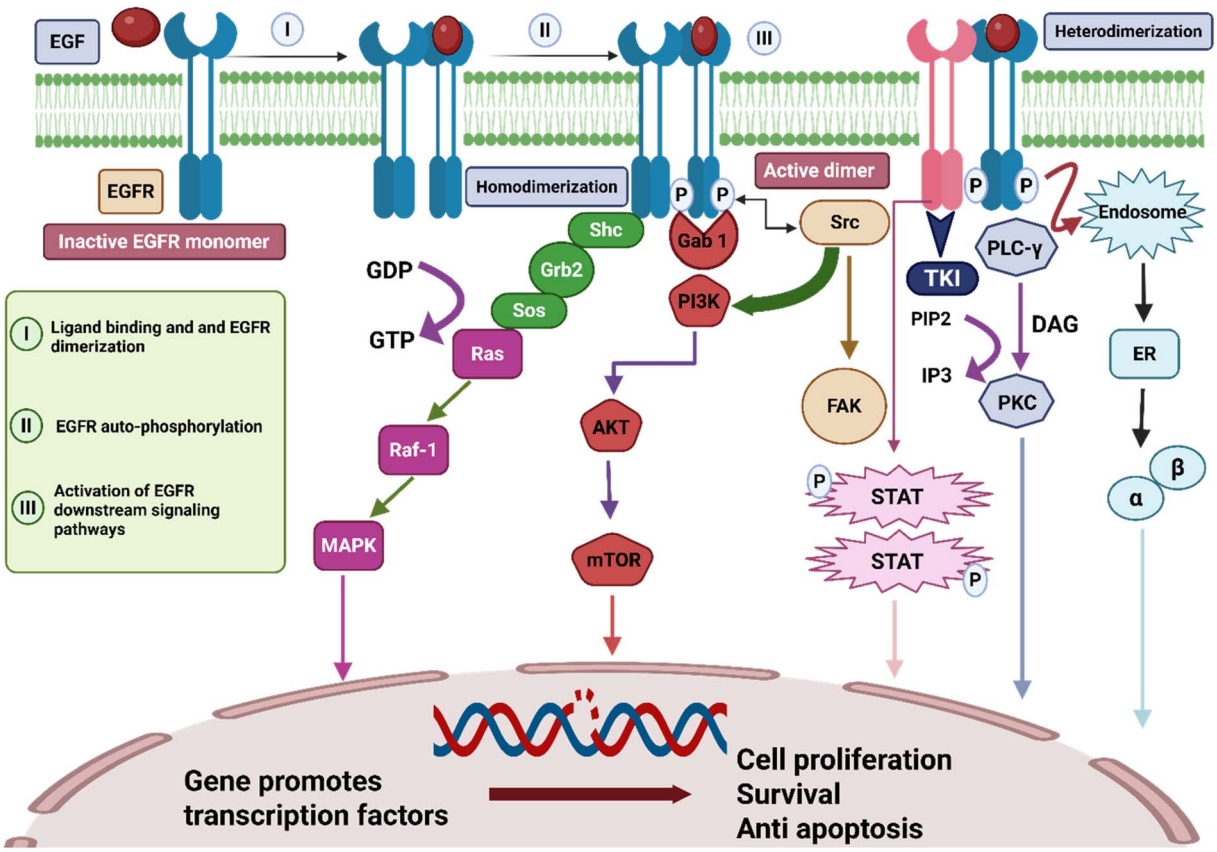

Fig. 1 EGFR activation and downstream signaling pathways.

Gab-1 to the intracellular domain (Fig. 1). This triggers multiple downstream signaling cascades, including the RAS/Raf-1/MAPK, PI3K/AKT, and PLC-γ/PKC pathways, which rely on adaptor proteins for transmission.[3] In contrast, phosphorylated receptors can directly activate the Src and STAT pathways.[35] Additionally, ligand-bound EGFR may undergo endocytosis and nuclear translocation, where it can directly regulate transcription of genes such as *Cox-2*, *iNOS*, *Aurora kinase A*, and *Cyclin D1* (ref. 36). These pathways converge to drive gene expression programs that promote cell proliferation, survival, invasion, and metastasis.

In tumors, EGFR is frequently dysregulated by overexpression or activating mutations. For example, EGFR is overexpressed in up to ∼50% of NSCLC cases and many head and neck squamous cell carcinomas.[37] Mutations in the kinase domain, such as exon 19 deletions or the L858R point mutation, result in constitutive signaling that drives oncogenesis in lung adenocarcinomas.[38] These tumors are highly dependent on EGFR ("oncogene addiction") and respond well to targeted tyrosine kinase inhibitors (TKIs).[39] First-generation reversible TKIs like gefitinib and erlotinib, which compete with ATP at the kinase site, initially produce significant clinical responses in EGFR-mutant NSCLC. However, resistance commonly arises within 8–14 months, often due to the T790M gatekeeper mutation.[40] The third-generation TKI osimertinib, which irreversibly targets T790 M-mutant EGFR, has since become first-line therapy.[41,42] Still, resistance mechanisms such as the C797S mutation or activation of bypass pathways limit long-term efficacy.[43] As a result, newer EGFR inhibitors and multi-targeted agents are developing to overcome resistance and suppress parallel oncogenic pathways (*e.g.*, VEGFR-2, MET).

An effective EGFR inhibitor must tightly bind the ATP-binding cleft of the kinase, often making specific hydrogen bonds to the hinge region (Met793 in EGFR) that anchors it in the site.[44] Ideally, it should exploit adjacent pockets for selectivity – for example, the hydrophobic region that accommodates the C-4 aniline of quinazoline inhibitors (as in erlotinib) or the solvent-exposed area for larger substituents.[45] Importantly, targeting EGFR in cancer cells inhibits proliferation and can trigger apoptosis by shutting down survival signals (AKT, NF-κB) and upregulating pro-apoptotic factors.[46] Many EGFR inhibitors have been shown to induce cell-cycle arrest (often G1 phase)[47] and promote apoptosis in tumor cells, especially those "addicted" to EGFR signaling.

While several EGFR-targeting agents are in clinical use, none of the current drugs incorporates a 1,2,3-triazole moiety. However, the modular nature of triazole click chemistry has allowed medicinal chemists to rapidly generate libraries of triazole-based analogues of known inhibitors or entirely novel hybrid scaffolds that can be tested for EGFR inhibition. The following sections will illustrate how such triazole derivatives have been designed to target EGFR alone or in combination with other cancer-relevant targets. We will see that many triazole-bearing compounds show inhibitory activity on the order of magnitude of standard EGFR TKIs (micromolar to nanomolar IC_{50} values), and in some cases, even greater potency or dual-target functionality. The incorporation of the triazole often enhances drug-like properties or enables attachment of additional pharmacophoric groups (*e.g.*, a solubilizing sugar or a second warhead for another enzyme). Thus, 1,2,3-triazoles have become a valuable motif in the contemporary toolkit for EGFR inhibitor development.

3. Importance of 1,2,3-triazoles in drug design

The 1,2,3-triazole ring offers multiple advantages in the design of bioactive molecules (Fig. 2), and its importance in drug discovery cannot be overstated.

3.1. Synthetic accessibility

The Cu(I)-catalyzed azide–alkyne cycloaddition ("click" reaction) provides an easy and robust route to 1,4-disubstituted 1,2,3-triazoles under mild conditions.[48] This reaction tolerates various functional groups, allowing medicinal chemists to rapidly assemble complex molecules by linking azide-bearing and alkyne-bearing fragments. This reaction's reliability and high yield accelerate the generation of analogues for SAR studies.

3.2. Stability

Once formed, the triazole ring is chemically inert to hydrolysis, enzymatic degradation, and extreme pH conditions. This means a triazole linkage in a drug candidate will not be easily cleaved *in vivo*, conferring metabolic stability. It can thus serve as a durable bioisosteric replacement for amide bonds, which are susceptible to amidases and peptidases. The triazole is often called a "non-classical bioisostere" of amides, esters, and peptide bonds. Replacing a labile amide with a triazole can maintain the geometry needed for binding while preventing rapid metabolism.[24,49]

3.3. Polarity and hydrogen bonding

The triazole ring contains multiple heteroatoms and has a dipole moment, enabling it to engage in polar interactions with proteins. It can function as a hydrogen bond acceptor *via* the N2 or N3 nitrogen lone pairs. In some cases (depending on substitution), the triazole's C5-bound hydrogen can act as a very weak H-bond donor, although generally the acceptor capability is exploited. In EGFR inhibitors, for example, a triazole N atom can form a hydrogen bond with the backbone NH or carbonyl of hinge residues (analogous to the N–H of an aniline in quinazolines forming a hinge bond). The triazole ring's planarity and aromaticity also allow for π–π stacking or hydrophobic interactions with aromatic amino acids in protein binding sites.

3.4. Tunable substituents

Being five-membered, the triazole ring has two positions (N1 and C4 in a 1,4-disubstituted triazole) that can be independently functionalized through the azide and alkyne components. This modularity means one can attach a wide range of R groups to the triazole – for instance, a pharmacophore known to interact with a target and a solubilizing or directing moiety – and join them *via* the triazole linker. In many EGFR inhibitor

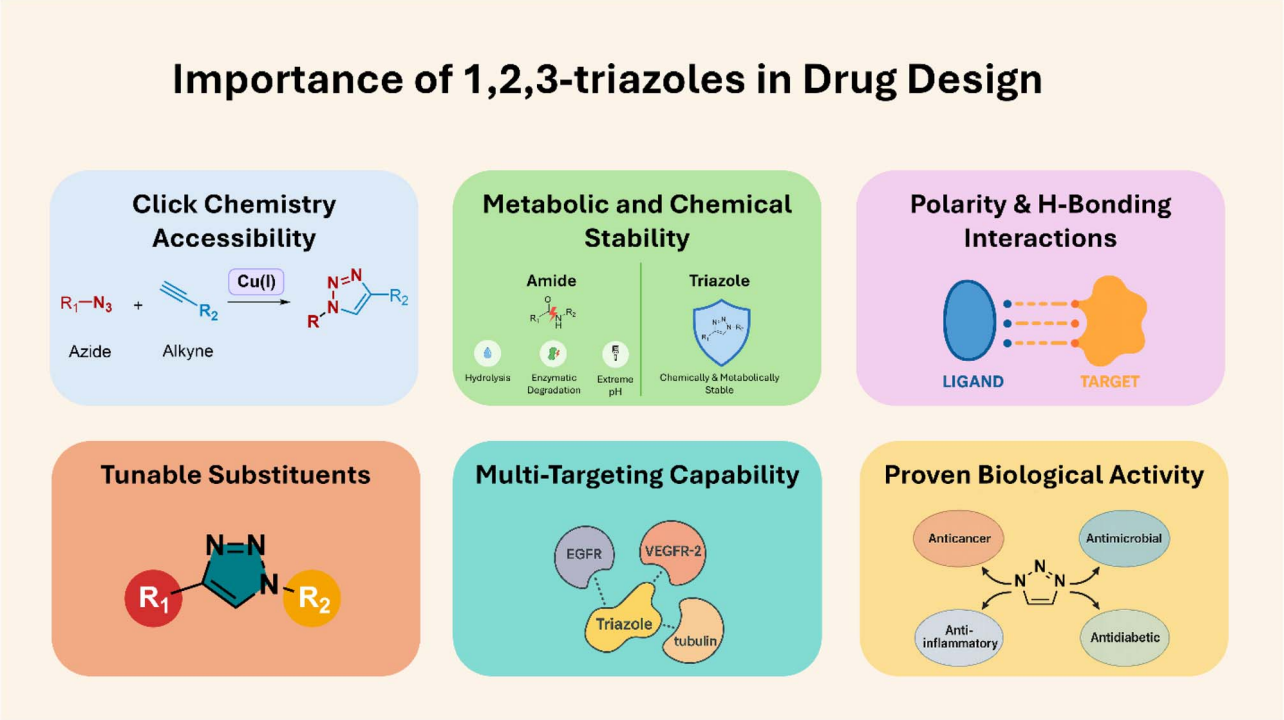

Fig. 2 Key features of 1,2,3-triazoles supporting their role in drug design.

studies, the triazole links a known EGFR-binding fragment (such as a quinazoline core mimicking ATP) with another functional fragment (such as an additional aryl group to occupy a secondary pocket or a fragment targeting a second enzyme). The ease of varying these substituents aids SAR exploration.

3.5. Multi-target potential

Because the triazole is relatively small and chemically inert, it can be incorporated into multi-target inhibitors without introducing reactive liabilities. Researchers have used triazoles to create bifunctional molecules that can engage two distinct targets – an EGFR kinase domain and another signaling protein – by tethering two ligands with a triazole linker. The triazole itself may also contribute to binding on both sides. This is exemplified by certain triazole hybrids simultaneously inhibiting EGFR and other kinases like VEGFR-2 or BRAF.

3.6. Proven bioactivity

Triazole-containing scaffolds have already yielded many compounds with potent anticancer effects across varied mechanisms.[50] They have been reported to interfere with tubulin polymerization, topoisomerase function, bromodomains, and others, in addition to kinases. In the context of EGFR, triazole-based analogues of quinazolines, pyrimidines, and indoles have shown that the triazole ring can adequately replace more common linkers without activity loss.

From a pharmacodynamic perspective, 1,2,3-triazoles can enhance binding specificity. Studies have noted that triazole-containing EGFR inhibitors often exploit a "selectivity pocket" adjacent to the ATP site, where the triazole ring forms favorable interactions that improve selectivity for EGFR over other kinases.[51] For instance, a triazole may orient an aryl group into a pocket unique to EGFR's conformation. In one report, a phenyl-triazole moiety in a hybrid inhibitor was "deeply embedded" in a hydrophobic pocket of EGFR, analogous to the way the phenylacetylene of erlotinib binds,[52] while the triazole N formed a hydrogen bond with a lysine residue (Lys721) in the active site. Such interactions underscore how the triazole can actively contribute to target affinity beyond just serving as a spacer.

In summary, the 1,2,3-triazole motif is a privileged structure in drug design due to its synthetic versatility, stability, and ability to engage biological targets through multiple interaction modes. These attributes have been capitalized on to create a new generation of EGFR inhibitors, as we will discuss in the following sections. Medicinal chemists often hybridize triazoles with known active scaffolds (*e.g.* quinazolines, benzimidazoles) to produce novel compounds, or use triazoles to rigidify molecules into bioactive conformations. The result, as evidenced by numerous recent studies, is a plethora of triazole-containing compounds with potent anticancer activity and, in many cases, impressive EGFR inhibition profiles. Below, we delve into the specific examples of such compounds, reviewing their biological activities and SAR in detail.

4. 1,2,3-Triazole-containing drugs

Several clinically approved drugs incorporate the 1,2,3-triazole ring, highlighting its pharmaceutical significance. For instance, Tazobactam is a β-lactamase inhibitor co-administered with β-lactam antibiotics such as piperacillin for the treatment of

Table 1 Approved and investigational drugs containing the 1,2,3-triazole scaffold, along with their primary therapeutic applications and current development status

Drug name	Chemical structure	Development status	Indication	Mechanism of action
Tazobactam	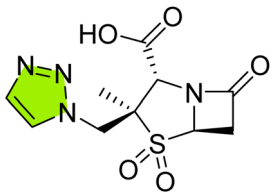	Approved	β-lactamase inhibitor (used with β-lactam antibiotics) for broad bacterial infections	Irreversibly binds and inhibits β-lactamases, protecting co-administered β-lactams
Cefatrizine	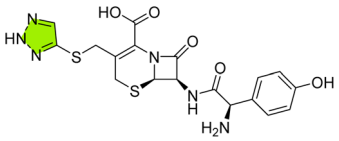	Approved	Broad-spectrum antibiotic (cephalosporin) for infections (*e.g.* RTIs, UTIs)	Inhibits bacterial cell wall synthesis by binding penicillin-binding proteins (β-lactam mechanism)
Rufinamide	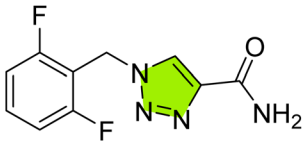	Approved	Adjunctive therapy for Lennox–Gastaut seizures	Modulates neuronal sodium channels (prolongs inactivated state), reducing excitability
Suvorexant	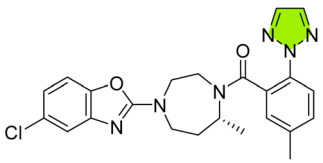	Approved	Insomnia	Dual orexin receptor (OX_1/OX_2) antagonist; blocks wake-promoting orexin neuropeptides
Ticagrelor	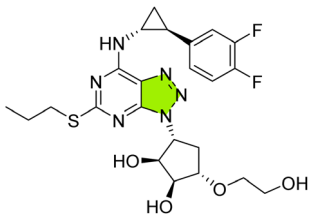	Approved	Acute coronary syndrome (antithrombotic)	Reversible antagonist of platelet $P2Y_{12}$ ADP receptor; inhibits ADP-induced platelet aggregation
Alizapride	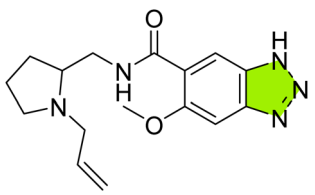	Approved	Nausea/vomiting (antiemetic, prokinetic)	Dopamine D_2 receptor antagonist in the chemoreceptor trigger zone
Daridorexant	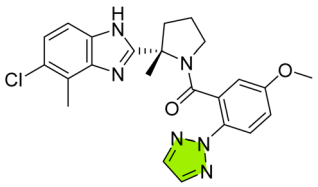	Approved	Insomnia	Dual orexin receptor antagonist (DORA), inhibits wake-promoting orexin signaling
Carboxyamidotriazole	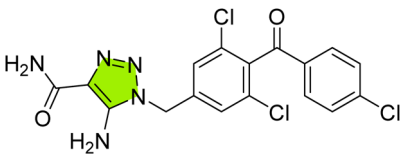	Investigational	Solid tumors (*e.g.* lung cancer)	Inhibits non-voltage-dependent Ca^{2+} channels; blocks NF-κB pathways to suppress tumor proliferation and angiogenesis
Zaprinast	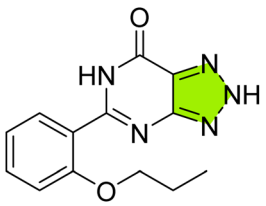	Investigational	Studied for cardiovascular/malaria	Phosphodiesterase inhibitor (PDE5/6/9/11); precursor of sildenafil (Viagra)

Table 1 (*Contd.*)

Drug name	Chemical structure	Development status	Indication	Mechanism of action
Vipadenant	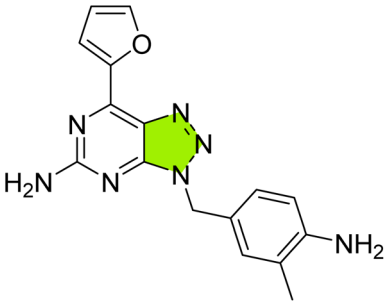	Investigational	Parkinson's disease (adjunctive)	Selective adenosine A_2A receptor antagonist (improves motor function)
Vorozole	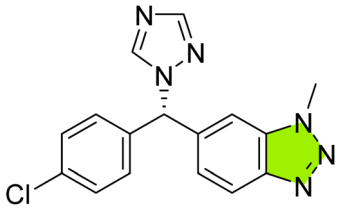	Investigational	Breast cancer imaging/ trials	Nonsteroidal aromatase inhibitor (blocks estrogen biosynthesis)
Mubritinib	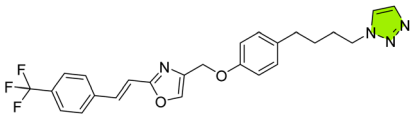	Investigational	Solid tumors (HER2-positive)	Selective inhibitor of HER2/ErbB2 tyrosine kinase
Ciforadenant	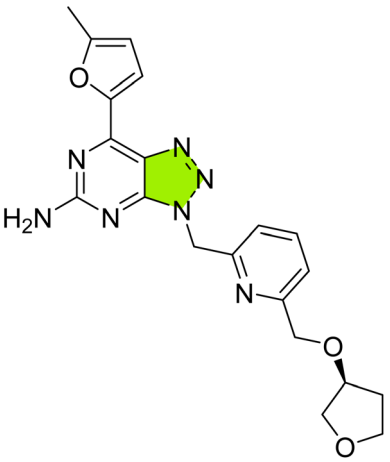	Investigational	Cancer immunotherapy	Oral A_2A adenosine receptor antagonist; restores T-cell antitumor activity
PRT062607	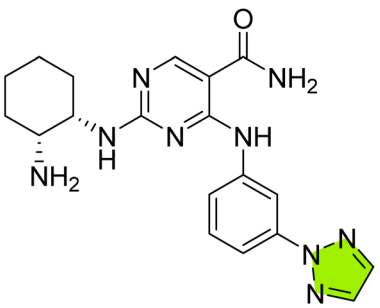	Investigational	Autoimmune/ inflammatory diseases	Potent, selective spleen tyrosine kinase (Syk) inhibitor
PF-04217903	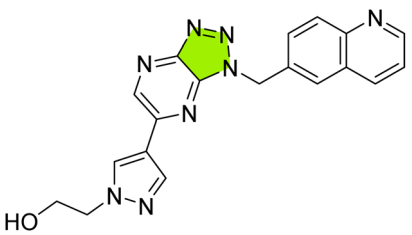	Investigational	Cancers (c-Met-driven models)	ATP-competitive MET kinase inhibitor (c-Met/ HGF receptor)

Table 1 (*Contd.*)

Drug name	Chemical structure	Development status	Indication	Mechanism of action
Milvexian	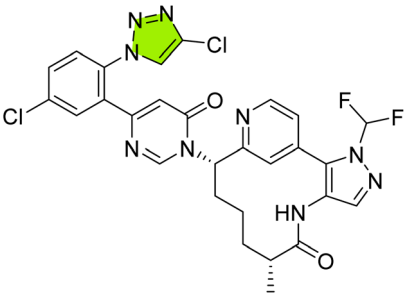	Investigational	Thromboembolic disorders (stroke, AF)	Oral factor XIa inhibitor (anticoagulant)
Radezolid	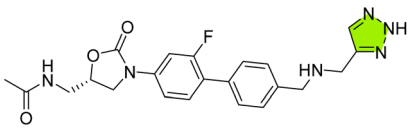	Investigational	Bacterial acne (investigational)	Oxazolidinone antibiotic; inhibits 50S ribosomal subunit (protein synthesis)
Savolitinib	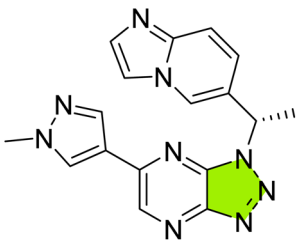	Investigational	NSCLC, gastric cancer	Oral c-Met (MET) tyrosine kinase inhibitor
Molidustat	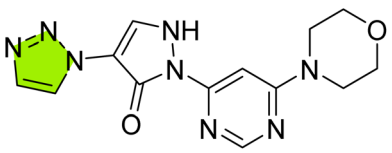	Investigational	CKD-associated anemia	HIF prolyl-hydroxylase (HIF-PH) inhibitor; increases endogenous erythropoietin
Bomedemstat	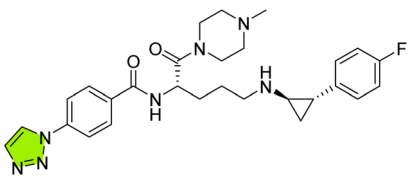	Investigational	Myeloproliferative neoplasms	Oral LSD1 (lysine-specific demethylase 1) inhibitor (epigenetic modulator)
PF-06446846	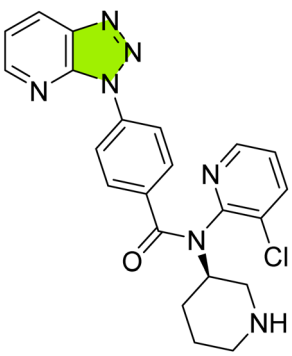	Investigational	Hypercholesterolemia	Small molecule that stalls ribosome on PCSK9 mRNA, reducing PCSK9 synthesis
BMS-986158	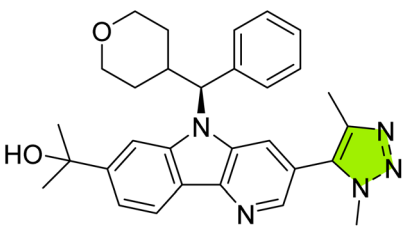	Investigational	Advanced cancers (solid tumors)	Potent BET bromodomain inhibitor (targets BRD2/3/4 epigenetic readers)

Table 1 (*Contd.*)

Drug name	Chemical structure	Development status	Indication	Mechanism of action
SB265610	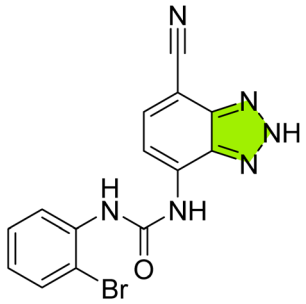	Investigational	Inflammation (preclinical models)	Allosteric CXCR2 chemokine receptor antagonist/inverse agonist
VAS2870	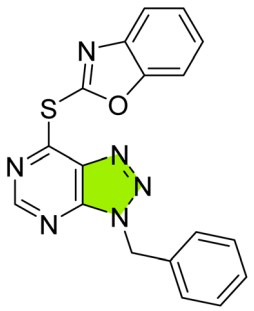	Investigational	Oxidative stress models	NADPH oxidase (NOX) inhibitor; suppresses reactive oxygen species formation
Seltorexant	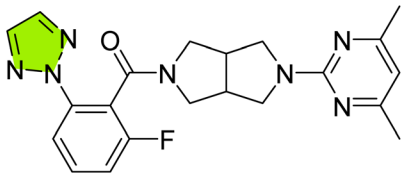	Investigational	Insomnia, depression	Dual orexin receptor (OX_1/OX_2) antagonist (improves sleep, mood)
Olitigaltin	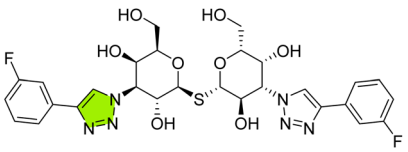	Investigational	Idiopathic pulmonary fibrosis	Inhaled galectin-3 inhibitor (anti-fibrotic)
JNJ-54175446	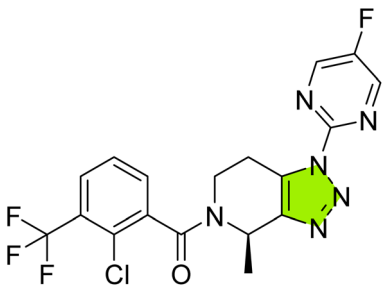	Investigational	Depression (MDD)	Selective $P2X_7$ purinergic receptor antagonist (anti-inflammatory/ neuroprotective)
ML-323	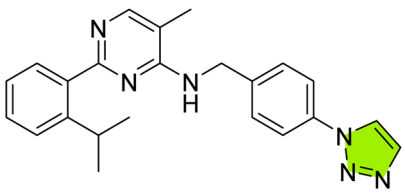	Investigational	Cancer (adjunct to DNA-damaging therapy)	Selective USP1/UAF1 deubiquitinase inhibitor; increases DNA damage in tumor cells

Table 1 (*Contd.*)

Drug name	Chemical structure	Development status	Indication	Mechanism of action
AR-C124910XX	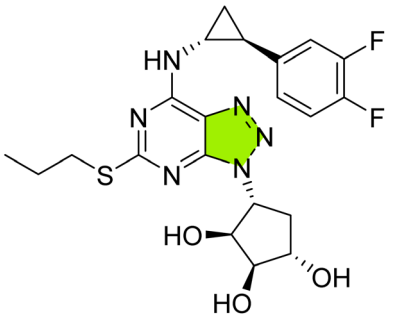	Investigational	(Active metabolite of ticagrelor)	Reversible $P2Y_{12}$ ADP receptor antagonist (similar to parent ticagrelor)
FTIDC	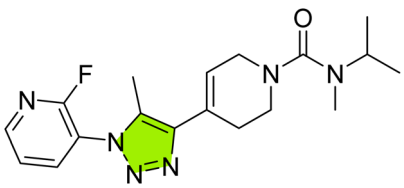	Investigational	(PET imaging tracer)	Radiotracer for 5-HT_2A serotonin receptors (investigational imaging agent)
Solithromycin	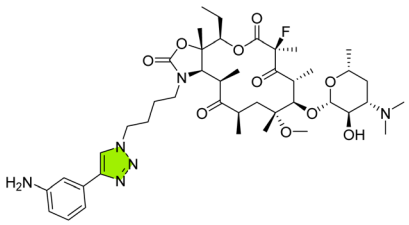	Investigational	Community-acquired pneumonia, gonorrhea	Fourth-generation ketolide antibiotic; binds 23S rRNA (50S subunit) to block protein synthesis
SM-164	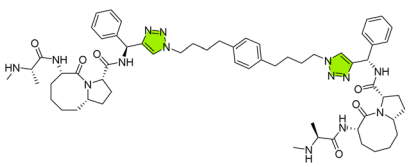	Investigational	Cancer (preclinical)	Bivalent SMAC mimetic; antagonizes IAP proteins (promotes apoptosis)
SN003	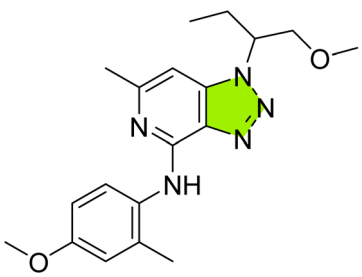	Investigational	Anxiety/depression (preclinical)	Corticotropin-releasing factor (CRF_1) receptor antagonist
Enmetazobactam	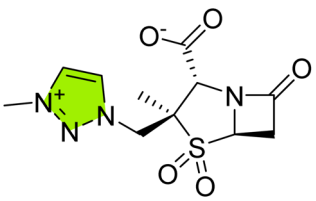	Investigational	Complicated UTI (with cefepime)	β-lactamase inhibitor; broadens cefepime activity against resistant Gram-negative bacteria

serious bacterial infections.[32] Cefatrizine is an orally active cephalosporin antibiotic used for respiratory and urinary tract infections; like other cephalosporins, it inhibits bacterial cell wall synthesis by binding to penicillin-binding proteins.[53] Rufinamide is an antiepileptic agent approved for Lennox–Gastaut syndrome, believed to act by prolonging the inactivated state of voltage-gated sodium channels.[54] Suvorexant and Daridorexant are dual orexin receptor antagonists (DORAs) approved for insomnia, functioning by blocking the wake-promoting orexin neuropeptides at OX_1 and OX_2 receptors.[55] Ticagrelor is an oral

antiplatelet agent used in the management of acute coronary syndromes, acting as a reversible antagonist of the $P2Y_{12}$ ADP receptor on platelets to inhibit aggregation.[56] Alizapride is an antiemetic and prokinetic agent that acts as a dopamine D_2 receptor antagonist in the central vomiting center.[57]

In addition to these approved drugs, numerous experimental and investigational compounds also contain the 1,2,3-triazole scaffold. Carboxyamidotriazole (CAI) is an anticancer agent that functions as a calcium channel blocker to inhibit tumor proliferation, angiogenesis, and metastasis.[58] Vipadenant (BIIB014) is a potent and selective adenosine A_2A receptor antagonist that has been investigated for its potential in treating neurodegenerative diseases such as Parkinson's disease.[59] Mubritinib (TAK-165) is a tyrosine kinase inhibitor originally developed to target HER2/ErbB2 in cancer therapy.[60] Ciforadenant is an adenosine A_2A receptor antagonist under investigation for its ability to enhance antitumor immune responses.[61] These approved and experimental 1,2,3-triazole-containing agents are presented in Table 1, which summarizes their therapeutic classes and development status.

5. 1,2,3-Triazole hybrids as EGFR inhibitors

To further elucidate the therapeutic relevance of 1,2,3-triazole-containing molecules as EGFR inhibitors, this review systematically classifies and analyzes the recent literature based on the nature of the core scaffold conjugated to the triazole ring. These hybrid systems include, but are not limited to, quinazoline, chromene, pyrimidine, quinoline, benzimidazole, indole, oxindole, and other privileged heterocycles. As illustrated in Fig. 3, diverse heterocyclic scaffolds can be tethered to the 1,2,3-triazole ring, which modulates interaction with the EGFR binding site to suppress downstream oncogenic signaling and induce apoptosis. By examining their cytotoxic activities, EGFR inhibitory profiles, and molecular modeling results, we aim to highlight the effect of the integration of 1,2,3-triazoles on the binding affinity, selectivity, and resistance-overcoming potential in these analogs. The following sections provide a scaffold-wise account of such triazole-based hybrids, beginning with quinazoline–triazole conjugates, long recognized as a foundational framework in EGFR-targeted therapy.

5.1. Quinazoline-1,2,3-triazole hybrids

The quinazoline scaffold has been a cornerstone of EGFR inhibitor design since the clinical success of gefitinib and erlotinib, which leverage hinge-binding interactions (*e.g.*, with Met793) to block kinase activity.[62] Recent efforts to enhance this pharmacophore have focused on integrating 1,2,3-triazole moieties—rigid, π-rich linkers capable of accessing adjacent kinase subpockets, improving solubility, and resisting

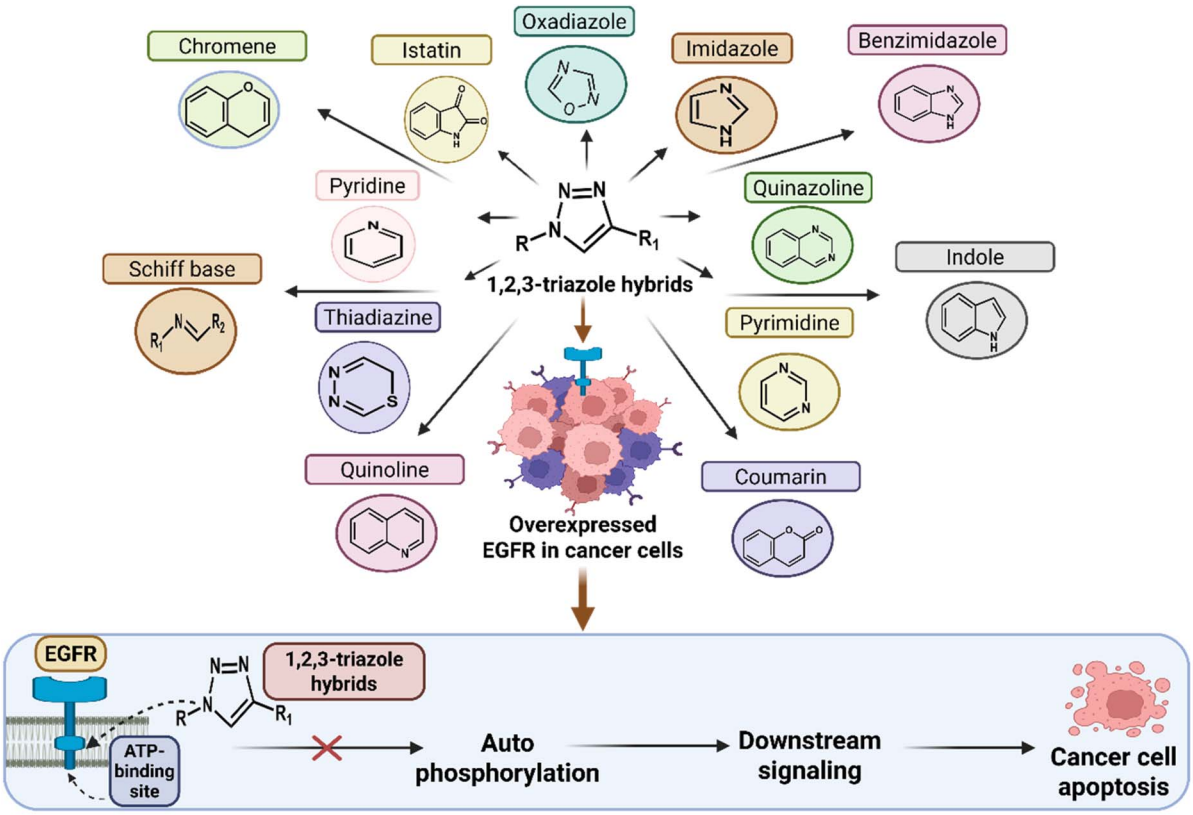

Fig. 3 Representative 1,2,3-triazole hybrids bearing diverse heterocyclic scaffolds as EGFR inhibitors.

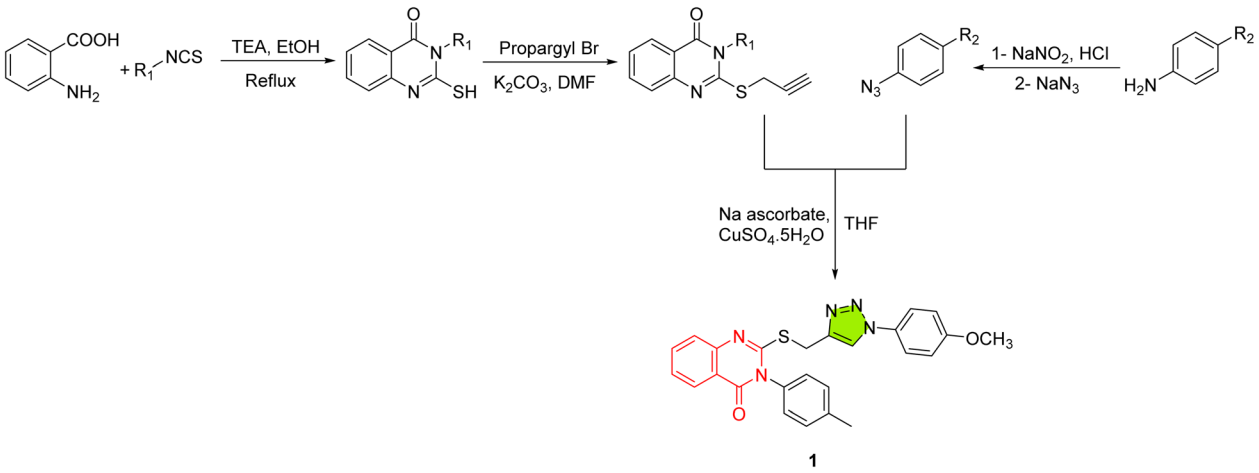

Scheme 1 Synthesis of 1,2,3-triazole hybrid **1**.

metabolic degradation. Researchers aim to preserve critical hydrogen bonds by hybridizing quinazolines with triazoles while introducing polypharmacology, mutant selectivity, and enhanced cellular uptake. This strategy has birthed a new multifunctional inhibitor class that transcends traditional ATP-competitive mechanisms.

The transformative potential of triazole–quinazoline hybrids was demonstrated by Mohamed *et al.*, who conjugated a phenyl-substituted triazole to the quinazoline core (Scheme 1) in good yields ranging from 66% to 80%, which are considered acceptable for multistep heterocyclic syntheses without requiring further optimization.[63] Their lead compound, **1**, outperformed erlotinib in antiproliferative assays (average $GI_{50} = 22$ nM *vs.* 30 nM) across MCF-7, Panc-1, and HT-29 cell lines. Beyond potency, **1** exhibited dual EGFR/$BRAF^{V600E}$ inhibition (IC_{50} = 49 nM and 66 nM, respectively), inducing G_1 arrest and apoptosis *via* Bax upregulation and caspase-3/-8 activation. Importantly, **1** showed negligible cytotoxicity toward normal human mammary epithelial MCF-10A cells, retaining 88% viability at 10 μM, underscoring a favorable safety margin. This work established the triazole linker as a versatile tool for engaging multiple kinase targets while maintaining quinazoline's hinge-binding efficacy.

Building on this dual-target paradigm, Ding *et al.* extended the triazole linker with hydroxamic acid chains, creating hybrids simultaneously inhibiting EGFR, HER2, and HDAC isoforms (obtained in moderate to excellent yields ranging from 47% to 94%) (Scheme 2).[64] Although some reactions yielded below 50%, the overall synthetic accessibility was acceptable considering the structural complexity of the hybrids. Their compound **2** achieved sub-nanomolar EGFR inhibition (IC_{50} = 0.12 nM) alongside potent HDAC1/6 activity (IC_{50} = 0.72 nM and 3.2 nM). In A431 and NCI-H1975 cells, **2** reduced viability (IC_{50} = 0.49 μM and 8.05 μM) while triggering EGFR dephosphorylation and histone H3 hyperacetylation—a testament to triazole's ability to merge disparate pharmacophores into unified polypharmacological agents.

To optimize hinge engagement and cell permeability, Le-Nhat-Thuy *et al.* redesigned the quinazoline core by fusing a dioxane ring and linking it *via* a 2-nitrophenyl triazole in consistently good yields of 70–90%, which are considered synthetically efficient and reproducible.[65] The resulting compound **3** (Scheme 3) exhibited remarkable potency gains, with IC_{50} values of 0.04 μM in KB cells and 0.14 μM in HepG2, 100-fold lower than erlotinib. SAR studies revealed the nitro group's role in enhancing π-stacking with Met769 and Thr766, while the dioxane moiety improved membrane penetration. Docking simulations across wild-type, inactive, and L858R mutant EGFR confirmed conserved hydrogen bonding, highlighting structural rigidity as a driver of mutant selectivity.

However, solubility remained a hurdle. Abdel-Rahman *et al.* addressed this by conjugating a xylopyranosyl glycoside to the

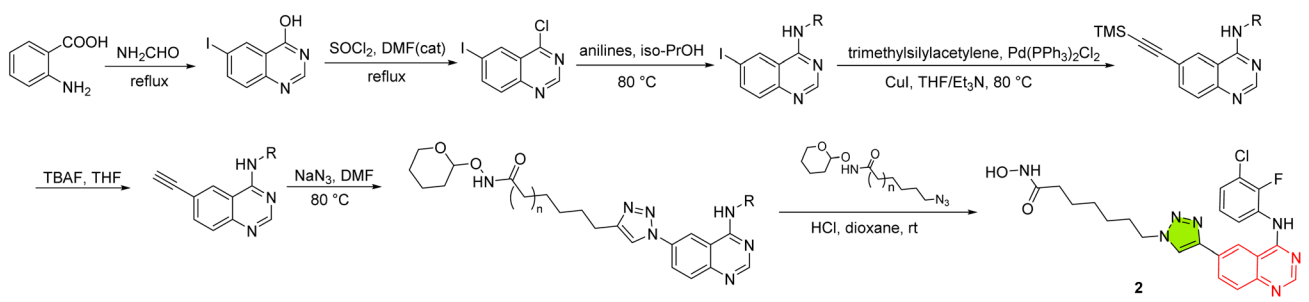

Scheme 2 Synthesis of 1,2,3-triazole hybrid **2**.

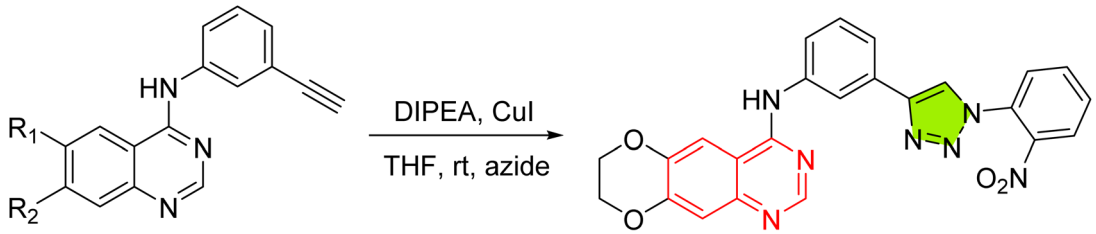

3

Scheme 3 Synthesis of 1,2,3-triazole hybrid **3**.

triazole–quinazoline scaffold in yields ranging from 58% to 87%, corresponding to moderate to very good efficiency.[66] While yields above 70% are considered satisfactory, reactions yielding near 58% may benefit from further optimization to enhance scalability. Their glycoside **4** (Scheme 4) inhibited EGFR (IC_{50} = 0.31 μM) and VEGFR-2 (3.20 μM) while improving aqueous solubility. In HCT-116 cells, **4** induced G_1 arrest (68.1% *vs.* 53.9% control) and apoptosis *via* Bax and p53 upregulation. The sugar moiety enhanced pharmacokinetics and positioned the quinazoline deeper into the kinase pocket, reinforcing interactions with Met769 and Cys919 in VEGFR-2. *In silico* ADMET profiling predicted that compound **4** complied with Lipinski's rule of five (no violations) but showed one Veber violation due to high topological polar surface area (TPSA = 160.8 $Å^2$). Its predicted lipophilicity ($M\log P$ = −0.33) indicated moderate polarity and favorable solubility, supporting improved bioavailability compared to aglycone analogues. Toxicological predictions further revealed that **4** is a P-gp non-substrate, reducing efflux-mediated resistance, and it showed no predicted hERG inhibition, suggesting a low risk of cardiotoxicity. Moreover, it was categorized as non-carcinogenic, non-biodegradable, and harmless in acute oral toxicity models, although AMES mutagenicity was positive, highlighting the need for further toxicological validation.

Meanwhile, Banerji *et al.* introduced halogenated aryl-triazoles to reduce non-specific cytotoxicity in good to very good yields of 73–88%, which reflect reliable synthetic accessibility.[67] Their lead **5** (Scheme 5) selectively inhibited MCF-7 cells (IC_{50} = 20.71 μM) while sparing normal kidney cells (IC_{50} = 40.32 μM) and erythrocytes (IC_{50} = 45.6 μM). Mechanistically, **5** disrupted EGFR phosphorylation *via* H-bonds to Met769 and halogen-π interactions with Met742, while ROS-mediated apoptosis (FITC MFI: 1683 *vs.* 765 control) and mitochondrial depolarization underscored its cancer-selective mechanism.

To directly combat resistance, Song *et al.* engineered triazoles tailored for $EGFR^{L858R/T790M}$ in yields ranging from poor to good (6–68%).[68] While the lower end of this range highlights synthetic inefficiency for some derivatives, optimization strategies could help improve scalability. Compound **6** (Scheme 6) inhibited the mutant kinase with 4 nM IC_{50}—17-fold selective over wild-type EGFR and 52-fold over HER2. In PC9 and H1975 cells, **6** achieved GI_{50} values of 0.9 nM and 505 nM, respectively, with minimal HER2 engagement (95-fold weaker than afatinib in SKBR3 cells). ADME profiling revealed moderate CYP2C9/2D6 inhibition and a favorable safety margin (HepG2 IC_{50} = 29 μM). Further profiling showed that the synthesized derivatives had negligible inhibition of CYP1A2, 2A6, 2B6, 2C19, 2E1, and 3A4 (<50% at 10 μM), but moderate inhibition of CYP2C9 and CYP2D6, indicating possible drug–drug interaction risk. Importantly, hERG patch-clamp assays revealed no significant cardiotoxicity. In hepatotoxicity assays, the compounds were far less toxic than the positive control nifedipine, reinforcing their acceptable safety profile.

Safavi *et al.* demonstrated that subtle triazole substitutions could fine-tune EGFR affinity and apoptotic efficacy in good yields of 65–75%, which are considered sufficient for medicinal chemistry campaigns without requiring extensive synthetic revision.[69] Their 4-methylphenyl derivative **7** (Scheme 7) inhibited aggressive lines like MDA-MB-231 and A549 with IC_{50} values of 12.05 μM and 8.06 μM, outperforming etoposide. Docking into the EGFR active site revealed hydrophobic interactions with Ala719/Val702 in the gatekeeper region, while AO/EB staining confirmed 39–40% apoptosis in breast cancer cells.

El Hamaky *et al.* further expanded the scaffold's versatility by targeting EGFR, VEGFR-2, and topoisomerase II in very good to excellent yields of 71–92%, reflecting robust and reliable synthetic methodology.[70] The lead compound, **8** (Scheme 8), inhibited all three targets (IC_{50} = 0.103 μM, 0.069 μM, and 19.74 μM) and induced G_2/M arrest (17.5%) and apoptosis (44.1%) in HeLa cells. Against cancer models, **8** displayed potent cytotoxicity with IC_{50} values of 2.57 μM (HeLa), 5.96 μM (HepG2), 6.41 μM (MCF-7), and 10.63 μM (HCT-116), while showing much weaker activity on normal WI-38 fibroblast cells (IC_{50} = 40.53 μM). Docking highlighted interactions with Met793 (EGFR),

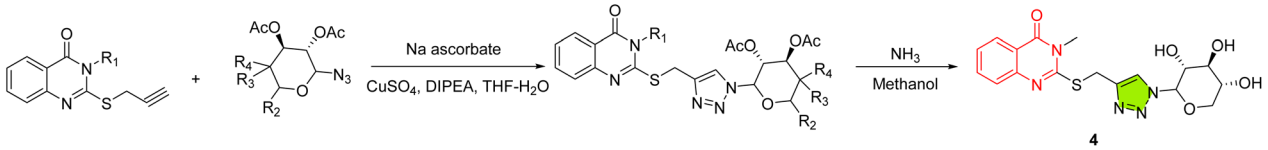

4

Scheme 4 Synthesis of 1,2,3-triazole hybrid **4**.

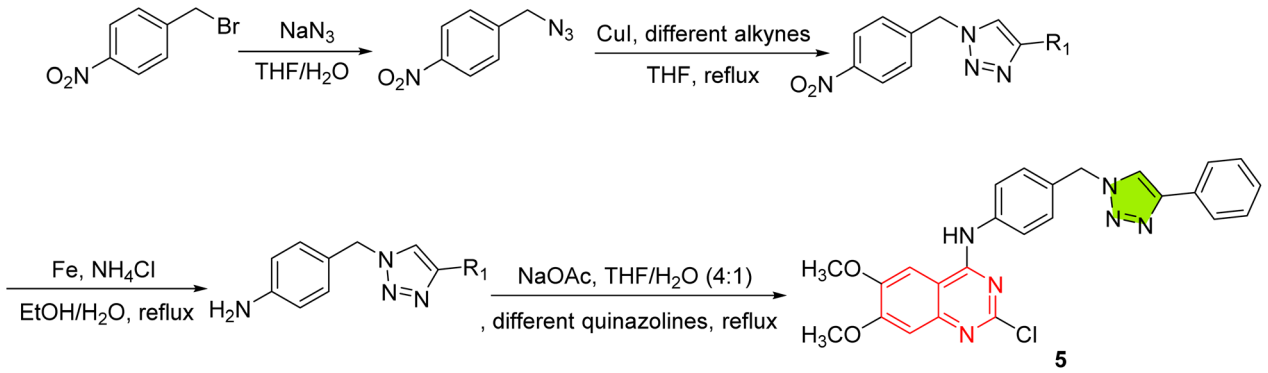

Scheme 5 Synthesis of 1,2,3-triazole hybrid **5**.

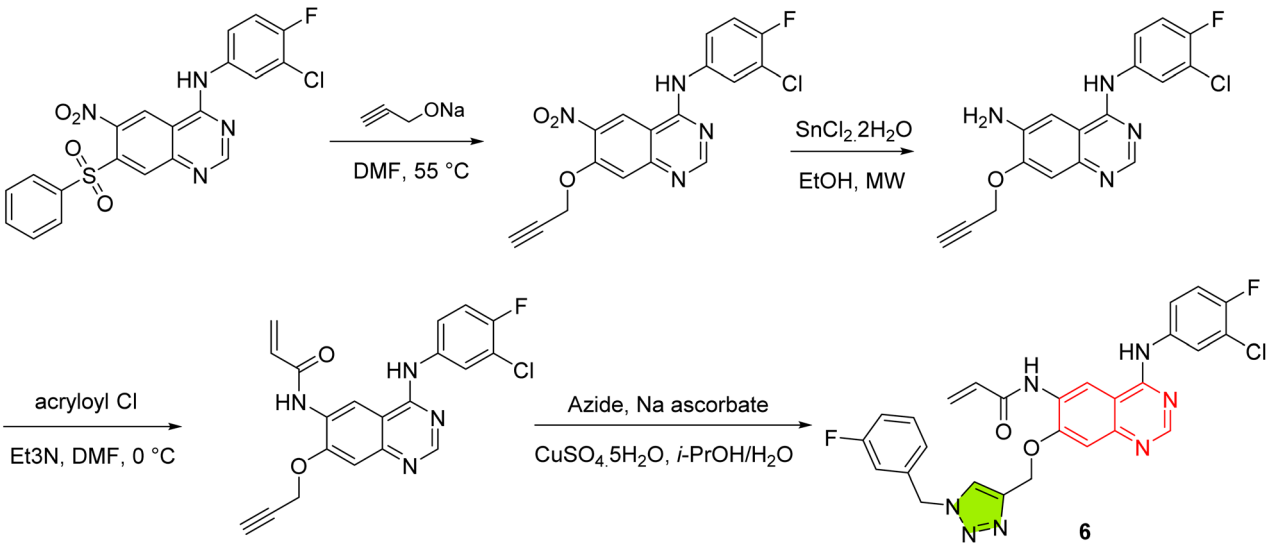

Scheme 6 Synthesis of 1,2,3-triazole hybrid **6**.

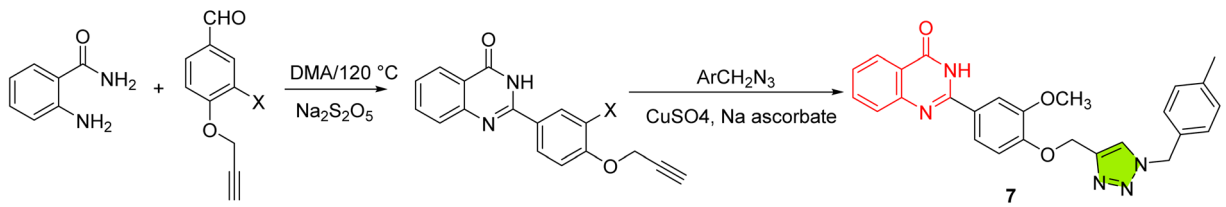

Scheme 7 Synthesis of 1,2,3-triazole hybrid **7**.

Cys919 (VEGFR-2), and Topo II's catalytic pocket, illustrating the hybrid's capacity to impair multiple oncogenic pathways.

In parallel, Lee *et al.* explored 3-hydroxyanilino quinazoline–triazoles against BRAF/EGFR kinases in yields spanning from poor to excellent (27–95%).[71] The wide variation indicates the need for optimization for certain structural variants, particularly those with lower synthetic efficiency. While **9** (Scheme 9) potently inhibited B-Raf^{V600E} (51 nM) and VEGFR2 (7 nM), its cellular efficacy in A375 melanoma was limited (GI_{50} >10 μM), suggesting permeability challenges. However, moderate activity in EGFR-mutant NSCLC lines (HCC827 GI_{50} = 1.3 μM) hinted at context-dependent utility. Structural analysis emphasized π–π-stacking with Trp531 in B-Raf and hinge-binding to Cys532/Cys919, reaffirming the scaffold's adaptability across kinase families.

5.2. Chromene/coumarin 1,2,3-triazole hybrids

Chromene and coumarin cores, when conjugated to a 1,2,3-triazole *via* Cu(I)-catalyzed click chemistry, combine two bioactive heterocycles that favor both hinge-binding and access to adjacent pockets in EGFR. Hajlaoui *et al.* applied microwave-assisted click chemistry to assemble chromene–triazole

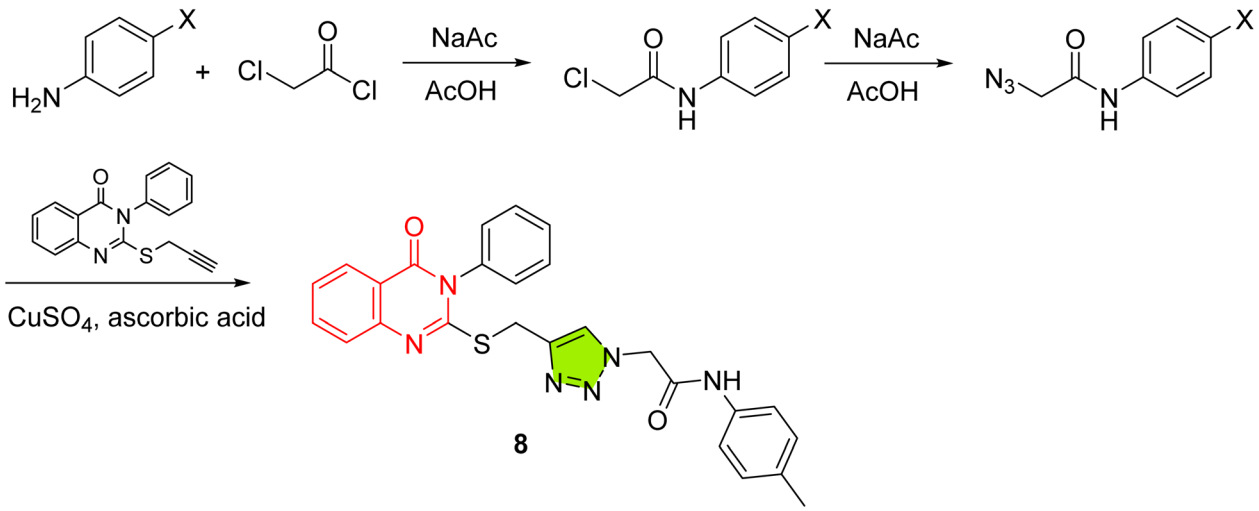

Scheme 8 Synthesis of 1,2,3-triazole hybrid **8**.

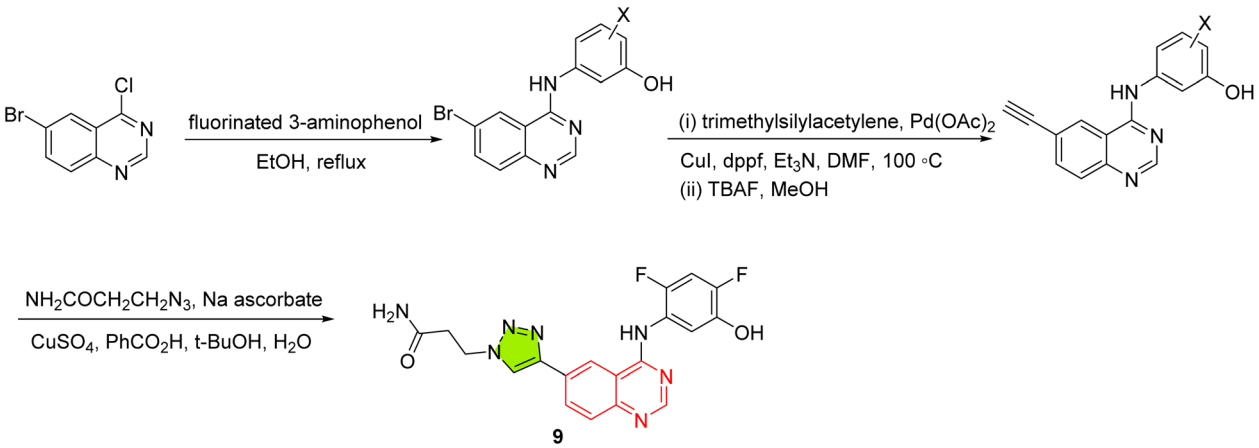

Scheme 9 Synthesis of 1,2,3-triazole hybrid **9**.

hybrids (Scheme 10) in very good to excellent yields of 82–92%, which reflect a highly efficient and reproducible synthetic process.[72] Among their series, compound **10** (4-trifluoromethylphenyl) emerged as the lead, inhibiting B16F10 and IGR39 melanoma cells with IC_{50} values of 69.0 ± 8.4 μM and 92.0 ± 6.0 μM, respectively, while docking to EGFR with −10.7 kcal mol^{-1} and forming a key H-bond to Lys721. A chlorinated analogue, **11**, excelled in α-amylase inhibition (IC_{50} = 9.13 ± 1.37 μM). Predicted ADMET data showed overall compliance with drug-likeness rules, acceptable solubility, and

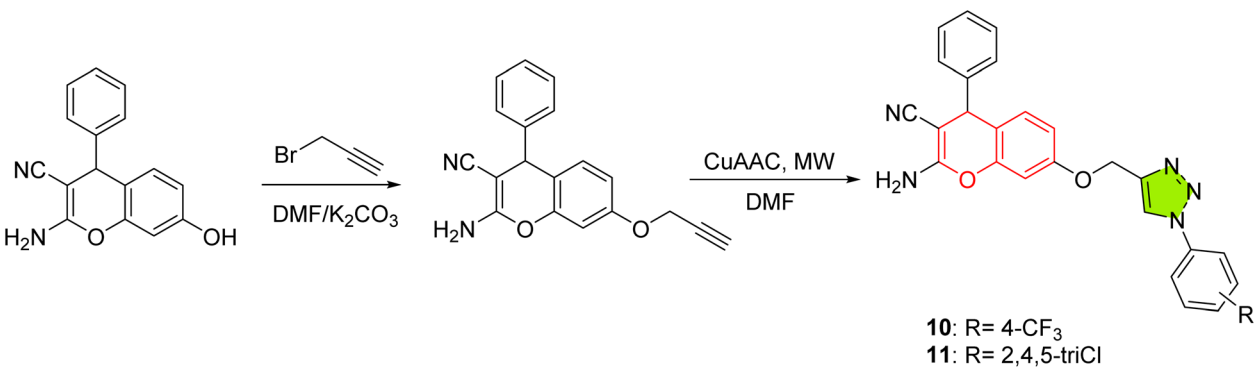

Scheme 10 Synthesis of 1,2,3-triazole hybrids **10** and **11**.

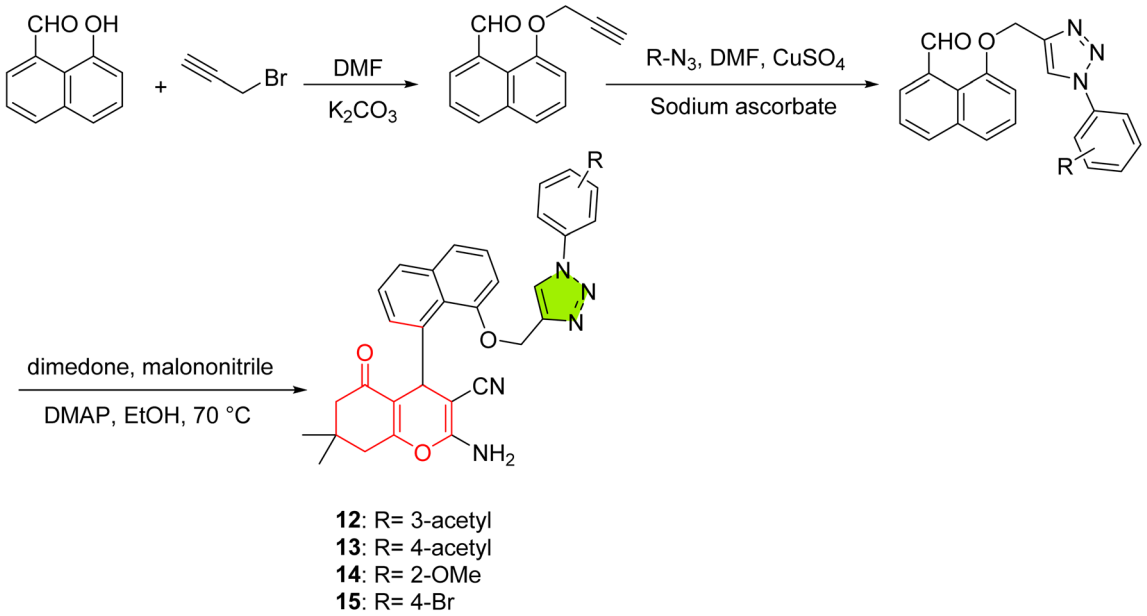

Scheme 11 Synthesis of 1,2,3-triazole hybrids **12**–**15**.

low acute oral toxicity (class IV–V). The hybrids were predicted non-carcinogenic and non-immunotoxic, with only nitro derivatives giving a mutagenicity alert, supporting their generally safe pharmacological profile.

Building on this foundation, Bojja and co-workers introduced acetyl groups at the phenyltriazole ring in good to very good yields of 76–85%, which are readily scalable and synthetically practical (Scheme 11):[73] the *meta*-acetyl derivative **12** achieved low-micromolar cytotoxicity ($IC_{50} = 2.67 \pm 0.03$ μM in MCF-7; 3.13 ± 0.03 μM in PC-3; 3.05 ± 0.05 μM in HeLa) and docked to EGFR with −10.5 kcal mol^{-1}, surpassing doxorubicin. Its *para*-acetyl isomer **13** mirrored this potency ($IC_{50} = 3.16$–4.68 μM), while derivatives such as **14** (−10.6 kcal mol^{-1} *vs.* FGFR2) and **15** (−10.9 kcal mol^{-1} *vs.* CDK2) highlighted the scaffold's multi-kinase versatility.

Building on Bojja's work, Vidya and colleagues introduced a 1,3,4-oxadiazole linker between chromene and the triazole, affording products in good to very good yields (70–89%), reflecting a balance between synthetic accessibility and functional diversity (Scheme 12). Among their series, **16** (3,5-dimethoxyphenyl) and **17** (4-methoxyphenyl) showed the strongest dual anticancer-EGFR profiles, with IC_{50} values of 9.24

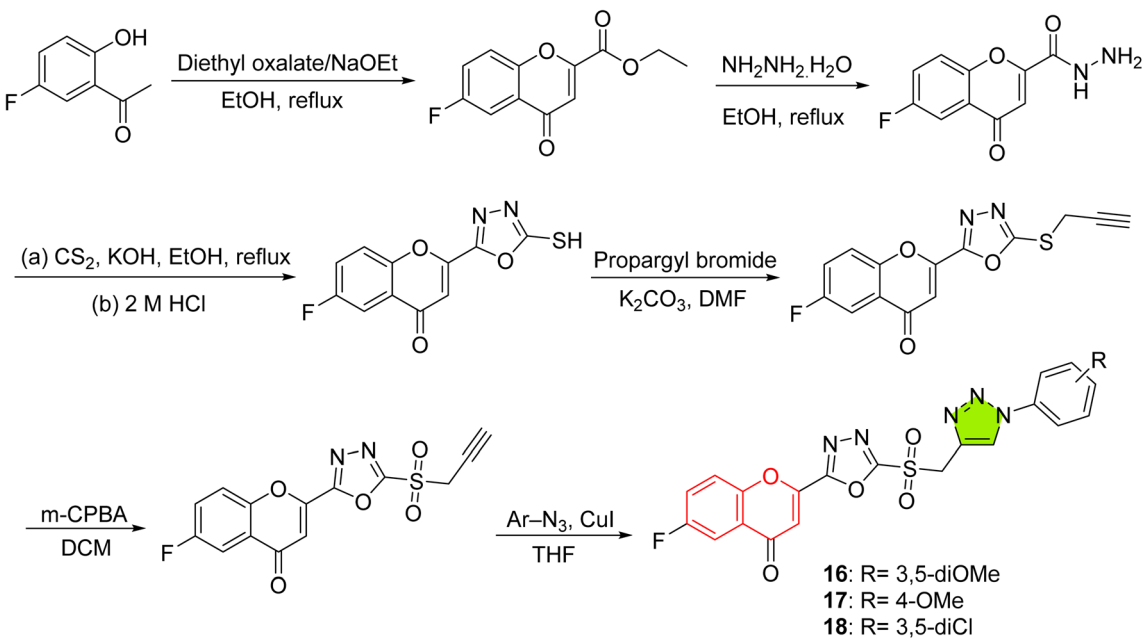

Scheme 12 Synthesis of 1,2,3-triazole hybrids **16**–**18**.

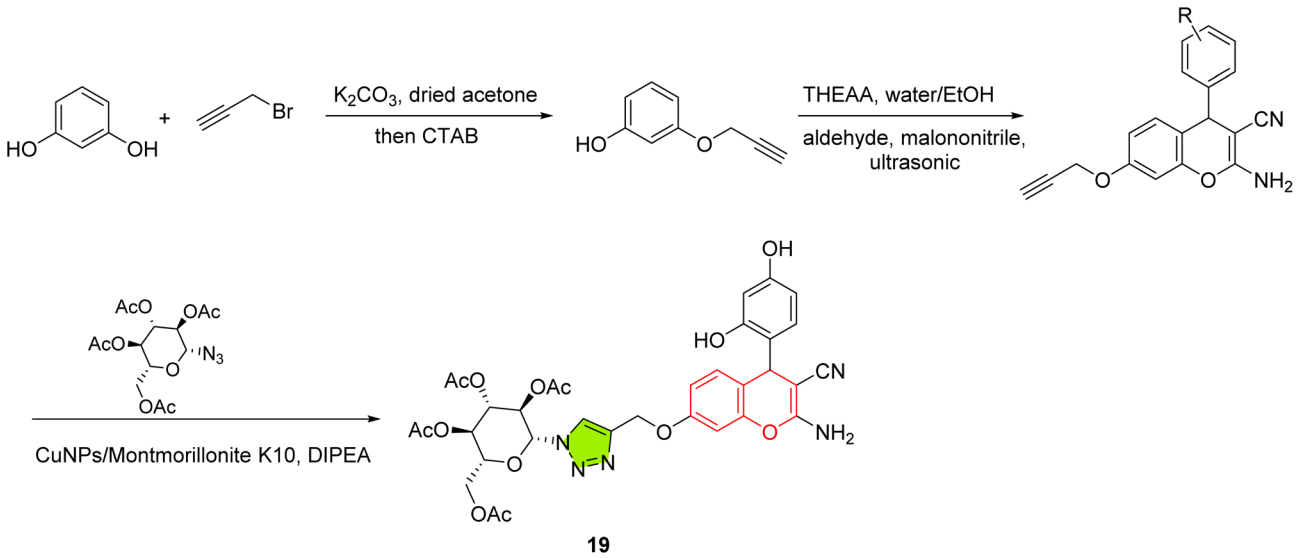

Scheme 13 Synthesis of 1,2,3-triazole hybrid **19**.

± 1.21 μM (MCF-7)/9.38 ± 1.15 μM (A-549) for **16** and 10.68 ± 1.08 μM/9.89 ± 0.93 μM for **17**, while EGFR inhibition reached submicromolar levels (0.480 ± 0.032 μM for **16**; 0.621 ± 0.082 μM for the 3,5-dichloro analogue **18**)—nearly matching erlotinib's 0.421 ± 0.030 μM benchmark.[74]

Seeking to merge cytotoxic and anti-angiogenic effects, Nguyen *et al.* grafted a D-glucose moiety onto the chromene–triazole core *via* a high-yielding and operationally simple approach (80–91%), reflecting excellent synthetic efficiency across the series (Scheme 13).[75] Their lead, **19** (2,4-dihydroxyaryl), potently suppressed HepG2, MCF-7, HeLa, and SK-LU-1 proliferation (IC_{50} = 3.83 ± 0.23 to 1.56 ± 0.22 μM) with minimal toxicity to WI-38 normal cells (IC_{50} = 97.5 ± 2.0 μM) and achieved nanomolar EGFR/VEGFR-2 inhibition (11.33 ± 0.41 nM and 19.23 ± 1.12 nM). Docking and 300 ns MD simulations confirmed stable Cys773/Lys721 interactions, while Annexin V assays revealed 27.7% total apoptosis *versus* 2.2% in controls.

To enhance drug-likeness, Kumar N. and co-workers pursued a different approach, applying a Ramachary–Bressy–Wang organocatalytic route to incorporate sulfonyl–benzimidazole onto the coumarin–triazole core. Their reported moderate to very good yields (55–89%) reflect a methodology still undergoing refinement, especially at the lower end where further optimization could improve throughput (Scheme 14).[76] Of their library, **20** and **21** delivered low-micromolar cytotoxicity (IC_{50} ≈ 2.6–3.7 μM in MCF-7/HeLa) and EGFR inhibition (0.204–0.210 μM)—nearly double the potency of erlotinib—while maintaining reduced toxicity toward normal cells, with **20** showing IC_{50} = 16.61 ± 0.72 μM (MCF-10A) and 13.77 ± 0.45 μM (HEK-293), and **21** showing IC_{50} = 22.26 ± 1.01 μM (MCF-10A) and 19.52 ± 0.87 μM (HEK-293). ADME profiling confirmed no Lipinski or Veber violations. Predicted pharmacokinetics further indicated good aqueous solubility and high intestinal absorption. Toxicological predictions categorized the compounds as non-carcinogenic, non-hepatotoxic, and with no hERG inhibition alerts, while AMES mutagenicity was flagged only for nitro-substituted analogues outside this series.

Moreover, Sanduja's systematic variation of linker length and halogenation in uracil–coumarin hybrids[77] revealed that **22** (n = 2, iodouracil) (Fig. 4) achieved a Glide gScore of −8.891 kcal mol^{-1} and Emodel −100.744 *versus* erlotinib's −8.538/−80.588, maintained complex stability over 50 ns MD

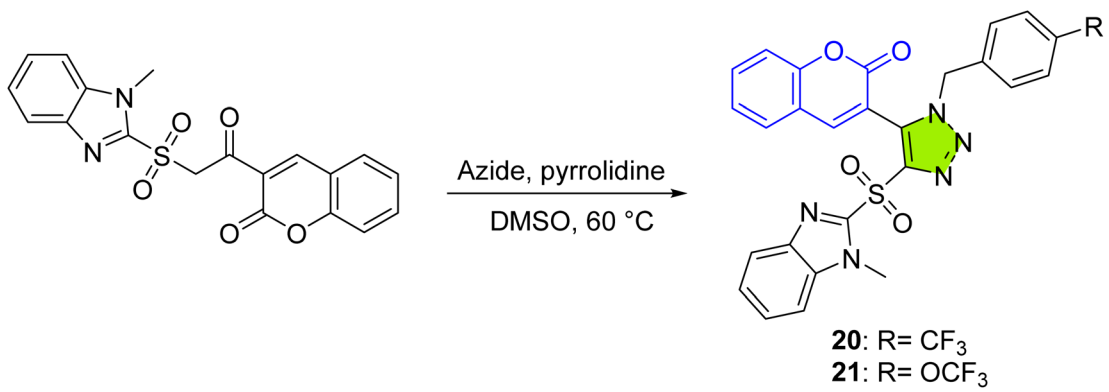

Scheme 14 Synthesis of 1,2,3-triazole hybrids **20** and **21**.

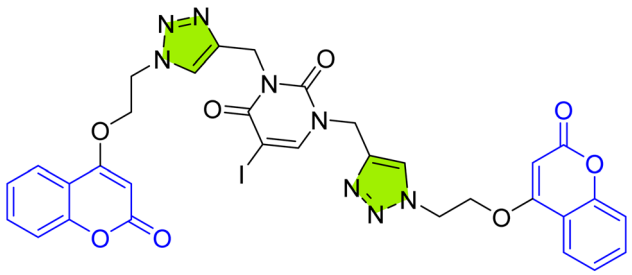

22

Fig. 4 Structure of 1,2,3-triazole hybrid 22.

(RMSD plateau ~0.3 nm), and formed four key H-bonds with Cys773, Met769, Lys721, and a water molecule—underscoring the power of halogen tuning for EGFR affinity.

5.3. Pyridine/pyrimidine-1,2,3-triazole hybrids

Both pyridine and pyrimidine scaffolds have been reported to exhibit EGFR inhibitory activity,[78,79] and their hybridization with 1,2,3-triazole linkers has proven an effective strategy to enhance kinase-binding affinity and antiproliferative potency against EGFR-driven cancers. Utilizing this, Sreerama *et al.* synthesized pyrido[4,3-*d*]pyrimidine–triazole derivatives in yields ranging from good to very good (66–82%) (Scheme 15),[80] representing synthetically favorable conditions with minimal need for optimization. Among the series, compound **23** (3-trifluoromethylphenyl) stood out for its cytotoxicity (MCF-7 IC_{50} = 2.27 ± 0.98 μM), surpassing doxorubicin (IC_{50} = 4.20 ± 0.73 μM). Additionally, compounds **24** (3,5-dichlorophenyl), **25**, and **26** surpassed erlotinib in EGFR inhibition (IC_{50} values of 0.24 ± 0.06, 0.28 ± 0.02, and 0.25 ± 0.05 μM, respectively). Docking against PDB 4HJO revealed that **25** formed a key H-bond with Ala698 and π–π stacking with Phe699, while **26** engaged Arg817—findings that underscore the versatility of this hybrid motif in achieving sub-micromolar kinase inhibition.

Expanding this scaffold, Bandi *et al.* crafted a series of pyrido[2,3-*d*]pyrimidine-thiazolidine-triazole hybrids in good yields (Scheme 16),[81] identifying **27** as the standout candidate: it inhibited EGFR with an IC_{50} of 0.39 ± 0.03 μM (*vs.* 0.42 ± 0.01 μM for erlotinib) and exerted superior cytotoxicity in MCF-7 (IC_{50} = 3.52 ± 0.12 μM) and A-549 (IC_{50} = 8.28 ± 0.26 μM) cells compared to the clinical inhibitor (MCF-7 IC_{50} = 4.32 ± 0.27 μM). Favorable docking interactions with Thr830, Cys773, and Met742 in the EGFR active site underpinned its activity. *In silico* pharmacokinetic predictions indicated moderate aqueous solubility and low gastrointestinal absorption for **27**, with no blood–brain barrier penetration. The compound adhered to Lipinski's criteria with only a marginal molecular weight deviation, and it was not predicted to be a P-gp substrate. However, CYP2C9 and CYP3A4 inhibition was predicted, which could

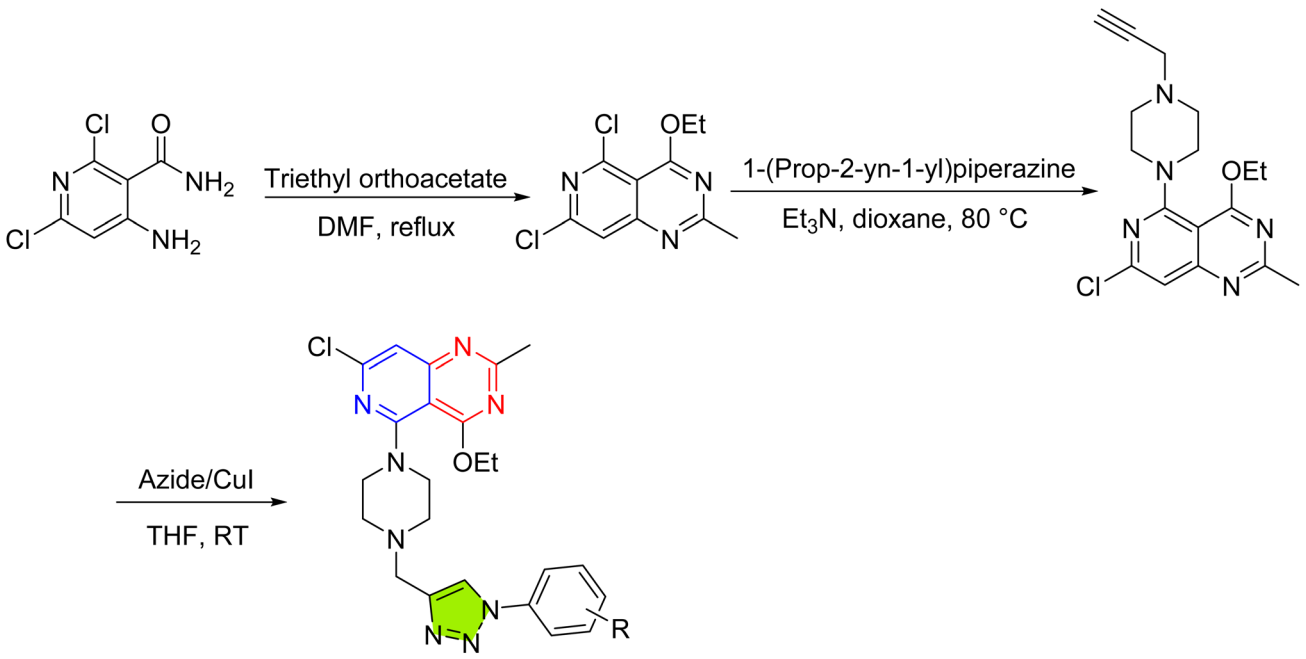

23: R= 3-CF_3
24: R= 3,5-diCl
25: R= 3-Cl
26: R= 4-Cl-3,5-diOMe

Scheme 15 Synthesis of 1,2,3-triazole hybrids 23–26.

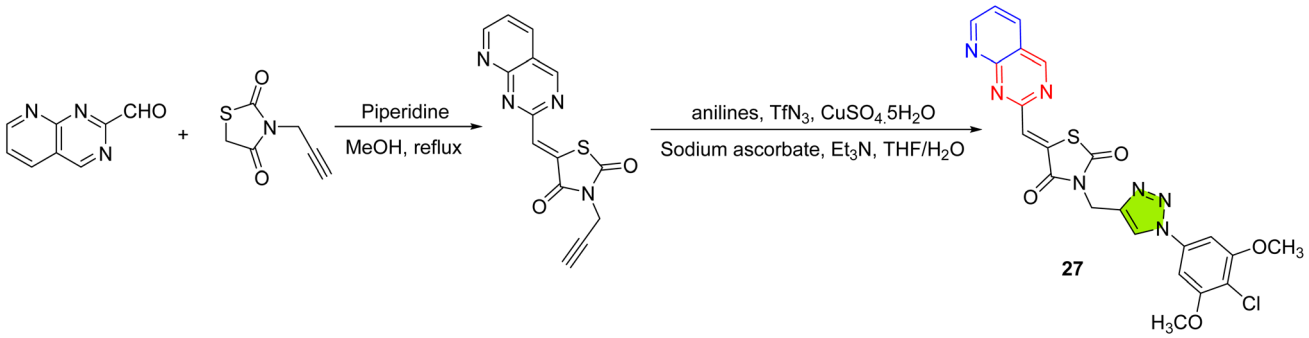

Scheme 16 Synthesis of 1,2,3-triazole hybrid **27**.

present potential metabolic liabilities. Its bioavailability score was modest (0.17), reflecting the need for further optimization.

Building on Bandi's work, Narasimhachar *et al.* explored pyrimidine-thio-triazole hybrids in strongly reproducible yields of 85–92% (Scheme 17),[82] reflecting excellent synthetic control and functional group tolerance. They identified **28** and **29** as leads in MCF-7 assays (IC_{50} = 29.62 μM and 41.8 μM, respectively). Though less potent than the fluorinated analogues, these sulfur-containing variants offered valuable mechanistic insights: docking into EGFR's ATP site (PDB 3W33) yielded binding energies of −7.27 and −7.45 kcal mol^{-1} for **28** and **29**, with **28** anchoring *via* strong H-bonding to Asp855 and a pi-cation interaction with Lys875. Molecular dynamics over 100 ns confirmed **28**'s superior complex stability (protein RMSD ~2.5 Å, ligand RMSD ~5.8 Å), establishing it as a promising scaffold for further optimization despite its moderate antiproliferative profile.

Capitalizing on the potency of pyrido-pyrimidine triazoles, researchers next turned to sugar-tethered hybrids to enhance both selectivity and cellular uptake. Thanh *et al.* synthesized a large panel of 4*H*-pyrano[2,3-*d*]pyrimidine-triazole glycoconjugates in uniformly high yields of 76–95% (Scheme 18).[83] These yields demonstrate superb efficiency, even across a chemically diverse 36-member library, facilitating systematic SAR exploration. The study identified four standout leads—**30**, **31**, **32**, and **33**. Compound **30** proved exceptional, combining sub-micromolar antiproliferative activity (MCF-7 IC_{50} = 1.36 ± 0.12 μM) with potent dual EGFR/HER2 inhibition (IC_{50} = 0.16 and 0.17 μM, respectively). Induced-fit docking into EGFR (PDB: 1M17) revealed that **30** formed hydrogen bonds with Met769, Cys773, and Thr830, mirroring erlotinib's hinge interactions while its glucose moiety improved water solubility. Flow cytometry confirmed apoptotic induction (37.1% total apoptosis *vs.* 1.7% in controls), underscoring its mechanistic promise.

In a parallel glycosylation strategy, Al-Sahaly and co-workers installed a glucopyranosyl spacer between a biphenyl/thienyl aryl system and the triazole ring in good yields of 75–79% (Scheme 19),[84] which are acceptable for glycosylated systems, though further optimization might be needed to push consistency toward the upper range. Their lead **34** achieved near-complete growth inhibition at 100 μM in A549 (98.5%), PC-3 (98.3%), and MCF-7 (97.7%) cells, with IC_{50} values of 6.50 ± 0.75 μM (A549) and 9.65 ± 4.83 μM (PC-3), while demonstrating negligible toxicity to BJ1 normal fibroblasts. Molecular docking scored −10.35 kcal mol^{-1} against EGFR and −11.35 kcal mol^{-1} against VEGFR-2, highlighting key interactions with Lys721 (EGFR) and Arg1027/Ala881 (VEGFR-2) that rationalize its dual-kinase profile.

5.4. Quinoline-1,2,3-triazole hybrids

Quinoline–triazole conjugates harness the well-established hinge-binding affinity of the quinoline core while exploiting the 1,2,3-triazole linker's rigidity and π-rich character to enhance kinase inhibition. Lavunuri *et al.* synthesized quinoline-fused 1,2,3-triazoles in good to very good yields of 68–85% (Scheme 20),[85] which are particularly commendable given the rigidity of the scaffold. They pinpointed compound **35** (4-methoxyphenyl) as a superior dual EGFR/HER2 inhibitor (IC_{50} = 0.12 μM and 0.34 μM *vs.* erlotinib's 0.42 μM/0.58 μM), with antiproliferative IC_{50} values of 2.8–6.4 μM across MCF-7, MDA-MB-468, and MDA-MB-231 cells; its 4-nitrophenyl analogue **36** mirrored this profile (EGFR/HER2 IC_{50} = 0.29/0.72 μM; cytotoxic IC_{50} = 3.5–7.5 μM), and docking confirmed key hinge interactions with binding energies around −9.0 kcal mol^{-1}.

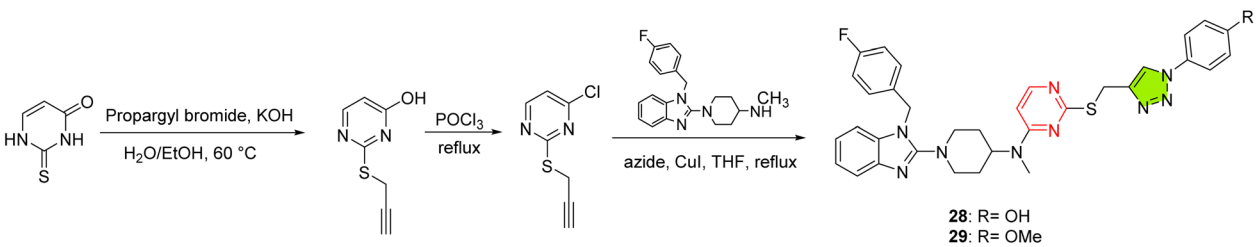

Scheme 17 Synthesis of 1,2,3-triazole hybrids **28** and **29**.

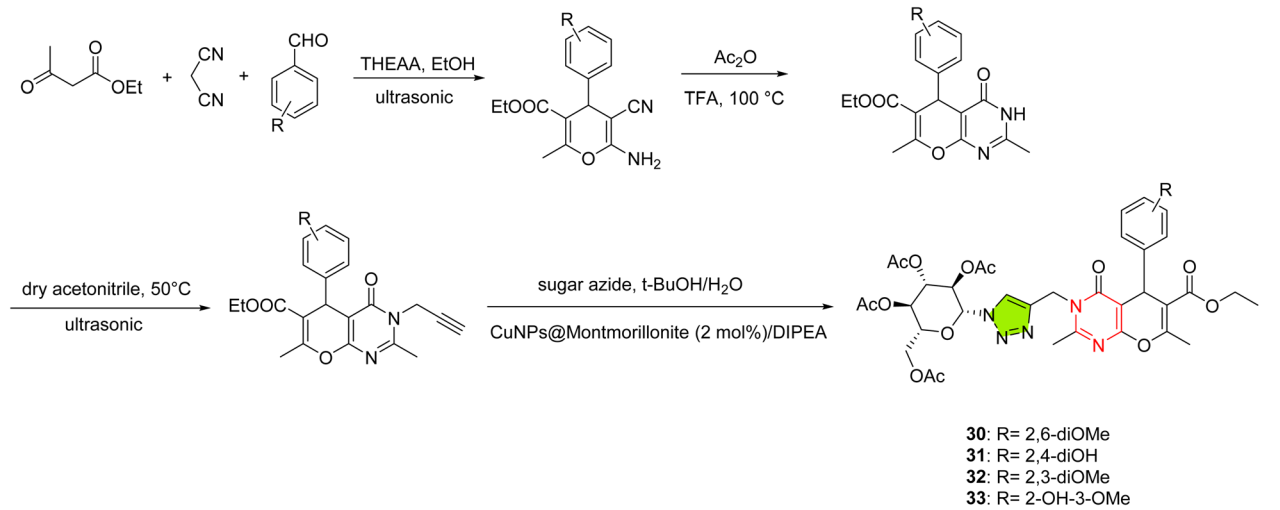

Scheme 18 Synthesis of 1,2,3-triazole hybrids **30–33**.

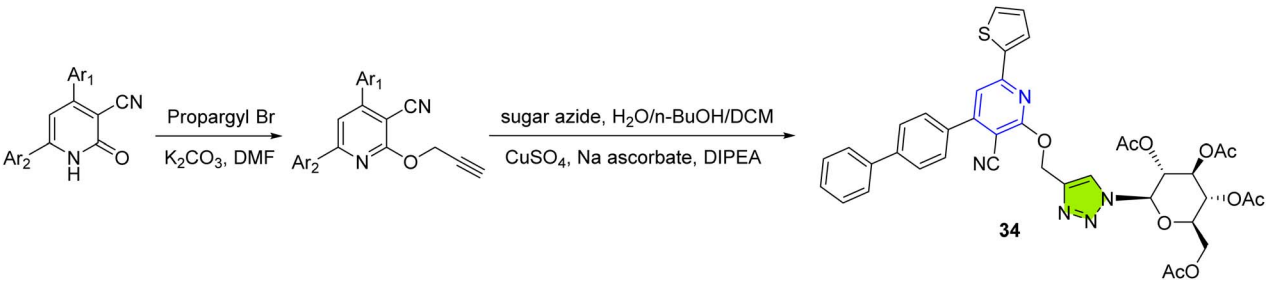

Scheme 19 Synthesis of 1,2,3-triazole hybrid **34**.

Mamidala *et al.* advanced these hybrids by introducing a morpholine moiety to the quinoline, obtained in good to very good yields of 72–88%, suitable for scale-up and functional group variation,[86] yielding compound **37** (Scheme 21), which achieved EGFR inhibition at 0.14 μM—over threefold more potent than erlotinib (0.42 μM)—and demonstrated GI_{50} values of 1.10 ± 0.08 μM (MCF-7), 4.55 ± 0.54 μM (A549), and 5.58 ± 0.68 μM (HepG2). The compound also exhibited poor activity against normal MCF-10A cells (IC_{50} = 95.05 ± 1.49 μM), reflecting its selective cytotoxicity toward malignant cell lines. Molecular docking placed **37** snugly within the Val702–Leu820 hydrophobic pocket (binding energy −9.96 kcal mol^{-1} *vs.* −7.69 kcal mol^{-1} for erlotinib), while *in silico* ADME profiling predicted excellent intestinal uptake, negligible CNS penetration, and adherence to Lipinski, Veber, Egan, and Muegge criteria. These features mark **37** as a promising, orally bioavailable EGFR-targeted agent with a favorable safety and PK profile.

In another study by the same group, they tethered a barbituric acid moiety through the triazole linker to generate multitarget hybrids in good to very good yields of 70–85% (Scheme 22).[87] These yields reflect smooth reaction conditions with minimal byproduct formation, suggesting that the synthetic protocol is well-suited for generating analogues at scale. Their lead, **38**, combined submicromolar EGFR inhibition (IC_{50} = 0.18 μM) with potent VEGFR-2 blockade (IC_{50} = 16.27 nM), outperforming erlotinib (0.40 μM) and sorafenib (35.64 nM). In MCF-7, MDA-MB-468, and MDA-MB-231 breast cancer lines, **38** delivered IC_{50} values of 3.8–4.6 μM, eclipsing 5-fluorouracil. Docking placed **38** deep in both EGFR and VEGFR-2 pockets ($\Delta G \approx -11.18$ and −12.48 kcal mol^{-1}), engaging hinge cysteines CYS751 and CYS919. ADMET predictions showed high intestinal absorption (>90%), moderate protein binding, and absence of CNS penetration, though CYP450 (including CYP2C19) inhibition and potential hepatotoxicity were noted, alongside compliance with major drug-likeness filters.

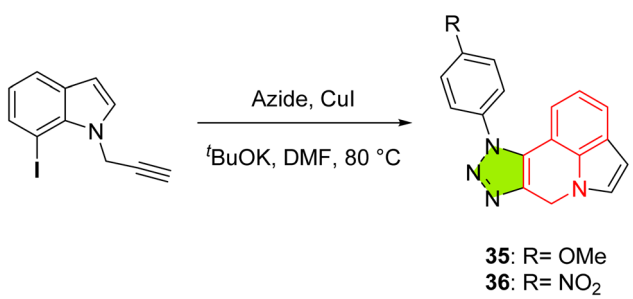

Scheme 20 Synthesis of 1,2,3-triazole hybrids **35** and **36**.

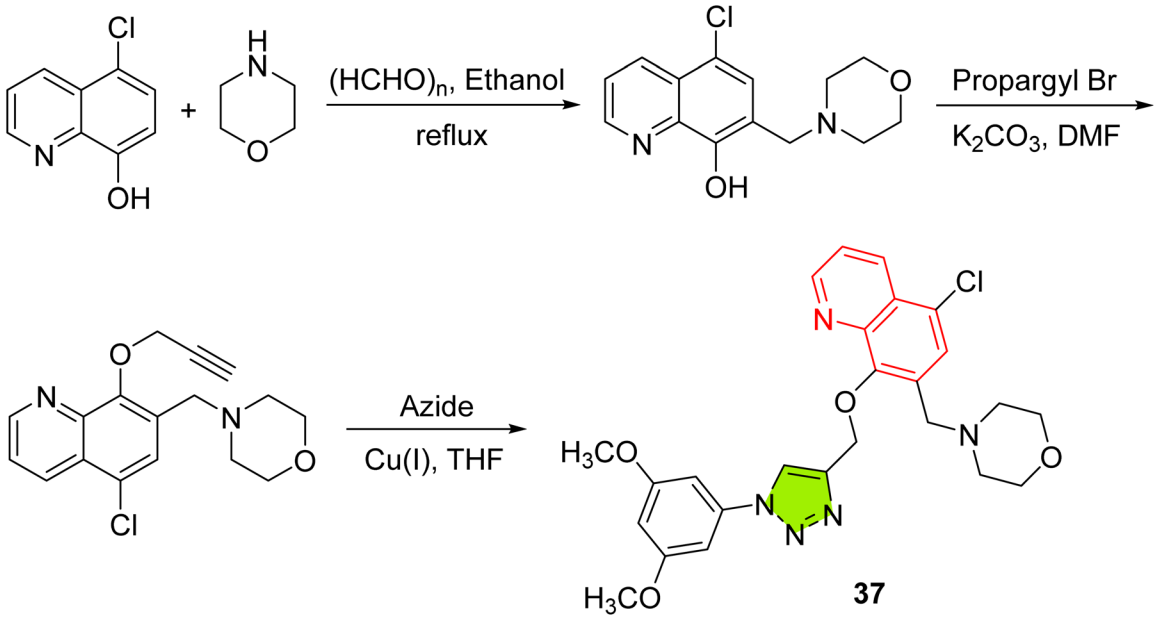

Scheme 21 Synthesis of 1,2,3-triazole hybrid **37**.

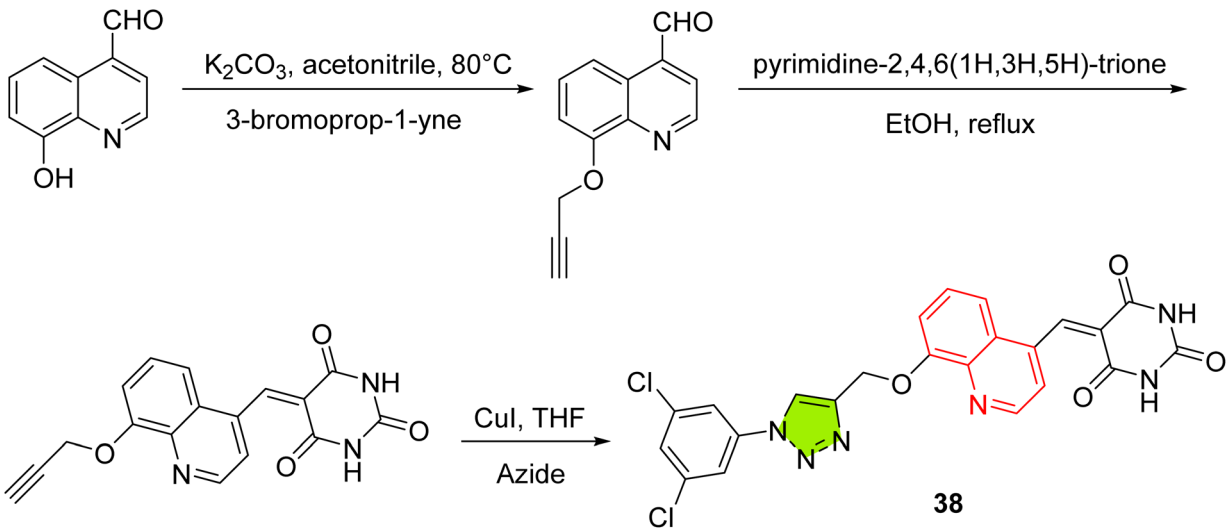

Scheme 22 Synthesis of 1,2,3-triazole hybrid **38**.

In a parallel design strategy, El-Sheref *et al.* crafted 4-(1,2,3-triazol-1-yl)quinolin-2(1*H*)-ones in good to excellent yields of 71–90% to exploit apoptosis pathways alongside kinase inhibition (Scheme 23).[88] These results indicate a consistently productive synthesis with good reproducibility across structural variations, supporting further medicinal chemistry exploration. Their standout compound, **39**, exhibited GI_{50} = 22 nM across Panc-1, MCF-7, HT-29, and A-549 cells—surpassing erlotinib (33 nM). Biochemical assays showed **39** inhibited EGFR (IC_{50} = 57 nM), $BRAF^{V600E}$ (68 nM), and the resistant $EGFR^{T790M}$ mutant (8.40 nM, *versus* osimertinib's 8.00 nM). In normal MCF-10A epithelial cells, **39** maintained 93% viability at 50 μM, underscoring its excellent selectivity for cancer cells. Mechanistically, **39** triggered robust apoptosis: caspase-3 rose to 715 pg mL^{-1}, caspase-8 to 2.35 ng mL^{-1}, and Bax to 336 pg mL^{-1}, while Bcl-2 fell to 0.60 ng mL^{-1}. Its antioxidant capacity (73.5% DPPH scavenging at 10 μM) further highlights its multifunctional anticancer profile.

5.5. Benzimidazole-1,2,3-triazole hybrids

Benzimidazole-1,2,3-triazole hybrids have emerged as sub-micromolar EGFR inhibitors demonstrating potent cytotoxic activity against different cancer cell lines. In one series, Pinnoju *et al.* designed benzimidazole–piperazine–triazole conjugates as EGFR-targeted breast cancer agents, synthesized in synthetically manageable yields between 63% and 82%, suggesting reliable conversion with no major scalability concerns (Scheme 24).[89] Their lead, **40**, combined sub-micromolar EGFR

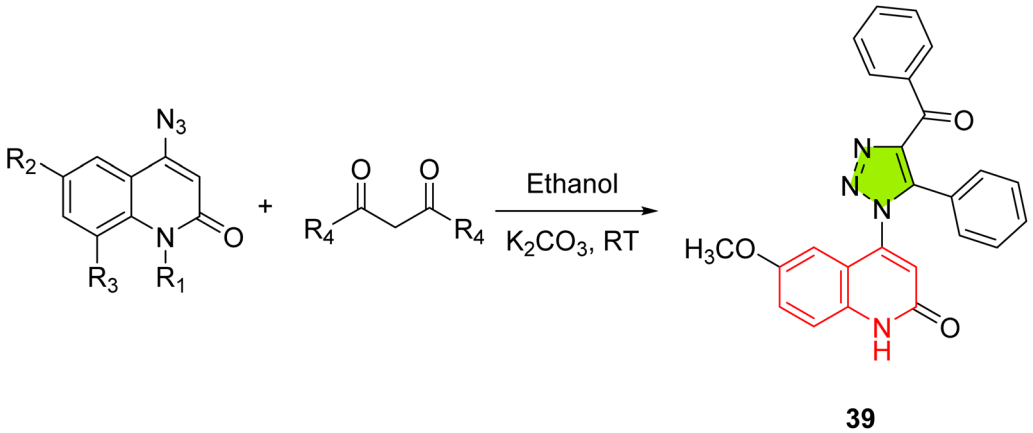

39

Scheme 23 Synthesis of 1,2,3-triazole hybrid **39**.

inhibition (IC_{50} = 0.19 μM, >2× more potent than erlotinib's 0.40 μM) with superior cytotoxicity in MDA-MB-231 (IC_{50} = 2.02 μg mL^{-1}) and MCF-7 (3.03 μg mL^{-1}) cells *versus* erlotinib (7.48 and 4.57 μg mL^{-1}). Docking into EGFR (PDB 4HJO) rationalized these results: **40** formed two hydrogen bonds with Met769 (ΔG = −10.33 kcal mol^{-1}, $K_i \approx$ 26.7 nM), underscoring how the piperazine–triazole extension enhances both affinity and cell-based potency while retaining drug-like properties.

Ahmed *et al.* expanded the series by exploring alternative benzimidazole–triazole hybrids in yields ranging from poor to excellent (20–94%).[52] While several derivatives were obtained efficiently, the lower-yielding reactions suggest scope for procedural optimization, especially for sensitive or electronically deactivated aryl substituents. Despite this, they identified **41** (Scheme 25) (GI_{50} = 25 nM *vs.* erlotinib's 33 nM in A-549, MCF-7, Panc-1, HT-29) and **42** (Scheme 26) (GI_{50} = 29 nM) as nanomolar EGFR inhibitors (IC_{50} = 73 ± 4 and 78 ± 5 nM, respectively). Both **41** and **42** exhibited minimal cytotoxicity in normal MCF-10A mammary epithelial cells, maintaining nearly 90% viability at 50 μM and highlighting their selectivity toward cancer cells. They also triggered marked apoptosis in MCF-7 cells—**41** upregulated caspase-3 by 12-fold, caspase-8 by 19-fold, and Bax by 36-fold while suppressing Bcl-2 by sevenfold; **42** showed similar trends. Docking highlighted key interactions with Met769, Thr766, and Leu694, and *in silico* ADMET projected good oral bioavailability and safety, although **41** carried AMES toxicity risk and **42** mild hepatotoxicity.

In a further expansion of the benzimidazole–triazole motif, Barothu *et al.* synthesized a series of 2-[2,4-bis-(1-phenyl-1*H*-[1,2,3]triazol-4-ylmethoxy)phenyl]-1*H*-benzimidazole derivatives in good yields of 60–75%, which are adequate for SAR studies but may benefit from optimization for large-scale access these compounds were evaluated for their broad-spectrum bioactivity (Scheme 27).[90] Their lead, **43**, bearing a 3-fluorophenyl substituent on the triazole, displayed potent cytotoxicity in MCF-7 (IC_{50} = 2.62 μM), PC-3 (3.87 μM), and HeLa (3.23 μM) cell lines, on par with doxorubicin. Docking into EGFR (PDB: 3W33) rationalized these results, with **43** and its analogue **44** achieving binding energies of −12.2 and −12.1 kcal mol^{-1}, respectively, compared to doxorubicin's −10.2 kcal mol^{-1}. Beyond oncology, **43** also inhibited key bacterial and fungal strains at levels comparable to streptomycin and amphotericin B, underscoring the versatility of benzimidazole–triazole hybrids as dual anticancer and antimicrobial agents.

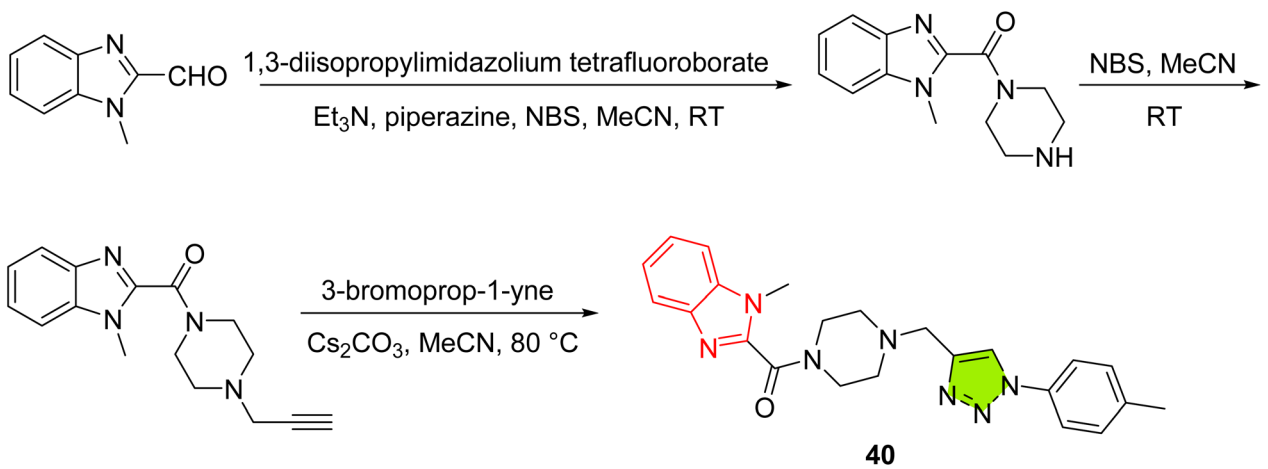

40

Scheme 24 Synthesis of 1,2,3-triazole hybrid **40**.

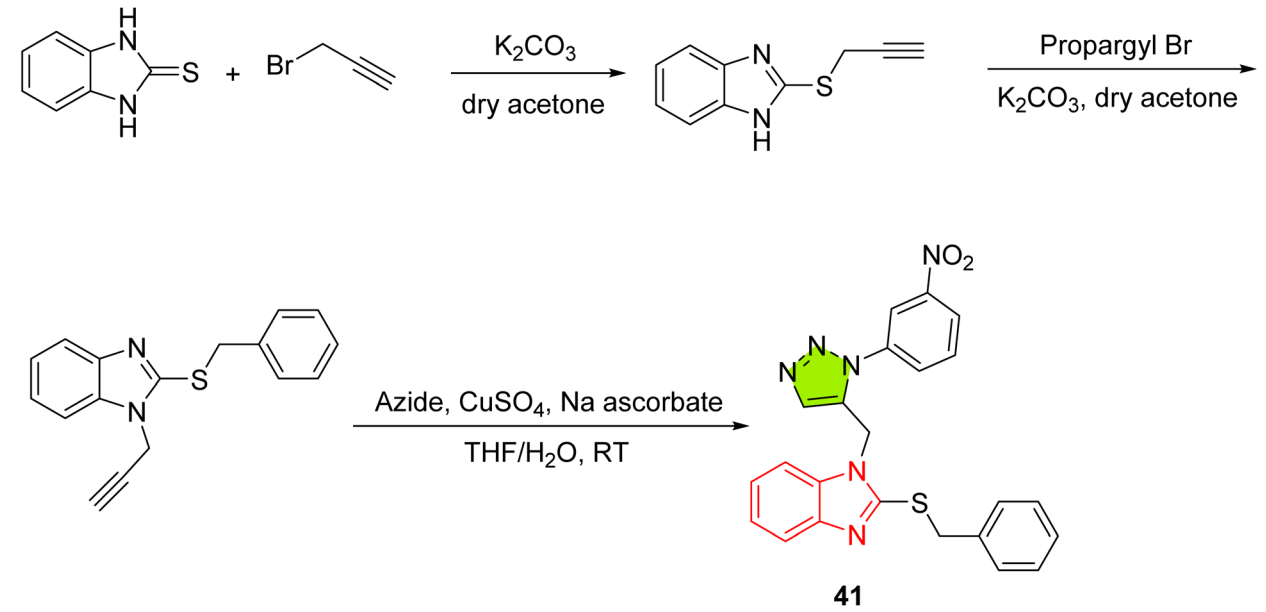

Scheme 25 Synthesis of 1,2,3-triazole hybrid **41**.

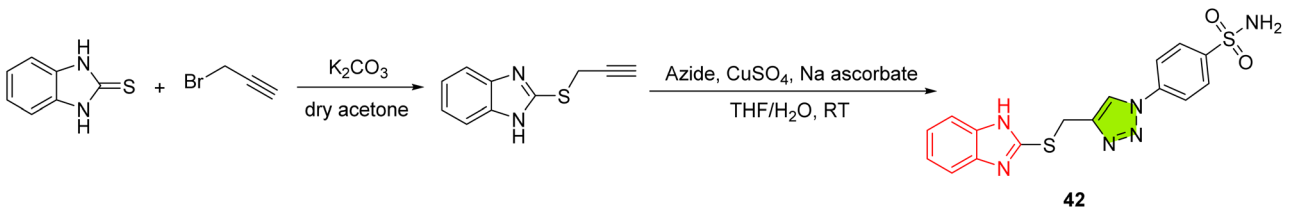

Scheme 26 Synthesis of 1,2,3-triazole hybrid **42**.

5.6. Indole-1,2,3-triazole hybrids

In recent studies, several indole–triazole hybrids have shown notable potential as EGFR inhibitors. Velidandla *et al.* presented indole-1,3,4-oxadiazole-sulfonyl triazoles bearing varied aryl groups in highly reproducible yields of 72–88%, indicating a well-optimized synthesis suitable for parallel library generation (Scheme 28).[91] Notably, **45** (3,5-dichlorophenyl) combined sub-5 μM cytotoxicity in MCF-7 (IC_{50} = 3.87 ± 0.21 μM) and A-549 (6.41 ± 0.35 μM) with potent EGFR inhibition (IC_{50} = 0.416 ± 0.036 μM), marginally surpassing erlotinib (0.422 ± 0.03 μM). Close behind, **46** (4-chloro-3,5-dimethoxyphenyl) showed similar efficacy (MCF-7/A-549 IC_{50}s

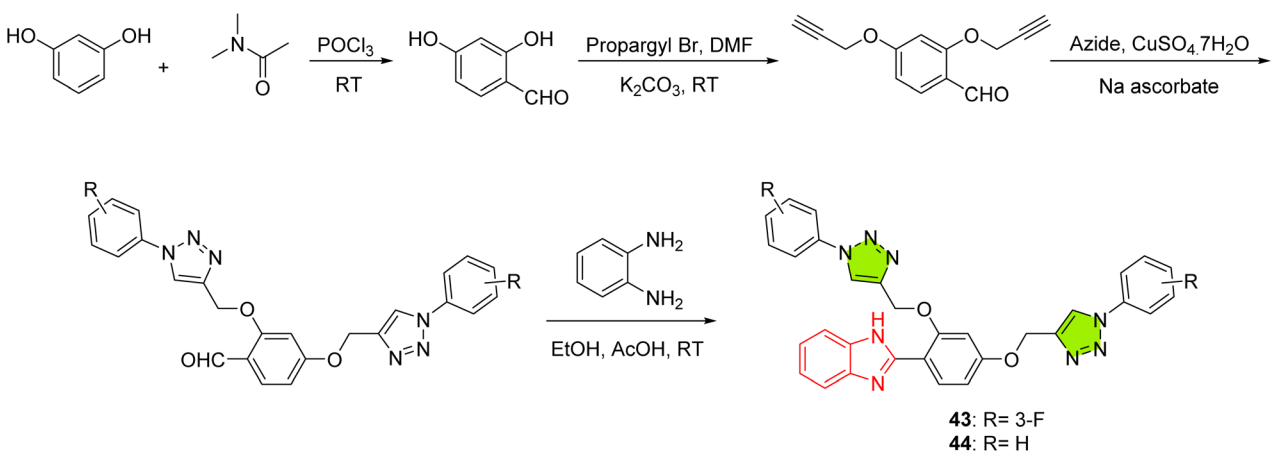

Scheme 27 Synthesis of 1,2,3-triazole hybrid **43** and **44**.

= 4.07 ± 0.28/7.39 ± 0.63 μM; EGFR IC_{50} = 0.453 ± 0.072 μM). Other analogues (**47**, **48**, **49**) retained sub-10 μM cytotoxicity and sub-micromolar EGFR activity, highlighting how subtle aryl modifications fine-tune enzymatic and cellular potency.

In a subsequent series, Perike *et al.* combined indole, thiazolidinedione, and triazole motifs in twelve hybrids obtained in good to very good yields of 75–82%, which reflect a highly practical synthetic route requiring no immediate optimization for compound accessibility (Scheme 29).[92] In this series, **50**, bearing a *meta*-acetylphenyl group on the triazole, outperformed doxorubicin across HePG2 (IC_{50} 4.43 μM), HCT-116 (4.46 μM), PC-3 (8.03 μM), and MCF-7 (3.18 μM). Docking against EGFR (PDB: 1M17; −10.1 kcal mol^{-1}) highlighted interactions with Cys773, Asp776, and Phe771, while CDK2 (PDB: 6GUE; −11.2 kcal mol^{-1}) and sorcin (PDB: 5MRA; −10.1 kcal mol^{-1}) scores underscored its multi-target profile.

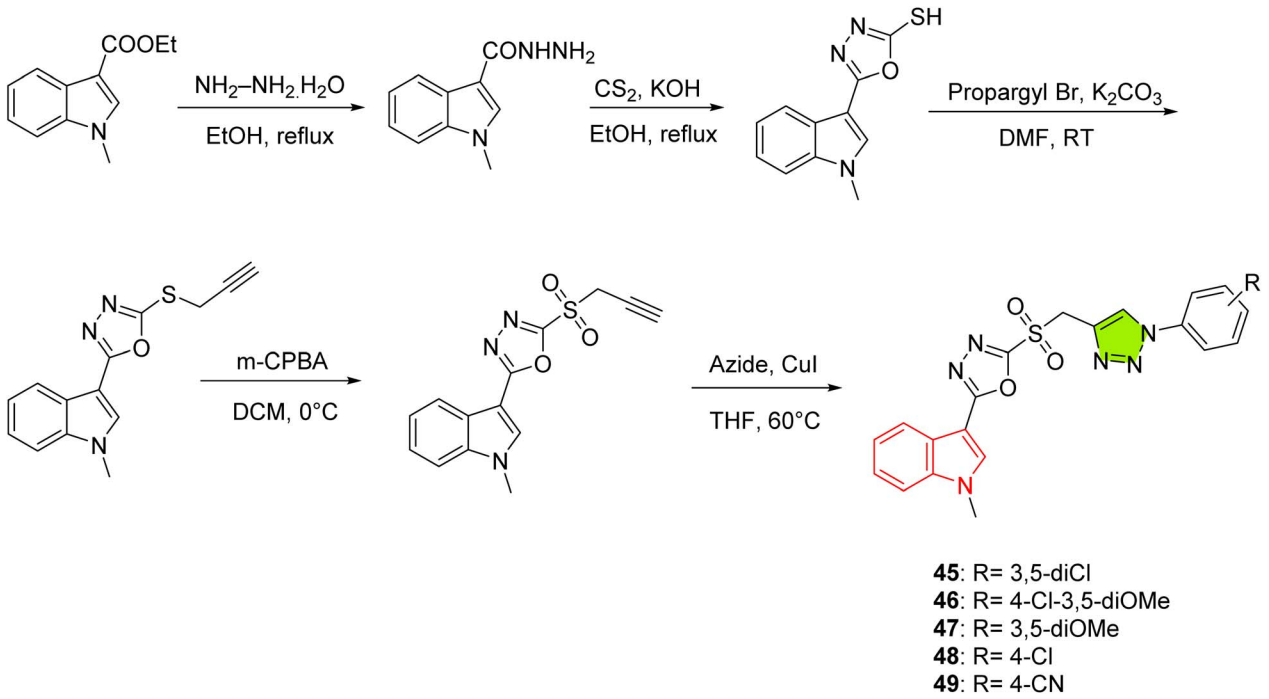

Scheme 28 Synthesis of 1,2,3-triazole hybrids **45–49**.

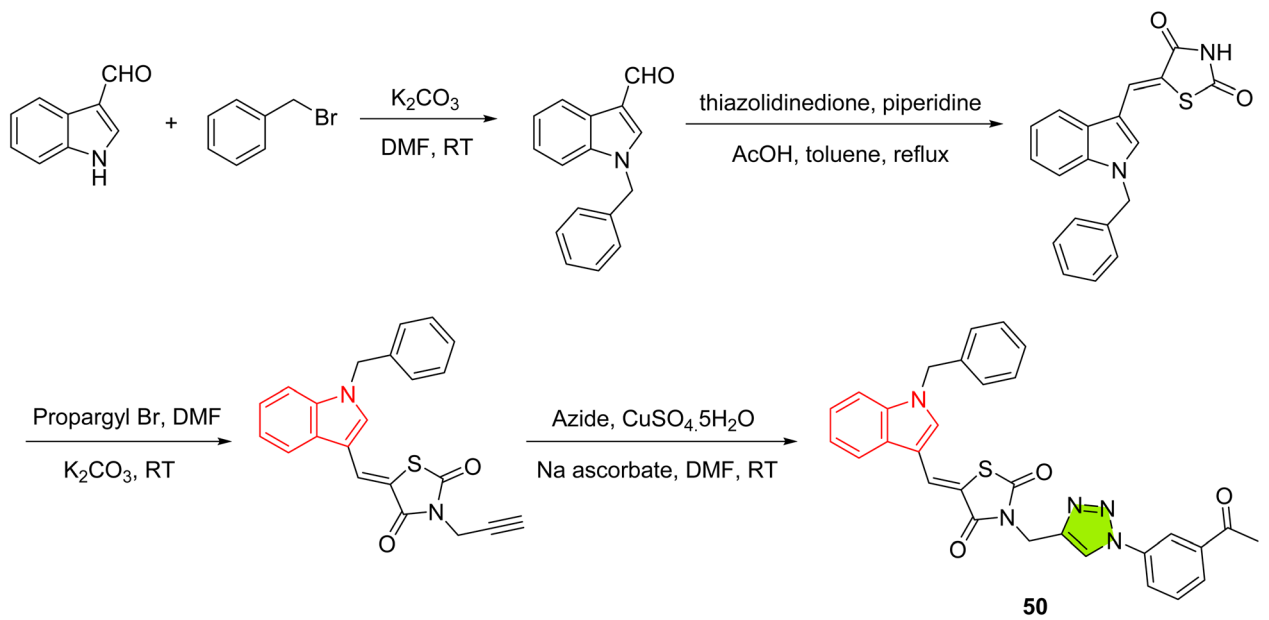

Scheme 29 Synthesis of 1,2,3-triazole hybrid **50**.

Importantly, **50** showed negligible toxicity on normal cells, indicating a favorable therapeutic window.

5.7. Oxindole/isatin-1,2,3-triazole hybrids

Oxindole- and isatin-based triazole hybrids have recently gained attention as dual inhibitors targeting EGFR and complementary oncogenic pathways. Building on this oxindole hybridization strategy, Nafie *et al.* introduced PARP-1 inhibition alongside EGFR targeting for liver cancer, synthesizing the series in consistently very good yields of 80–89%, indicating reliable and scalable synthesis for further development (Scheme 30).[93] Compound **51** exhibited the strongest HepG2 cytotoxicity (IC_{50} = 1.9 μM), while **52** combined PARP-1 IC_{50} = 2.01 nM with EGFR IC_{50} = 74.6 nM and spared normal THLE-2 cells (IC_{50} > 40 μM). Mechanistic assays showed **52** induced a 6.6-fold increase in apoptosis and upregulated p53, Bax, caspase-3, and caspase-9 (4.6–9.3-fold) while suppressing Bcl-2. Docking and dynamics confirmed stable binding at Arg817 (EGFR) and Asp766 (PARP-1).

Furthermore, Das *et al.* explored 1,2,3-triazole-indolin-2-one hybrids for broad-spectrum anticancer activity, obtained in moderate to good yields of 46–73%, which, although sufficient for early SAR exploration, may benefit from further reaction refinement to enhance overall efficiency (Scheme 31).[94] Compound **53** equaled melphalan in L1210 (IC_{50} = 3.0 ± 0.9 μM *vs.* 2.13 ± 0.02 μM) and CEM (1.5 ± 0.6 μM *vs.* 1.4 ± 0.4 μM) assays, and showed similar potency in HeLa (3.4 ± 0.6 μM). Against normal HEK293T embryonic kidney cells, **53** was less cytotoxic (7.5 μM), confirming its relative selectivity for malignant cells. Mechanistic studies confirmed that **53** activates intrinsic and extrinsic apoptotic pathways, arrests the cell cycle, and is non-genotoxic as demonstrated by assays excluding DNA damage or mutagenic potential. Docking into EGFR (PDB: 6P8Q) positioned **53** in the ATP pocket *via* H-bonds with Met793, π-sulfur interactions at Met790, and π-alkyl contacts with Leu788/Ala743. Favorable SwissADME predictions further validate **53** as a promising EGFR-targeted lead.

Shifting to an isatin core, Ghosh *et al.* employed MM/PBSA calculations to design a series of isatin-1,2,3-triazole hybrids bearing various alkyl and aryl substituents as dual EGFR/CDK2 inhibitors.[95] Compound **54** (Fig. 5), bearing a 4-methoxyphenyl group, achieved the best MM/PBSA EGFR binding energy (−23.25 ± 0.33 kcal mol^{-1}) *versus* −15.50 ± 0.28 kcal mol^{-1} for CDK2, demonstrating kinase selectivity. A 100 ns MD run gave an average RMSD of 1.8 Å with persistent H-bonds to Met769 and Asp831. DFT analysis revealed a HOMO–LUMO gap of 3.2 eV conducive to strong electronic interactions, and SwissADME predicted log *P* = 2.8, TPSA = 85 $Å^2$, full Lipinski/Ghose/Veber/Egan compliance, and low CYP450 risk. By contrast, **55** (3-chlorophenyl) (Fig. 5) bound CDK2 (−9.55 ± 0.34 kcal mol^{-1}) and EGFR (−18.09 ± 1.13 kcal mol^{-1}) with slightly higher MD RMSD (2.3 Å), suggesting a broader kinase profile.

5.8. Imidazole-1,2,3-triazole hybrids

Imidazole–triazole hybrids have recently emerged as potential EGFR inhibitors with promising antiproliferative profiles. Alluru *et al.* synthesized a series of 1*H*-naphtho[2,3-*d*] imidazole-4,9-dione-triazole hybrids and evaluated their cytotoxicity in MCF-7, HeLa, and A-549 cells (Scheme 32).[96] Their standout, **56** (4-nitrophenyl), delivered IC_{50} values of 1.53 ± 0.23

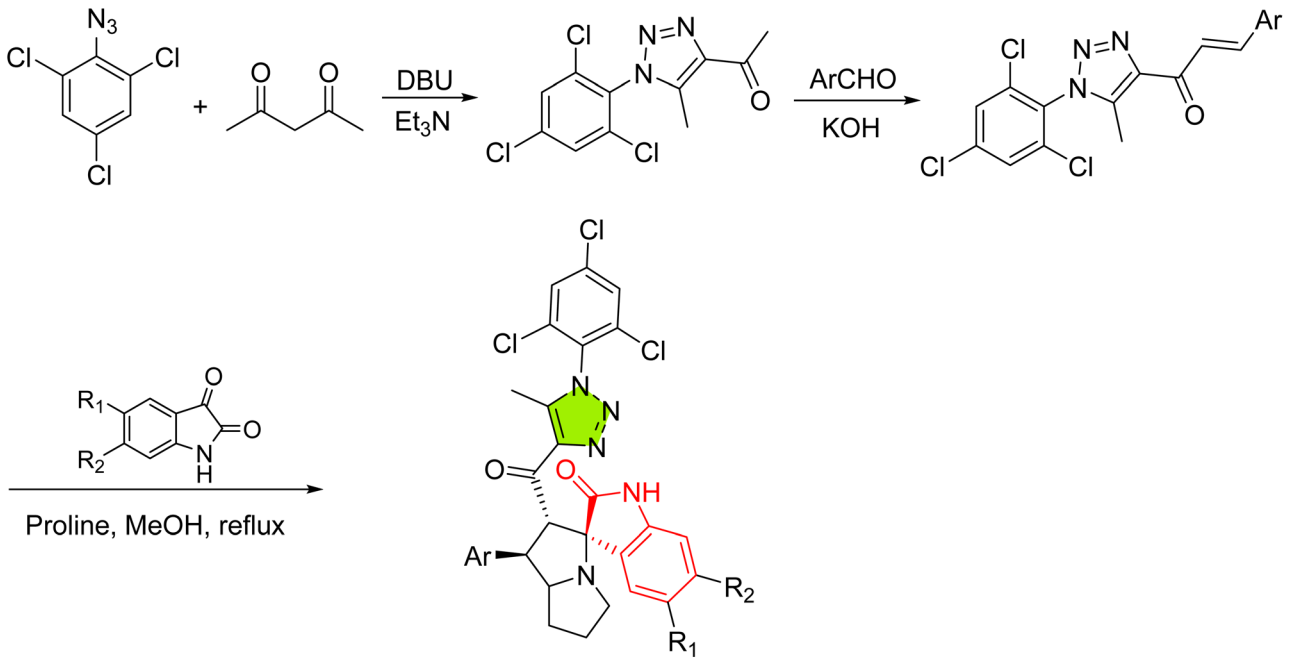

Scheme 30 Synthesis of 1,2,3-triazole hybrid **51** and **52**.

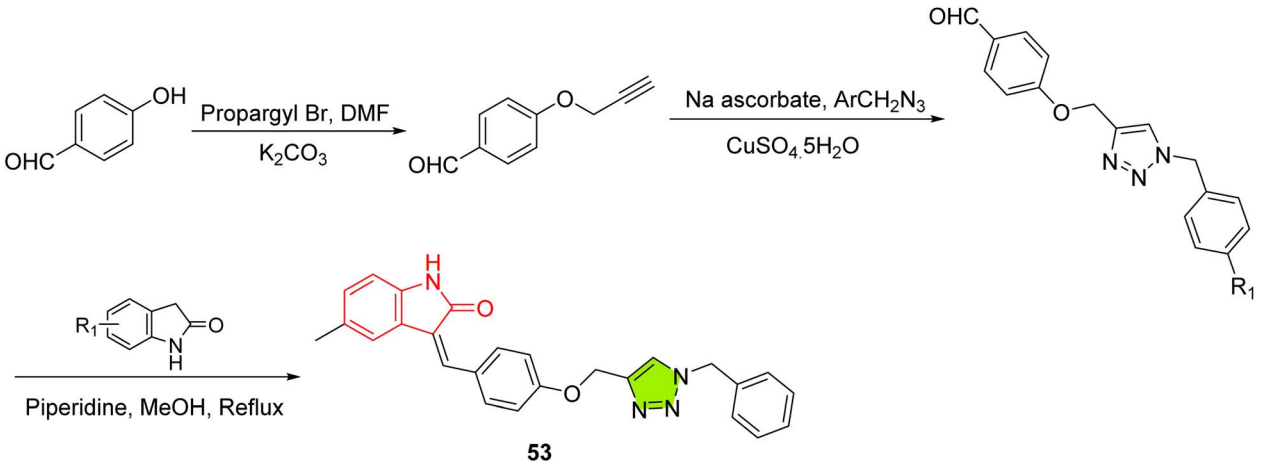

53

Scheme 31 Synthesis of 1,2,3-triazole hybrid **53**.

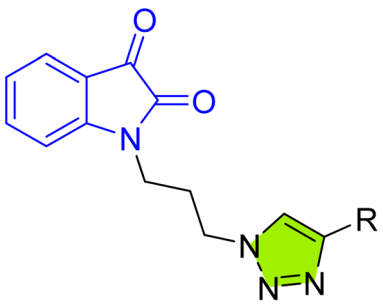

54: R= 4-Me-ph
55: R= phenanthren-9-yl

Fig. 5 Structures of 1,2,3-triazole hybrids **54** and **55**.

μM (MCF-7), 4.52 ± 0.65 μM (HeLa), and 1.45 ± 0.25 μM (A-549), outperforming doxorubicin (2.18, 5.51, and 2.02 μM). Docking into EGFR (PDB: 4HJO) confirmed its potency ($\Delta G = -11.86$ kcal mol; $K_i \approx 2.02$ nM), with key hydrogen bonds to Lys721, Lys704, and Lys692. Substituents at C-4—such as the bromo in **57** and isopropyl in **58**—also exceeded doxorubicin in two cell lines. In contrast, **59** (4-cyano) demonstrated comparable activity, illustrating how aryl variation finely tunes both kinase engagement and antiproliferative efficacy.

Johnpasha *et al.* explored fused imidazole-imidazo[1,2-*c*][1,2,3]triazoles *via* a PEG-400-mediated ultrasonic one-pot reaction, affording products in good yields of 65–79%, which suggests good overall efficiency under green chemistry conditions (Scheme 33).[97] Compounds **60** and **61** emerged with IC_{50} values of 4.02 ± 0.74 μM and 4.23 ± 0.65 μM against MCF-7, surpassing erlotinib (4.70 ± 0.11 μM), and matched or

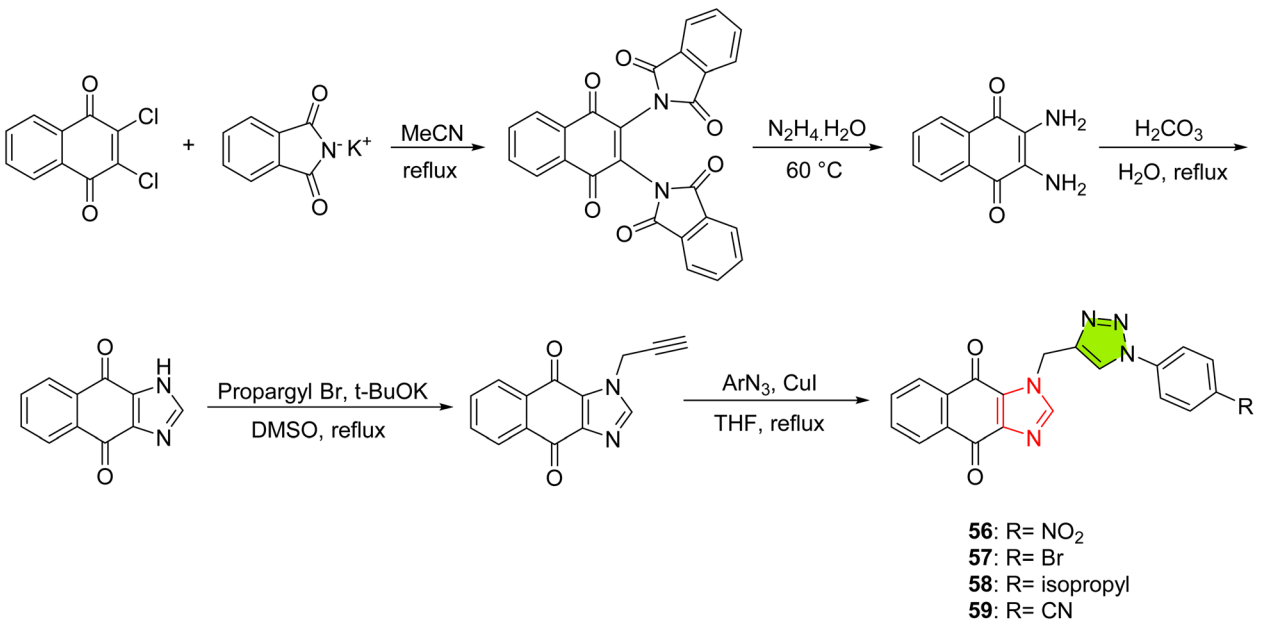

56: R= NO_2
57: R= Br
58: R= isopropyl
59: R= CN

Scheme 32 Synthesis of 1,2,3-triazole hybrids **56–59**.

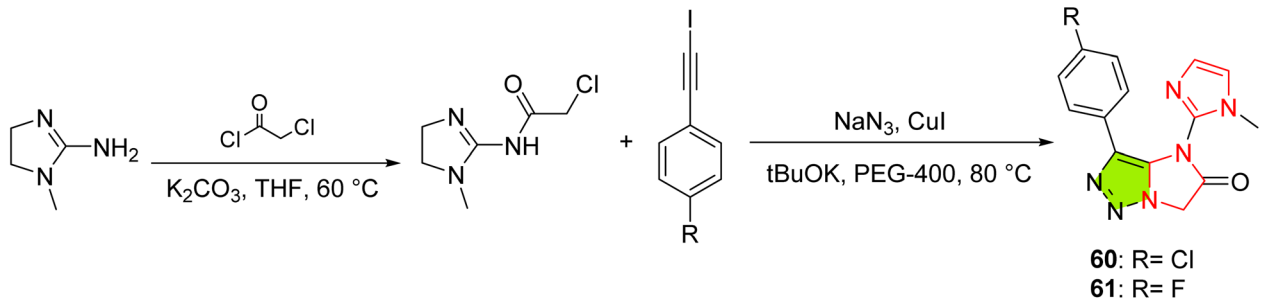

Scheme 33 Synthesis of 1,2,3-triazole hybrids **60** and **61**.

exceeded its EGFR inhibition ($IC_{50} = 0.38 \pm 0.02$ μM and 0.42 ± 0.05 μM *vs.* 0.42 ± 0.04 μM). On normal MCF-10A mammary epithelial cells, **60** and **61** showed reduced cytotoxicity with IC_{50} values of 13.68 ± 0.83 μM and 10.88 ± 0.93 μM, respectively, highlighting their selectivity toward malignant cells. Docking revealed that both form hydrogen bonds with Met769 and engage in π-alkyl and hydrophobic contacts mirroring erlotinib's EGFR ATP-site interactions, validating their capacity to recapitulate key kinase-binding motifs.

Samala *et al.* broadened the scope by synthesizing a series of fused coumarine-imidazo[1,2-*c*][1,2,3]triazoles in very good yields (Scheme 34).[98] The lead, **62**, displayed an EGFR IC_{50} of 0.367 ± 0.02 μM—outpacing erlotinib (0.460 ± 0.06 μM)—and cytotoxicity in A-549 cells ($IC_{50} = 3.54 \pm 0.33$ μM). Meanwhile, **63** and **64** were most active in MCF-7 (3.36 ± 0.13 and 4.06 ± 0.18 μM *vs.* 4.25 ± 0.08 μM for erlotinib). Docking scores for top analogues as EGFR inhibitors were below −9.0 kcal mol^{-1}, with **65** leading at −9.75 kcal mol^{-1} *via* an H-bond to Lys721. *In silico* ADMET predicted high intestinal absorption, compliance with Lipinski, Veber, Egan, and Muegge rules, absence of BBB penetration, and manageable hERG II and hepatotoxicity risks alongside favorable solubility and pharmacokinetics.

5.9. Oxadiazole-1,2,3-triazole hybrids

Recent efforts have explored oxadiazole–triazole conjugates as scaffolds capable of simultaneously modulating EGFR and parallel oncogenic pathways. Mahmoud *et al.* designed a series of 1,2,3-triazole/1,2,4-oxadiazole conjugates in moderate to very good yields of 46–84%—reflecting variable reaction efficiency likely influenced by electronic effects of the substituents—to achieve dual inhibition of EGFR and VEGFR-2 (Scheme 35).[99] Their standout compound, **66**, bearing a 3,4,5-trimethoxyphenyl group, delivered a GI_{50} of 28 nM across A-549, MCF-7, Panc-1, and HT-29 cells, surpassing erlotinib (33 nM). It inhibited EGFR with an IC_{50} of 76 ± 6 nM and VEGFR-2 at 2.40 ± 0.02 nM, and drove apoptosis by raising caspase-3 (587 pg mL^{-1}), caspase-8 (2.55 ng mL^{-1}), and Bax (362 pg mL^{-1}) while lowering Bcl-2 to 0.60 ng mL^{-1}. Analogues **67** and **68** showed similarly potent dual activity ($GI_{50} = 32$–35 nM; EGFR $IC_{50} = 82$–89 nM; VEGFR-2 $IC_{50} = 3.80$–4.70 nM). Docking studies revealed that **66** mimics a DFG-in conformation in EGFR and a DFG-out conformation in VEGFR-2, suggesting a hybrid type I/II inhibition mechanism at both ATP sites.

In a related study, Ayoup *et al.* synthesized a series of 1,2,4-oxadiazole-triazole hybrids in yields ranging from 61% to 87%, which are generally acceptable for this scaffold, though some reactions may benefit from optimization to enhance overall efficiency (Schemes 36 and 37).[100] Designed to target the EGFR–PI3K–AKT–mTOR signaling axis in lung (A549) and colon (Caco-2) cancer models, the series yielded several biologically active candidates. Compound **69** (Scheme 36) led in A549 with an IC_{50} of 3.56 μM, simultaneously reducing EGFR mRNA to 23% of

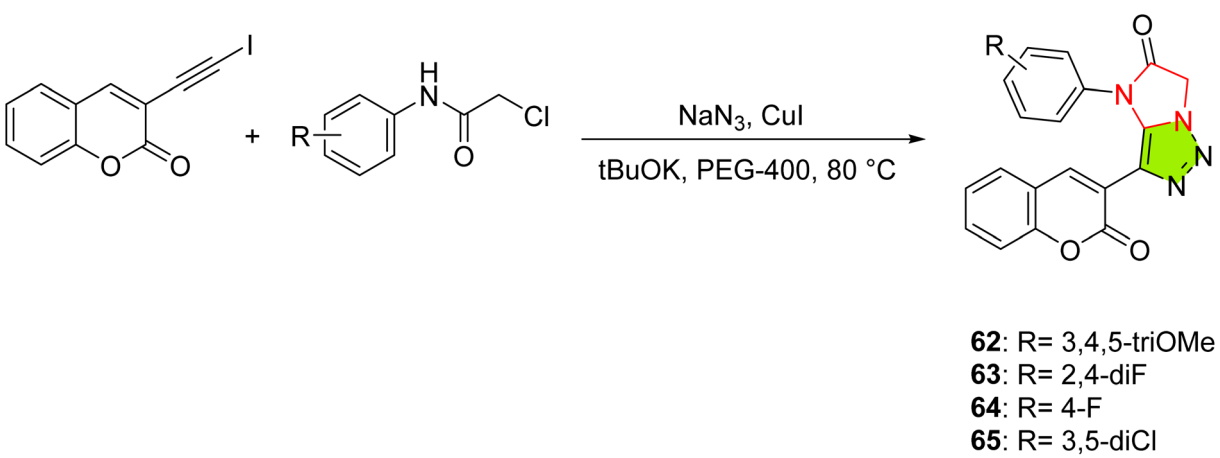

Scheme 34 Synthesis of 1,2,3-triazole hybrids **62**–**65**.

control, while **70** (IC_{50} = 12.73 μM) induced p53 expression by 6.5-fold. In Caco-2 cells, **71** (Scheme 37) (16.38 μM) and **70** (14.09 μM) showed the greatest growth inhibition. Docking against EGFR (PDB: 2ITY; −6.85 to −7.91 kcal mol^{-1}) highlighted interactions with Met793 and key hydrophobic pockets. All top hits demonstrated high gastrointestinal absorption, zero Lipinski or Veber violations, and minimal blood–brain barrier penetration, underscoring their potential as selective, low-CNS-risk anticancer agents.

Shifting focus to 1,3,4-oxadiazoles, Mahmoud *et al.* explored a series of 1,3,4-oxadiazole–1,2,3-triazole conjugates across Panc-1, MCF-7, HT-29, and A-549 cells, synthesized in excellent yields of 92–94% indicating a highly efficient and reproducible synthetic route with minimal byproduct formation (Scheme 38).[101] Among these, **72**, which incorporates a 4-chlorophenyl-thiazole moiety, matched erlotinib in growth inhibition (GI_{50} = 0.23 μM *vs.* 0.06 μM) and blocked EGFR with an IC_{50} of 0.11 μM. Compound **72** showed negligible impact on normal MCF-10A cells, retaining 86% viability at 50 μM and underscoring its cancer selectivity. Mechanistic assays linked **72**'s efficacy to intrinsic apoptosis—caspase cascades activation, a 14-fold surge in cytochrome c release, and a dramatic shift in the Bax/Bcl-2 ratio, while flow cytometry revealed that 41.5% of Panc-1 cells accumulated in G_1. Computational docking (ΔG = −10.65 kcal mol^{-1}) mirrored erlotinib's binding pose, and ADME predictions confirmed a favorable oral profile.

5.10. Thiadiazine-1,2,3-triazole hybrids

Some triazolo–thiadiazine derivatives have demonstrated selective EGFR inhibition alongside potent antiproliferative

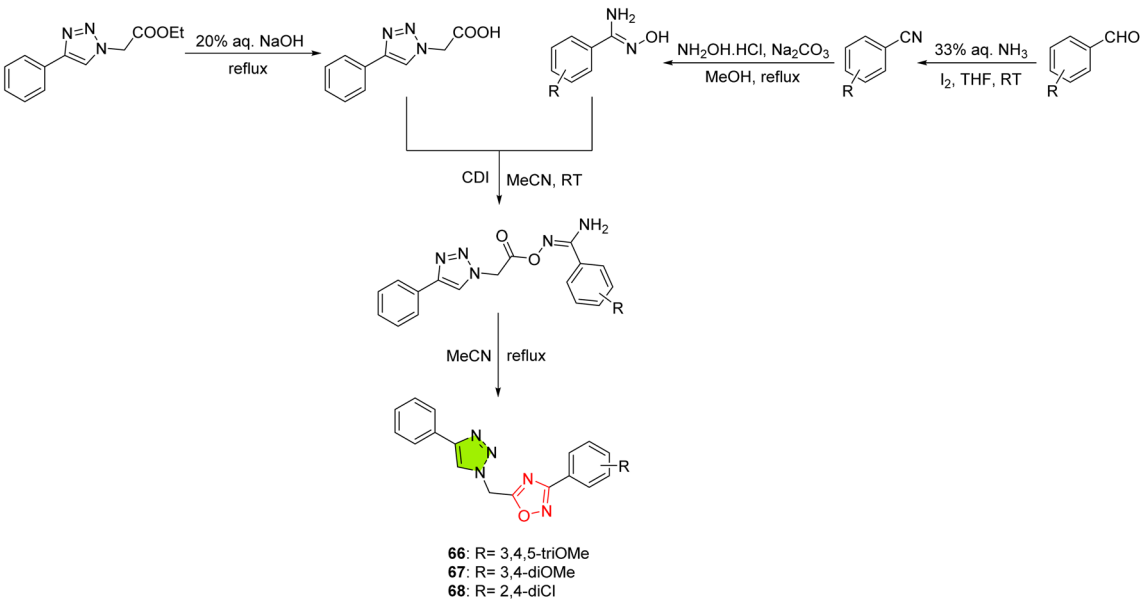

Scheme 35 Synthesis of 1,2,3-triazole hybrids **66**–**68**.

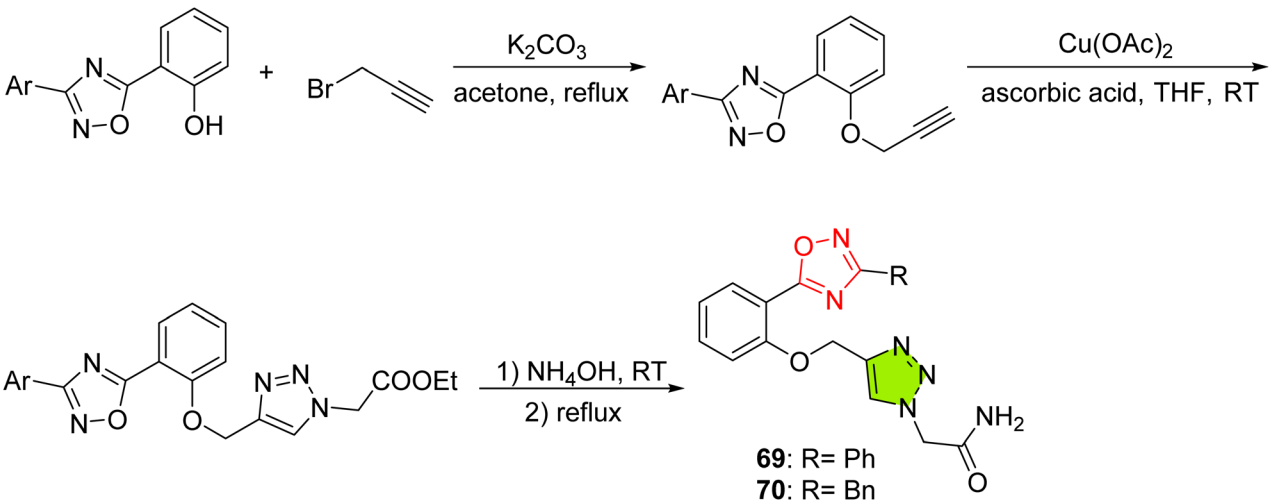

Scheme 36 Synthesis of 1,2,3-triazole hybrids **69** and **70**.

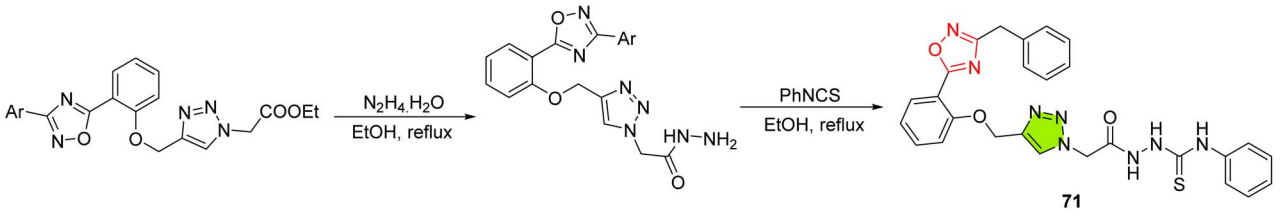

Scheme 37 Synthesis of 1,2,3-triazole hybrid **71**.

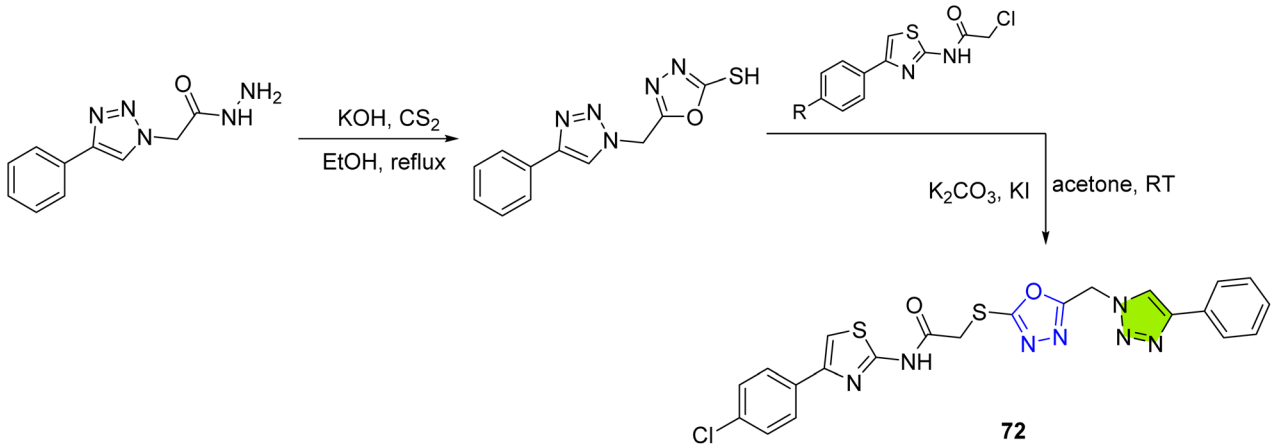

Scheme 38 Synthesis of 1,2,3-triazole hybrid **72**.

effects in breast cancer models. Telukuntla *et al.* synthesized a series of phenyl-linked triazolo[3,4-*b*][1,3,4]thiadiazines in good yields of 68–75% (Scheme 39), which are acceptable for initial lead discovery but may benefit from further optimization for scalability. These derivatives were evaluated their anti-proliferative effects in MCF-7 and MDA-MB-231 breast cancer models as well as their EGFR inhibition.[102] Compounds **73** (3,5-dichlorophenyl) and **74** (4-fluorophenyl) emerged as the most efficacious, achieving IC_{50} values of 3.86 ± 0.51 μM and 4.10 ± 0.71 μM in MCF-7 cells, and 6.98 ± 0.61 μM and 8.01 ± 0.69 μM in MDA-MB-231 cells, each surpassing erlotinib. Against normal MCF-10A epithelial cells, **73** and **74** showed markedly reduced toxicity with IC_{50} values of 41.26 ± 1.82 μM and 39.84 ± 1.65 μM, respectively, underscoring their favorable selectivity indices. In enzymatic assays, **73** inhibited EGFR with an IC_{50} of 0.312 ± 0.02 μM, marginally more potent than erlotinib (0.421 ± 0.03 μM), while **74** followed closely at 0.419 ± 0.05 μM. Molecular docking into the EGFR kinase domain (PDB: 4HJO) revealed conserved hydrogen bonds to Asn818 and Cys773, complemented by hydrophobic interactions of the halogenated phenyl rings.

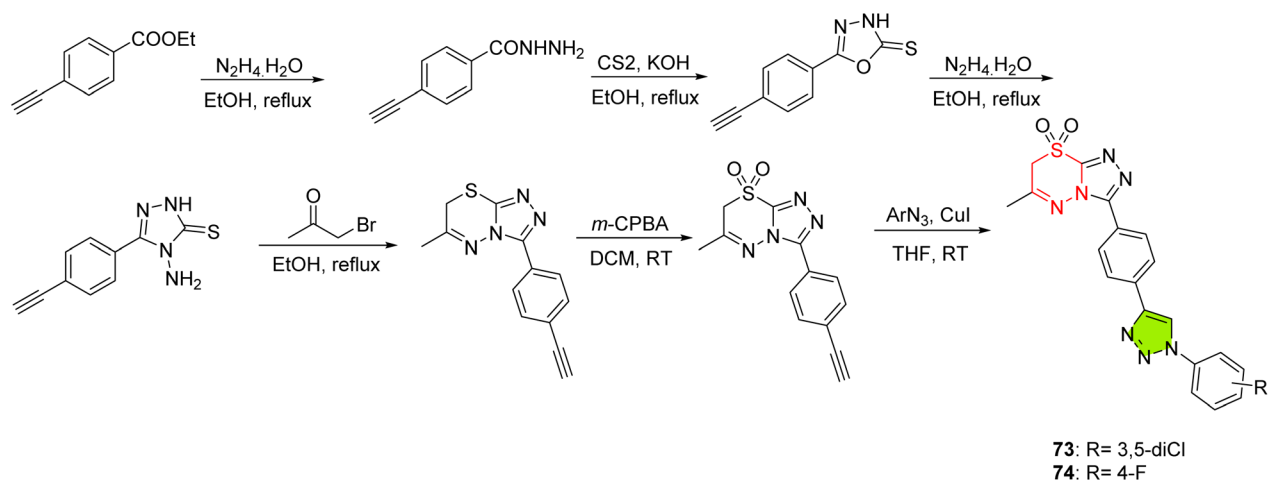

Scheme 39 Synthesis of 1,2,3-triazole hybrids **73** and **74**.

Building on this work, Chirra *et al.* employed a PEG-400-mediated ultrasonic one-pot protocol to access an expanded library of fused triazolo–thiadiazine–triazole hybrids, afforded in good yields of 66–79% (Scheme 40).[103] These yields represent efficient transformations using green chemistry principles, though the lower end may be improved through tuning of ultrasonic parameters or substrate scope. Among them, compound **75** exhibited superior cytotoxicity ($IC_{50} = 3.52 \pm 0.12$ μM in MCF-7; 5.52 ± 0.23 μM in MDA-MB-231), and **76** (bearing an alternative aryl substitution) showed comparable potency (4.09 ± 0.25 μM and 6.09 ± 0.58 μM, respectively). EGFR inhibition assays confirmed **77** as the most potent enzyme inhibitor ($IC_{50} = 0.38 \pm 0.02$ μM) with **76** at 0.41 ± 0.05 μM (erlotinib = 0.42 ± 0.02 μM). Docking studies highlighted interactions with Met769 and surrounding hinge residues that closely mimic those of clinical EGFR inhibitors—in silico ADMET analysis projected acceptable solubility, minimal hERG liability, and favorable pharmacokinetic parameters for these thiadiazine-containing hybrids.

5.11. Natural-product-inspired hybrids

Drawing on the inherent bioactivity of monoterpenoid phenols, researchers have fused 1,2,3-triazole linkers to natural-product cores, such as carvacrol and thymol, to create multi-target anticancer agents that engage kinase, apoptosis, and cytoskeletal pathways. Enneiymy *et al.* harnessed the carvacrol scaffold to assemble a series of triazole hybrids, obtained in good to very good yields of 66–88%,[104] which are synthetically efficient and generally consistent across the series. This culminated in compound **78** (Scheme 41) as the lead multitarget inhibitor. **78** exhibited sub-nanomolar affinity for EGFR ($K_i = 1.87$ nM) and $BRAF^{V600E}$ ($K_i = 1.03$ nM), and nanomolar activity against tubulin polymerization ($K_i = 39.67$ nM)—dramatically outperforming encorafenib (EGFR $K_i = 580.74$ nM), sorafenib ($BRAF^{V600E}$ $K_i = 6920$ nM), and colchicine (tubulin $K_i = 708.73$ nM). Molecular docking into EGFR's ATP site revealed key interactions with Lys745 and Met766, while parallel simulations in $BRAF^{V600E}$ and tubulin confirmed stable contacts with Asp593/Trp530 and Tyr224/Gly143, respectively. A 100-ns molecular dynamics trajectory showed low RMSD fluctuations. It maintained compact ligand–protein complexes, and *in silico* ADME profiling forecasted high oral bioavailability, non-mutagenicity, and favorable bioactivity scores, positioning **78** as a compelling candidate for further preclinical evaluation.

Riadi *et al.*[105] extended this strategy to a parathoxythymol core, generating triazole derivatives that simultaneously target EGFR and the anti-apoptotic protein Bcl-2, synthesized in good yields of 70–75% (Scheme 42).[106] Among these, compound **79** demonstrated the strongest *in silico* affinities (-28.8 kJ mol^{-1} for EGFR; -29.2 kJ mol^{-1} for Bcl-2), driven by multiple hydrogen bonds and hydrophobic contacts with Met769, Lys721, Leu820, and Asn11. Density functional theory calculations revealed a high dipole moment (260.4 D) and elevated polarizability, indicative of favorable reactivity. In 100-ns dynamics, the **79** – Bcl-2 complex maintained an RMSD around 1.7 Å with persistent hydrogen bonding. ADMET predictions further underscored **79**'s drug-likeness (TPSA = 86.47 $Å^2$; log *P* = 4.03), excellent intestinal absorption, blood–brain barrier permeability, and compliance with Lipinski's rule, alongside minimal toxicity flags. Importantly, solubility analysis predicted a log *S* of −4.76, indicating low aqueous solubility, a common feature of lipophilic drug-like molecules, which may necessitate formulation strategies to enhance bioavailability. These *in silico* data advocate for **79**'s progression into biological validation as a stable, multitarget anticancer agent.

5.12. Schiff-base & thiosemicarbazone hybrids

Integrating imine (Schiff-base) and thiosemicarbazone linkers into 1,2,3-triazole frameworks has yielded hybrids that combine potent EGFR inhibition with pronounced effects on cell cycle, apoptosis, and migration—key hallmarks for breast cancer therapeutics. Nawareg *et al.* prepared a series of

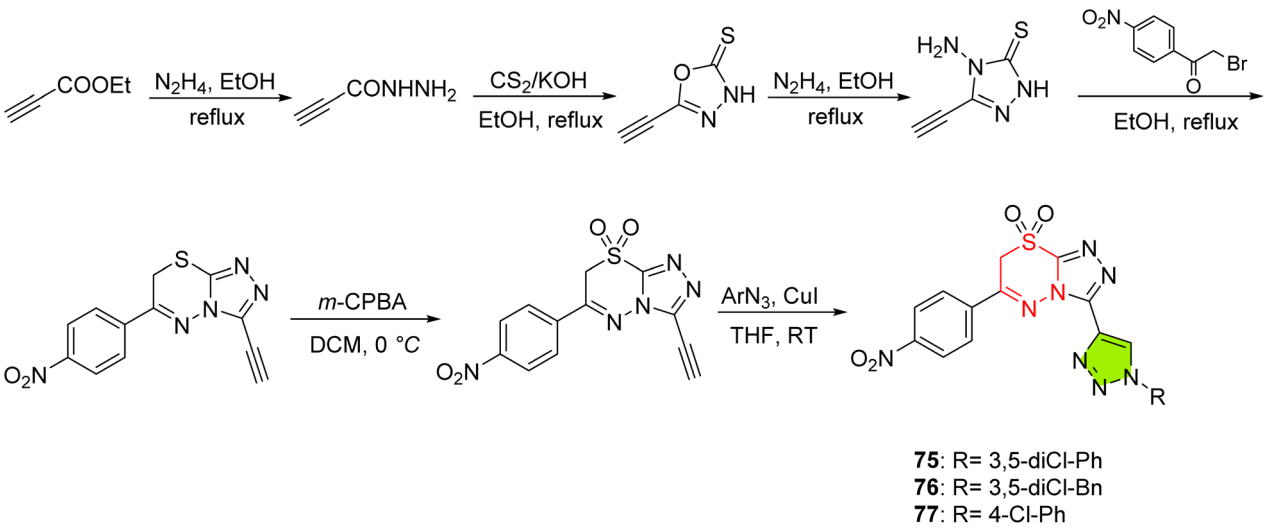

Scheme 40 Synthesis of 1,2,3-triazole hybrids **75–77**.

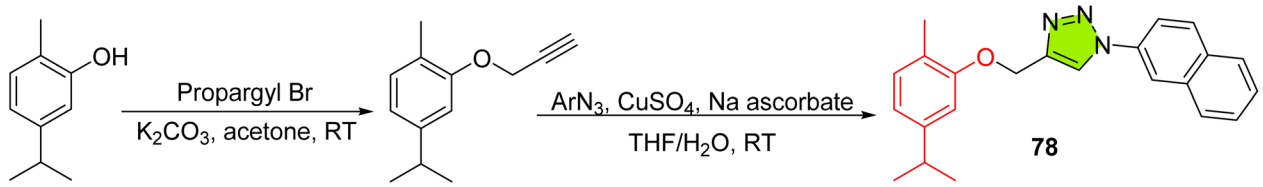

Scheme 41 Synthesis of 1,2,3-triazole hybrid **78**.

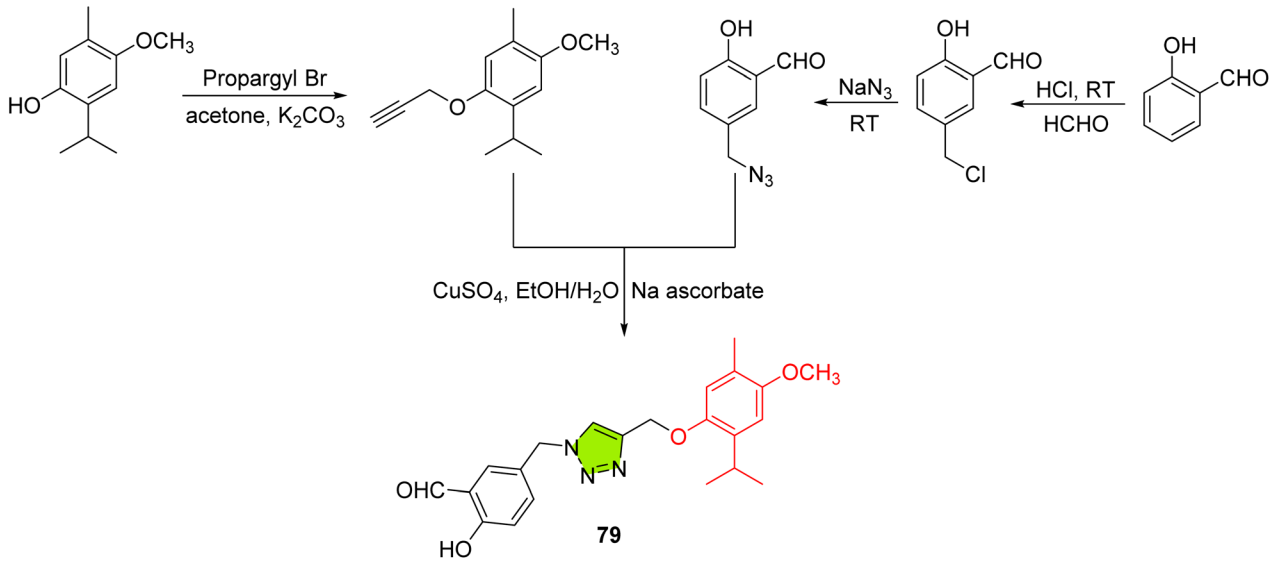

Scheme 42 Synthesis of 1,2,3-triazole hybrid **79**.

triazole-Schiff's base conjugates in moderate to very good yields of 57–85% (Scheme 43),[106] a range acceptable for lead development. Though some reactions may benefit from improved conversion. They identified **80** as leading EGFR inhibitor. Compound **80** blocked EGFR with an IC_{50} of 0.15 μM (gefitinib = 0.081 μM) and exhibited selective cytotoxicity in MCF-7 (IC_{50} = 15.63 μM) and MDA-MB-231 (18.01 μM) cells while showing markedly weaker activity against normal WI-38 fibroblasts (IC_{50} = 78.58 ± 3.5 μM) and MCF-10A epithelial cells (IC_{50} = 37.43 ± 1.26 μM), thereby confirming its cancer-selective profile. Mechanistically, **80** induced G_2/M arrest and elevated apoptotic populations by 48-fold, accompanied by Bax upregulation, Bcl-2 suppression, and activation of caspases-8 and -9. Molecular docking into EGFR's ATP pocket revealed hydrogen bonds to Lys745 and Gly719 and a binding energy of −7.23 kcal mol^{-1}. *In silico* ADMET profiling predicted favorable absorption, distribution, metabolism, and excretion parameters, underscoring **80**'s promise for further EGFR-targeted breast cancer studies.

Aljuhani *et al.* explored benzothiazole–triazole hybrids equipped with hydrazone or thiosemicarbazone linkers, synthesized in very good to excellent yields of 88–91% (Scheme 44),[107] indicating high synthetic efficiency. Compounds **81** and **82** displayed cytotoxicity against T47-D breast cancer cells (IC_{50} = 17 ± 1 and 13 ± 1 μM, respectively) and inhibited EGFR with IC_{50} values of 0.69 ± 0.01 μM (98.5% inhibition) and 1.16 ± 0.02 μM (96.8%), rivaling erlotinib (1.3 μM). Both hybrids were non-toxic to normal fibroblasts (IC_{50} > 500 μM). Docking studies highlighted key interactions with Met769 *via* the triazole ring and hydrophobic stabilization by the benzothiazole core, yielding binding energies of −29.48 kcal mol^{-1} (**8a**) and −27.27 kcal mol^{-1} (**8b**). Additionally, **81** impeded A549 cell migration, reducing wound closure by 92.4% at its IC_{50}—demonstrating dual EGFR inhibition and anti-migratory activity.

5.13. Drug-1,2,3-triazole hybrids

Building on approved EGFR tyrosine kinase inhibitors, researchers have hybridized 1,2,3-triazole moieties with existing drugs to enhance potency against wild-type and resistant EGFR, promote apoptosis, and overcome drug resistance. Gao *et al.* modified gefitinib by click-coupling a triazole linker to generate a novel hybrid series synthesized in moderate to very good yields of 47–85% (Scheme 45). While some reactions afforded moderate yields, the upper range reflects good synthetic efficiency for these triazole-based derivatives. This series was profiled in wild-type non-small cell lung cancer (NSCLC) lines[108] which resulted in compounds **83** and **84** emerging as the most active, with **83** inhibiting proliferation in NCI-H1299, A549, and NCI-H1437 cells at IC_{50} values of 3.94 ± 0.17, 3.16 ± 0.11, and 1.83 ± 0.13 μM, respectively; **84** showed comparable potency

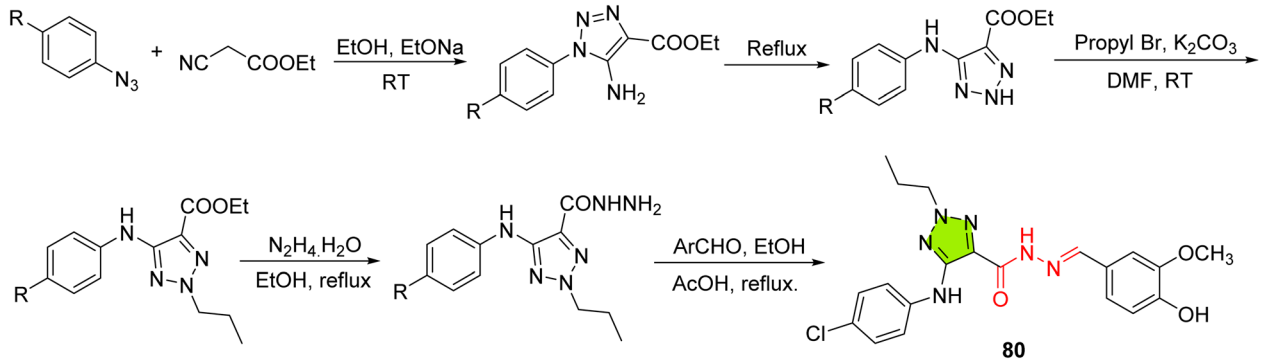

Scheme 43 Synthesis of 1,2,3-triazole hybrid **80**.

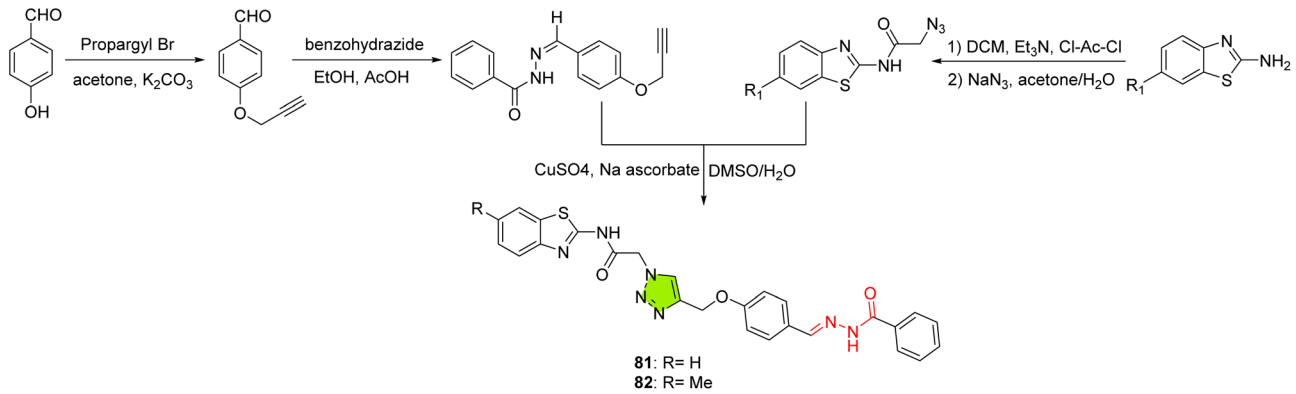

Scheme 44 Synthesis of 1,2,3-triazole hybrids **81** and **82**.

(3.84–1.69 μM) and both outperformed gefitinib (14.62–20.56 μM). Functional assays demonstrated that **83** and **84** suppressed colony formation, impaired wound-healing and transwell assays migration, and induced mitochondrial-pathway apoptosis in H1299 cells (up to 65.8% total apoptosis at 8 μM). Western blotting confirmed downregulation of Bcl-2, caspase-9, and MMP9 alongside cleaved caspase-3 and PARP activation. Toxicity studies revealed that both **83** and **84** exhibited much weaker cytotoxicity toward normal hepatocytes (L02) with IC_{50} values of 18.87 ± 1.03 and 17.68 ± 0.52 μM, respectively, and

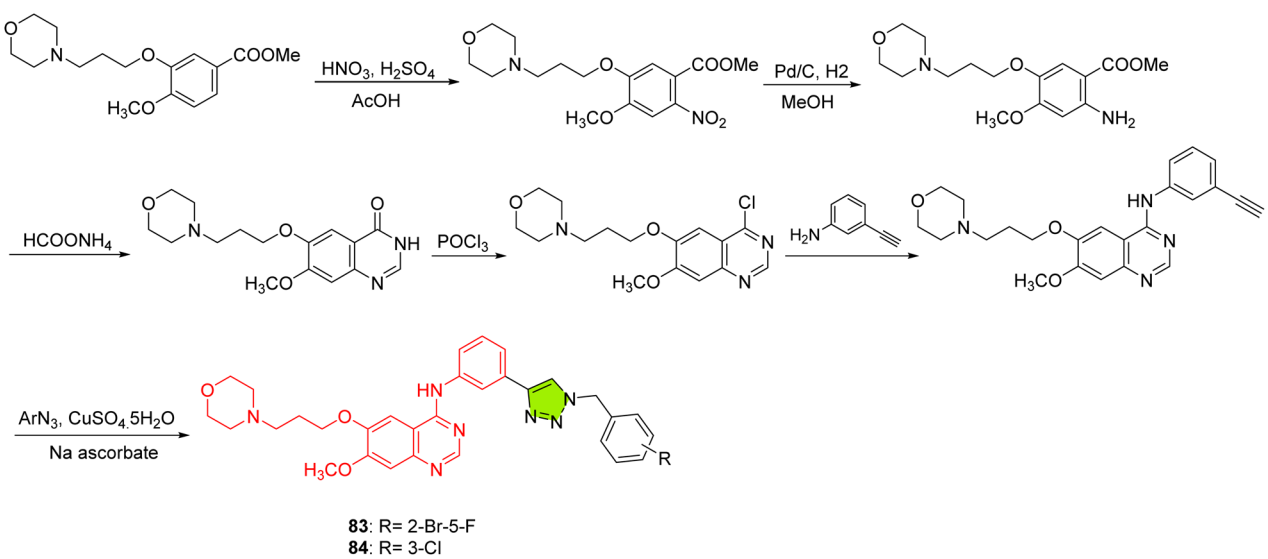

Scheme 45 Synthesis of 1,2,3-triazole hybrids **83** and **84**.

survival rates of 70–90% at 4 μM, underscoring their selectivity for cancer cells. Moreover, acute oral toxicity assessment in mice confirmed excellent safety: no deaths, no body weight loss, no pathological changes in organs, and normal serum ALT, AST, BUN, and creatinine levels were observed, indicating no hepatic or renal impairment. *In vivo*, **83** further demonstrated an excellent safety profile, with no adverse effects on organ histology or serum biochemistry.

Deng *et al.* applied a similar triazole-click strategy to erlotinib, synthesizing 14 analogues and evaluating them in HeLa cervical cancer cells (Scheme 46).[109] Compound **85** demonstrated the highest cytotoxicity (IC_{50} = 3.79 μM *vs.* erlotinib's 39.50 μM), while **86**, **87**, **88**, **89**, and **90** ranged from 4.16 to 8.21 μM. Notably, **89** and **88** induced up to 87.3% apoptosis and caused G_2/M cell-cycle arrest, with **88** also showing the strongest EGFR inhibition (IC_{50} = 1.76 μM; **89** = 13.01 μM; **86** = 49.39 μM). These multifunctional profiles highlight how triazole derivatization can drastically improve erlotinib's efficacy in non-lung cancer contexts.

Biegański *et al.* took a divergent approach by conjugating a ferrocenyl moiety to erlotinib *via* a methylene spacer, yielding five ferrocenyl-erlotinib hybrids in moderate to very good yields of 46–82% (Scheme 47) given the steric and redox-active nature of the ferrocenyl group.[110] Their lead, compound **91**, reduced viability in erlotinib-resistant NSCLC lines H1650 and H1975 to 14% and 19% at 20 μM, respectively—far exceeding erlotinib's effect. Mechanistic studies revealed that **91** generated two to three times more reactive oxygen species (ROS) than erlotinib; this ROS-mediated cytotoxicity was reversed by *N*-acetylcysteine, confirming its dependence on oxidative stress. Compound **91** also disrupted mitochondrial membrane potential, activated caspase-9 and caspase-3 (~2- to 3-fold increases), induced G_2/M arrest, and upregulated γH2AX, indicating DNA damage. Docking into the EGFR kinase domain (higher score than erlotinib) suggested that **91** retains canonical ATP-site interactions while adding a ROS-generating mechanism.

Meanwhile, Alsayad *et al.* explored metronidazole-derived triazoles by linking the antibiotic core to a 1,2,3-triazole, obtaining products in good yields of 61–68% (Scheme 48).[111] While these yields are acceptable for small-molecule synthesis, they may benefit from further optimization to enhance overall efficiency and scalability. Five analogues were tested in A549 lung cancer cells, among which compounds **92** and **93** showed the greatest antiproliferative effects (IC_{50} = 3.21 ± 1.21 μM and 4.10 ± 1.43 μM), whereas **94–96** were less active (9.06–12.67 μM). Docking against the EGFR kinase (PDB: 1M17) revealed that **93** achieved the strongest binding (−8.45 kcal mol^{-1}) through interactions with Met769, Lys721, and dual Cys773 residues; **92** followed (−8.16 kcal mol^{-1}) by engaging Met769, Lys721, Asp831, and Thr766. The *para*-biphenyl and benzene–sulfonamide substituents at the triazole's 4-position appear to be key for cytotoxicity and kinase affinity, supporting **92** and **93** as promising EGFR-targeted leads.

5.14. Miscellaneous hybrids

Şenol *et al.* synthesized sixteen triazole hybrids—arylidenhydrazides and thiazolidin-4-ones—in good to excellent yields (75–96%), reflecting excellent synthetic accessibility for both series, and evaluated their activity against HER2, EGFR, and VEGFR1 in MCF-7 cells (Scheme 49).[112] Among these, **97** (hydrazide series) and **98** (thiazolidin-4-one series) stood out, with IC_{50} values of 8.48 μM and 4.38 μM, respectively, while exhibiting minimal toxicity toward MCF-10A cells (IC_{50} = 114.8 μM and 170.6 μM). The selective index for **98** reached 38.9—nearly tenfold higher than doxorubicin, correlating with docking scores around −9.01 kcal mol^{-1} for HER2, EGFR, and VEGFR1. Key hydrogen bonds with Lys-805 and Pro-802 in HER2, and Asp-831 in EGFR, were mediated by **98**'s electron-donating substituents, rationalizing its dual-target profile.

In another study, Rezki *et al.* tethered sulfa drug moieties to benzothiazole–triazoles, synthesized in very good to excellent yields of 84–90% (Scheme 50), which are synthetically robust

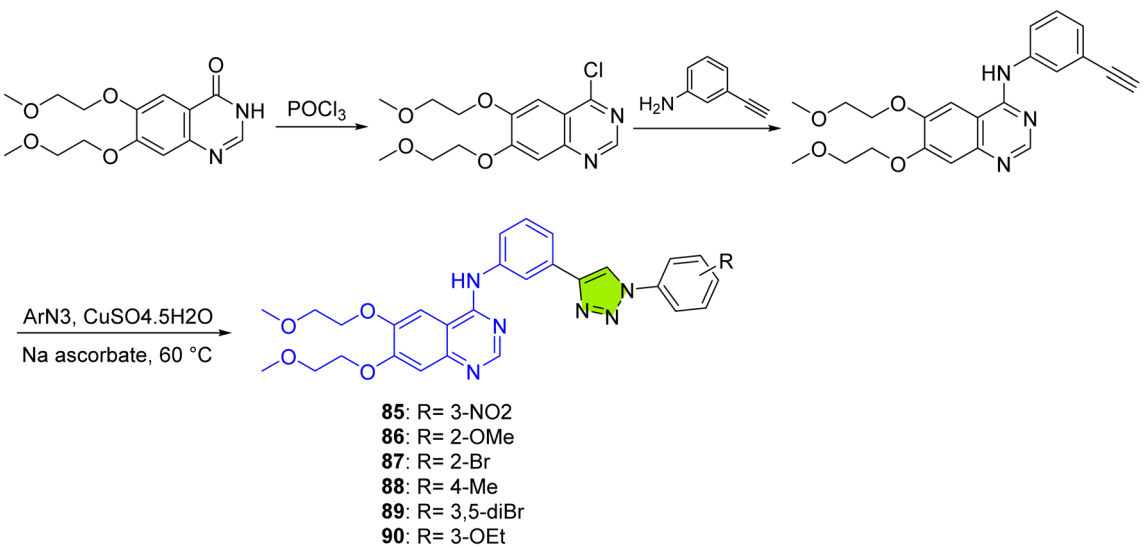

Scheme 46 Synthesis of 1,2,3-triazole hybrids **85–90**.

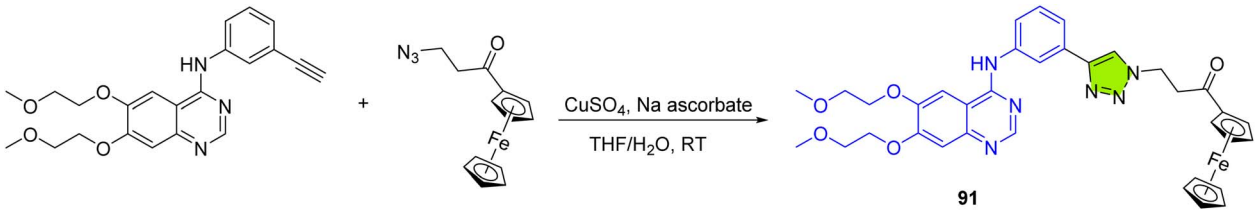

Scheme 47 Synthesis of 1,2,3-triazole hybrid **91**.

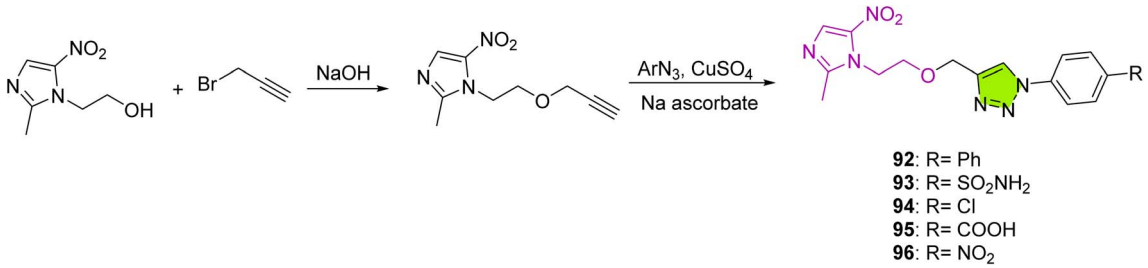

Scheme 48 Synthesis of 1,2,3-triazole hybrids **92–96**.

and reproducible, supporting further optimization.[113] Compounds **99** (3-methylbenzothiazole) and **100** (4-fluorobenzothiazole) delivered EGFR IC_{50} values of 104.3 ± 0.2 nM and 103.8 ± 1.2 nM—on par with erlotinib (76.6 ± 1.2 nM). Against HepG2, they achieved IC_{50} values of 1.49 ± 0.01 μM and 1.78 ± 0.01 μM *versus* staurosporine's 16.98 ± 0.25 μM, and **99** inhibited MCF-7 at 2.45 ± 0.04 μM without WI-38 toxicity (IC_{50} > 500 μM). Flow cytometry showed up to 30% apoptosis and G_2/M arrest. Docking highlighted persistent H-bonds to Met769 and Leu694, plus hydrophobic contacts with Val702 and Phe723; 50 ns MD gave RMSD < 2.0 Å. ADMET profiling indicated high intestinal absorption (98.6% for **99**, 97.7% for **100**), good aqueous solubility (log *S* −3.28 and −3.09, better than erlotinib's −4.73), and compliance with drug-likeness rules. Both compounds were predicted non-AMES mutagenic, non-hERG I inhibitors, but flagged as potential hERG II inhibitors and hepatotoxic, suggesting manageable but noteworthy safety concerns. These features, combined with their strong cytotoxicity and selectivity, reinforce their candidacy as orally active EGFR-targeted agents.

Meanwhile, Chaidam *et al.* assembled a library of 1,6-bis-triazole-linked α-galactoside derivatives, synthesized in good yields (Scheme 51), and screened them across nine cancer cell lines.[114] The omega-undecylenyl analogue **101** displayed potent activity against P-388 murine leukemia (IC_{50} = 4.45 μM) and broad-spectrum efficacy (13.2–32.7 μM) in HT-29, MCF-7, and A549 cells, whereas the coumarinyl derivative **102** selectively inhibited K-100 cholangiocarcinoma (IC_{50} = 4.87 μM) and MCF-7. Docking analyses linked cytotoxicity to dual engagement of EGFR (Cys-773 interactions) and CDK-2 (H-bonds with Thr-14, Lys-129, Gln-131), with both compounds forming stabilizing π-anion and hydrophobic contacts *via* their triazole and sugar moieties.

Furthermore, Fadaly *et al.* designed bis-triazole hybrids bearing nitric oxide-donating oxime groups to achieve multi-target inhibition, synthesized in moderate to very good yields of 54–89% (Scheme 52).[115] These yields indicate generally

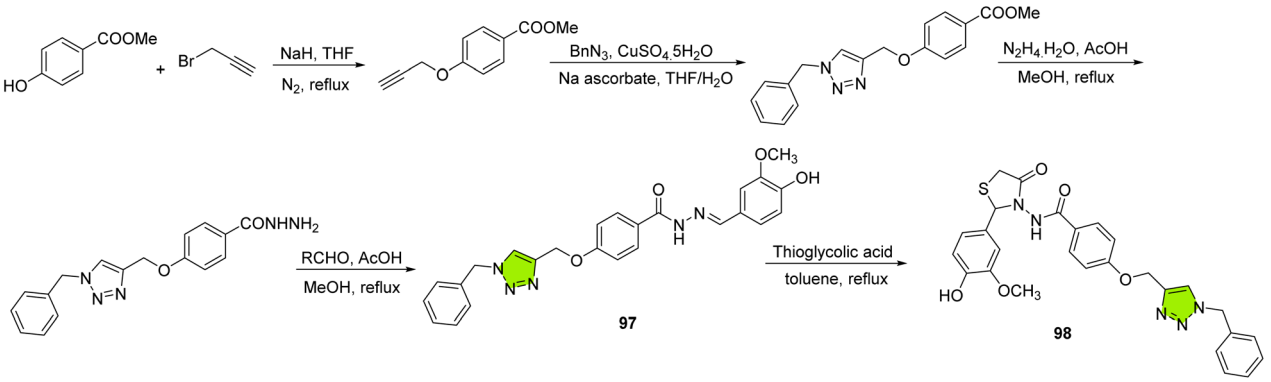

Scheme 49 Synthesis of 1,2,3-triazole hybrids **97** and **98**.

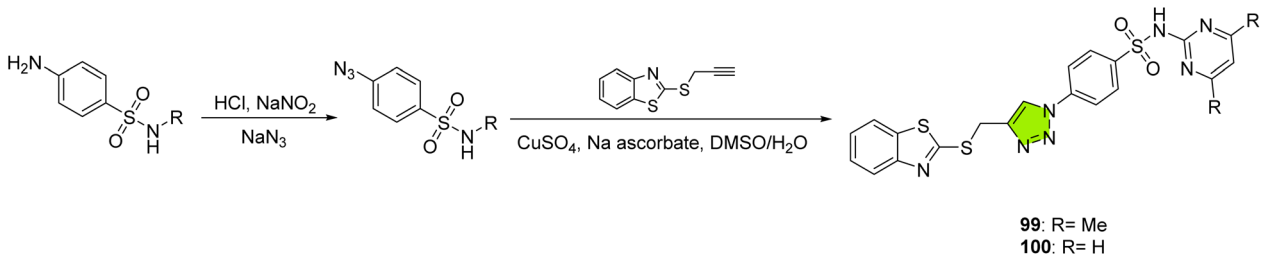

Scheme 50 Synthesis of 1,2,3-triazole hybrids **99** and **100**.

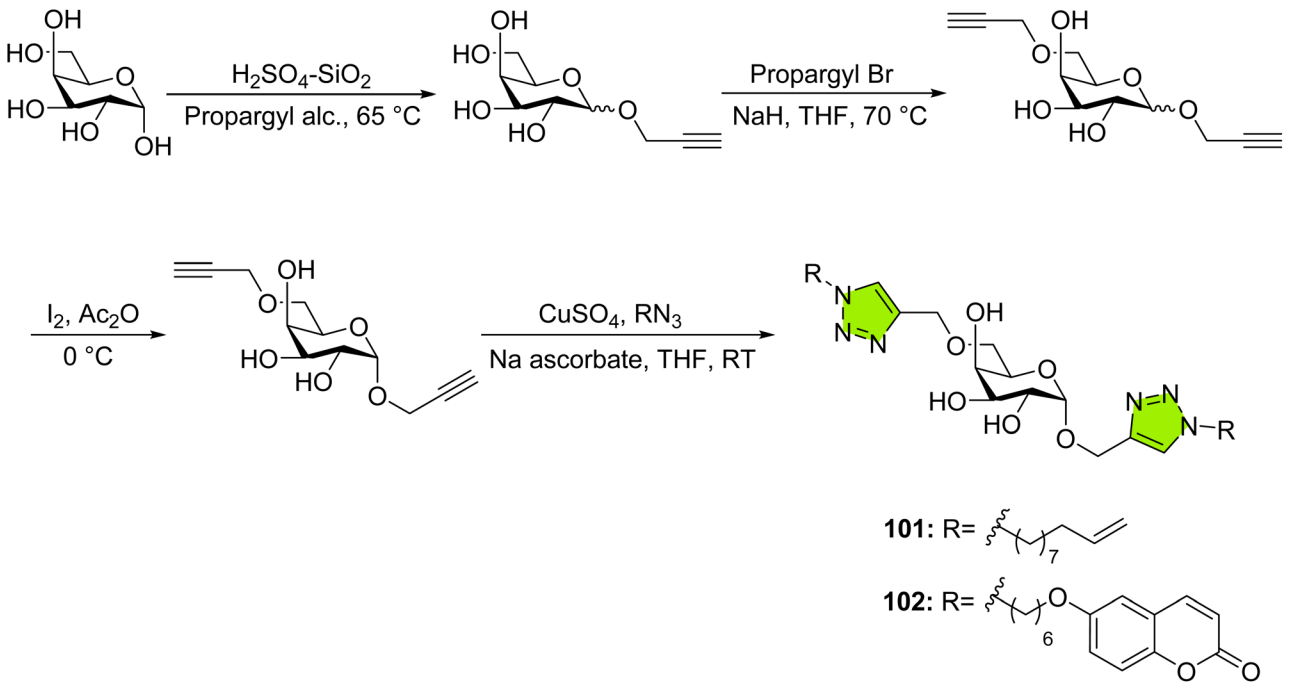

Scheme 51 Synthesis of 1,2,3-triazole hybrids **101** and **102**.

acceptable synthetic accessibility for structurally diverse hybrids, though some reactions could potentially benefit from further optimization. Compounds **103**, **104**, **105**, and **106** exhibited potent antiproliferative activity across several cancer cell lines, with IC_{50} values of 9–16 μM in MCF-7 cells, outperforming tamoxifen; 4.5–14 μM in Hep3B, 5.3–13.7 μM in HCT-116, and 3–4.5 μM in A549 cells (*versus* 6 μM for 5-FU). These hybrids also demonstrated strong EGFR inhibition (IC_{50} = 0.066–0.205 μM) and $BRAF^{V600E}$ inhibition (IC_{50} = 0.05–0.09 μM), with **106** emerging as the most potent against both kinases. Additionally, they inhibited aromatase (IC_{50} = 22.4–30.3 μM) and showed favorable COX-2 selectivity, with selectivity indices ranging from 18 to 49 compared to celecoxib's 21.1—suggesting synergistic nitric oxide release alongside kinase and enzyme blockade.

Subsequently, Mahmoud *et al.* explored 1,2,3-triazole-carboximidamide hybrids for dual EGFR/VEGFR-2 inhibition, obtained in yields of 67–88%, spanning good to very good efficiency (Scheme 53),[116] reflecting robust and efficient synthetic performance. Their lead, **107** (3,4-dimethoxy), delivered a GI_{50} of 31 nM across Panc-1, MCF-7, HT-29, and A-549 cells—slightly surpassing erlotinib's 33 nM. Enzymatically, **107** inhibited VEGFR-2 at 1.8 ± 0.05 nM and EGFR at 83 ± 5 nM (erlotinib = 80 ± 5 nM), and triggered apoptosis (caspase-3 up 531.5 pg mL^{-1}, Bax 298.6 pg mL; Bcl-2 down to 0.85 ng mL^{-1}). Docking revealed **107** occupies both kinase ATP sites with hinge-binding patterns analogous to sorafenib and erlotinib. *In silico* ADME predicted good oral bioavailability, negligible blood–brain barrier penetration, and compliance with drug-likeness filters.

Maghraby employed a chalcone–triazole hybridization strategy in another series to target EGFR and BRAF (Scheme 54).[117] Several derivatives—including **108**, **109**, **110**, **111**, **112**, and **113**—achieved IC_{50} values of 0.95–1.80 μM across four cancer lines (doxorubicin = 1.14 μM). Notably, **109** emerged as the most potent, inhibiting cell growth at 0.95 μM and EGFR kinase at 0.09 ± 0.05 μM (erlotinib = 0.05 ± 0.03 μM), while moderately blocking BRAF (0.90 ± 0.10 μM). Docking confirmed that **109** fits snugly in the EGFR-TK ATP pocket *via* H-bonds and π–π stacking. Flow cytometry showed G_1 arrest, linking its kinase blockade to cell-cycle disruption.

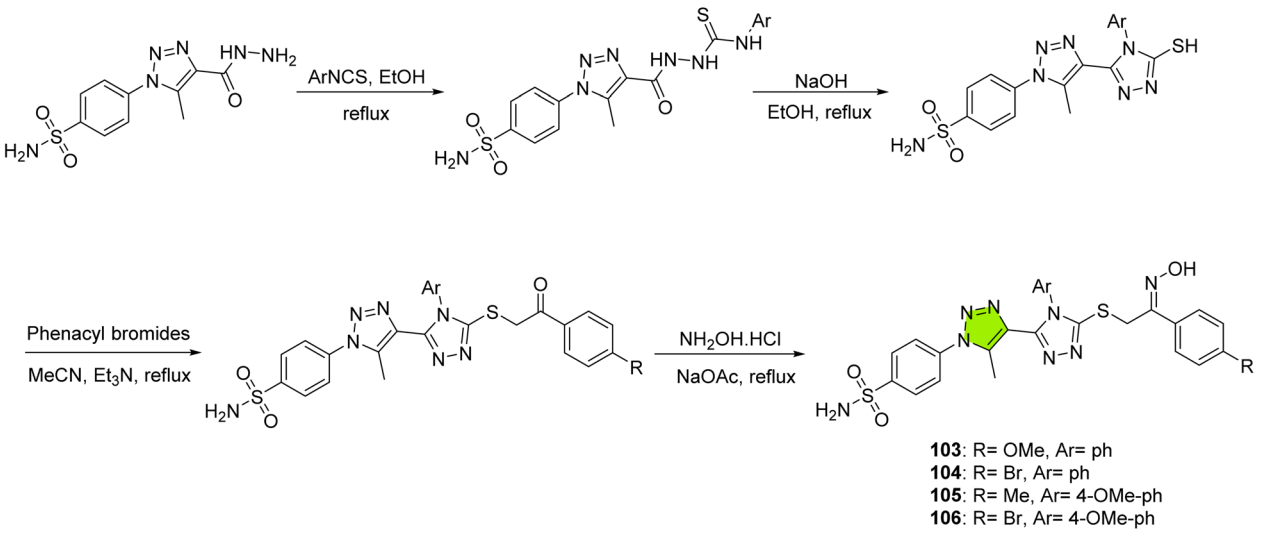

Scheme 52 Synthesis of 1,2,3-triazole hybrids **103–106**.

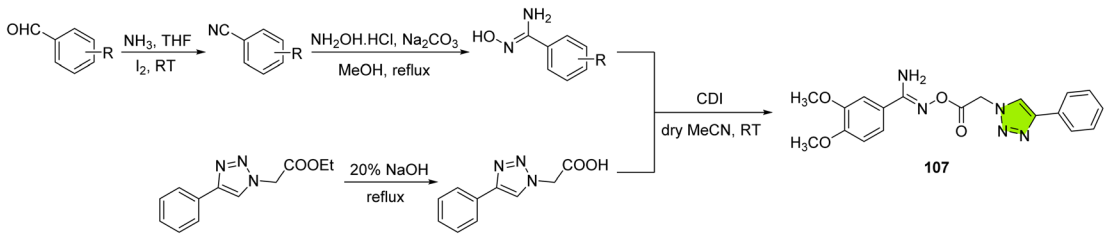

Scheme 53 Synthesis of 1,2,3-triazole hybrid **107**.

Exploring dimerization as a strategy to enhance EGFR inhibition, Deshmukh *et al.* synthesized aryloxy-bridged, amide-linked dimeric triazoles and evaluated their antiproliferative and EGFR-TK phosphorylation inhibitory activities, obtained in very good to excellent yields of 85–94% (Scheme 55), supporting the efficiency and scalability of their method.[118] Compounds **114** and **115** stood out: **114** inhibited MCF-7 cells at 4.18 μM with 88.3% EGFR-TK inhibition—approaching gefitinib—while **115** achieved 2.80 μM (MCF-7) and 5.61 μM (A549) with 72.7% kinase blockade. Both exhibited favorable selectivity (MCF-10A IC_{50} = 33.4 μM and 14 μM, respectively). Docking into EGFR (PDB: 4HJO) revealed H-bonds with Met793 and π-cation interactions with Lys745, mirroring gefitinib's binding mode

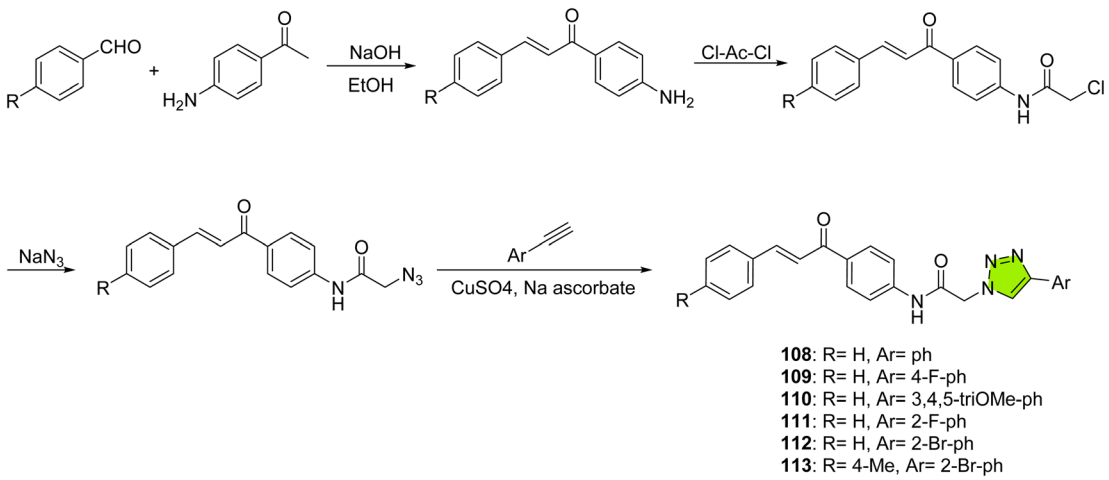

Scheme 54 Synthesis of 1,2,3-triazole hybrids **108–113**.

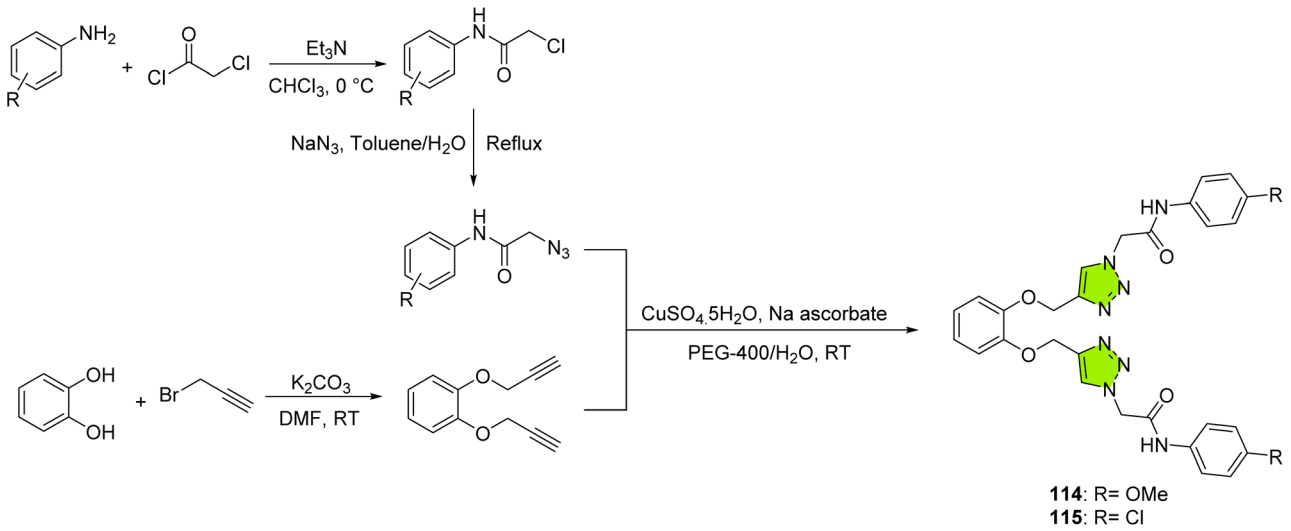

Scheme 55 Synthesis of 1,2,3-triazole hybrids **114** and **115**.

and supporting their dual antiproliferative and kinase inhibitory profiles.

Acheampong *et al.* targeted EGFR-dependent triple-negative breast cancer by hybridizing estradiol with a 1,2,3-triazole linker.[119] Their lead, **116** (Fig. 6), exhibited potent cytotoxicity in MDA-MB-231 ($IC_{50} = 8.12 \pm 0.85$ μM) and MDA-MB-468 ($IC_{50} = 25.43 \pm 3.68$ μM) cells, surpassing sorafenib in MDA-MB-231. Mechanistically, **116** induced G_0/G_1 arrest, downregulated cyclin D1 and Dyrk1B, and inhibited both total and phosphorylated EGFR and downstream PI3K/AKT/mTOR and RAS/ERK pathways. Apoptosis was mediated *via* mitochondrial release of cytochrome c, APAF1 activation, PARP1 cleavage, and Annexin V positivity. Molecular dynamics confirmed stable cation-π interactions between the triazole and Lys721 (EGFR) and Lys52/Lys149 (ERK). *In silico* ADMET predictions further highlighted its suitability as a drug-like candidate, with high gastrointestinal absorption, favorable Caco-2 and MDCK permeability, acceptable bioavailability and half-life, and no P-gp liability. Importantly, **116** showed non-carcinogenicity, low risk of hepatotoxicity, drug-induced liver injury, AMES mutagenicity, and eye irritation, and only moderate probability of hERG channel inhibition—indicating a favorable safety margin compared to most analogs. These features position **116** as a promising multi-target EGFR-pathway inhibitor for TNBC.

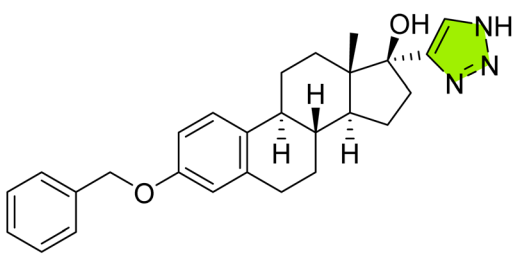

116

Fig. 6 Structure of 1,2,3-triazole hybrid **116**.

Vanga *et al.* explored Meldrum's acid-7-azaindole-triazole hybrids across five human cancer cell lines (MCF-7, HeLa, DU-145, HepG2, K562).[120] The 4-methyl derivative **117** (Fig. 7) emerged with broad-spectrum potency—$IC_{50} = 4.44 \pm 0.32$ μM in HeLa and 6.67–12.38 μM in MCF-7, DU-145, and HepG2—while inducing G_2/M arrest and apoptosis (Hoechst staining, Annexin V-FITC). Docking revealed **117** engages EGFR and anti-apoptotic Mcl-1 through hydrogen bonds, π-cation interactions, and hydrophobic contacts. Methoxy-substituted analogues **118** and **119** (Fig. 7) showed selective HeLa activity ($IC_{50} \approx 9.6$ μM), underscoring the role of aryl substitution in tuning anticancer efficacy.

Boruah and co-workers demonstrated that a catalyst-free [3 + 2] cycloaddition of phenacyl azides with maleimides or 1,4-naphthoquinone can yield high-purity triazoles in yields ranging from 72% to 92% (good to excellent efficiency) (Scheme 56).[121] These yields reflect high synthetic efficiency without the need for metal catalysis. Screening of 21 derivatives

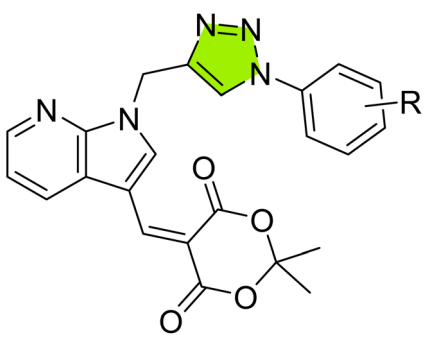

117: R= 4-Me
118: R= 3,5-diOMe
119: R= 3,4,5-triOMe

Fig. 7 Structure of 1,2,3-triazole hybrids **117–119**.

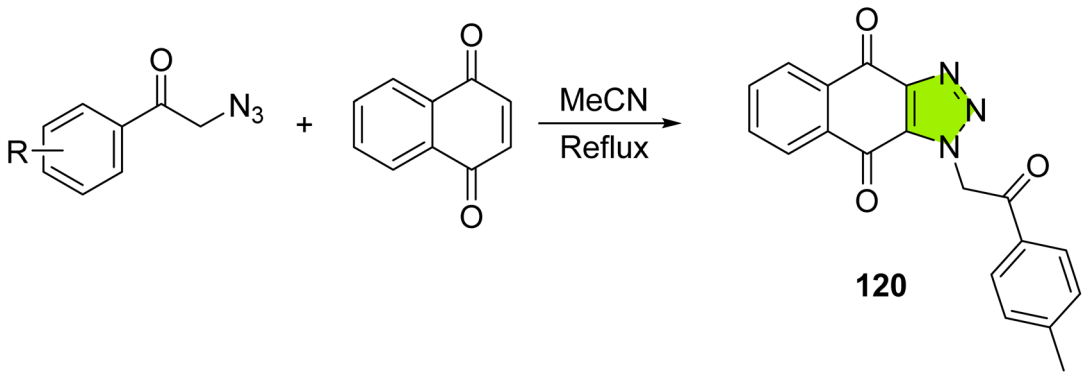

Scheme 56 Synthesis of 1,2,3-triazole hybrid **120**.

by molecular docking against EGFR (PDB: 6TFU) identified **120** (a naphthoquinone conjugate) as the top candidate (-8.8 kcal mol^{-1} *vs.* gefitinib's -5.81 kcal mol^{-1}). This compound forms fifteen significant interactions—including π–π-sulfur and π–π-alkyl contacts with Met790, Leu788, and Lys745—highlighting the synthetic route's potential to deliver potent EGFR inhibitors *via* green chemistry.

Boda *et al.* leveraged the planar phthalazine-1,4-dione scaffold to design 1,2,3-triazole hybrids, synthesized in good to very good yields of 76–87% (Scheme 57).[122] These yields are synthetically reliable, requiring no extensive optimization and suitable for library generation. The 4-nitrophenyl analogue **121** exhibited IC_{50} values of 2.33 ± 0.43 μM, 7.21 ± 0.61 μM, and 3.96 ± 0.41 μM, respectively, surpassing doxorubicin in lung and breast assays. Docking into EGFR (PDB: 4HJO) confirmed a binding energy of -11.16 kcal mol^{-1} ($K_i = 6.55$ nM) *via* a hydrogen bond to Lys721 and extensive hydrophobic contacts. Analogues **122** and **123** also achieved scores beyond -11 kcal mol^{-1} and low-micromolar cytotoxicity, underscoring the phthalazine–triazole framework as a versatile EGFR-targeted scaffold.

Focusing on pyrazole cores, Swapna *et al.* synthesized 1,2,3-triazole-linked pyrazole hybrids, obtained in good to very good yields of 78–86%—reflecting consistent and reproducible conditions—and screened them across MCF-7, IMR-32, and

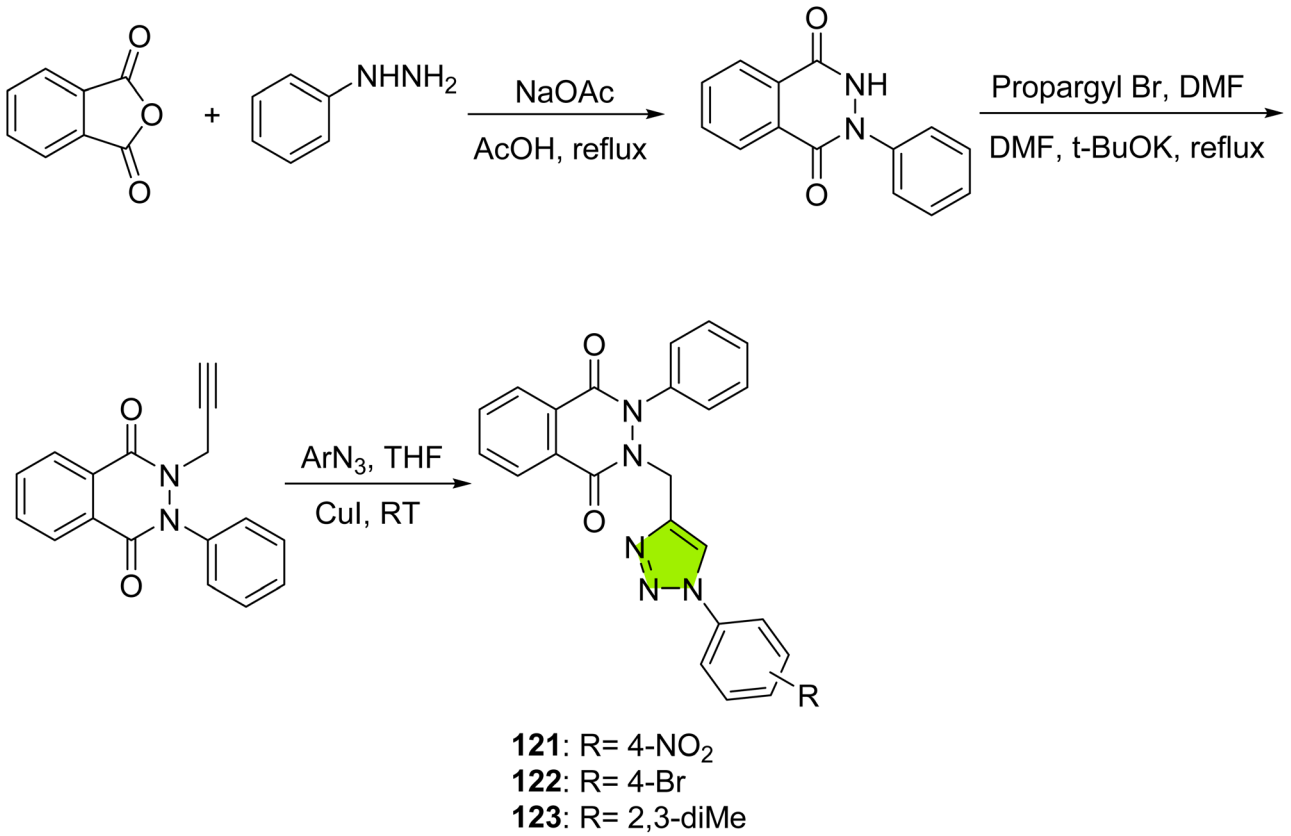

Scheme 57 Synthesis of 1,2,3-triazole hybrids **121–123**.

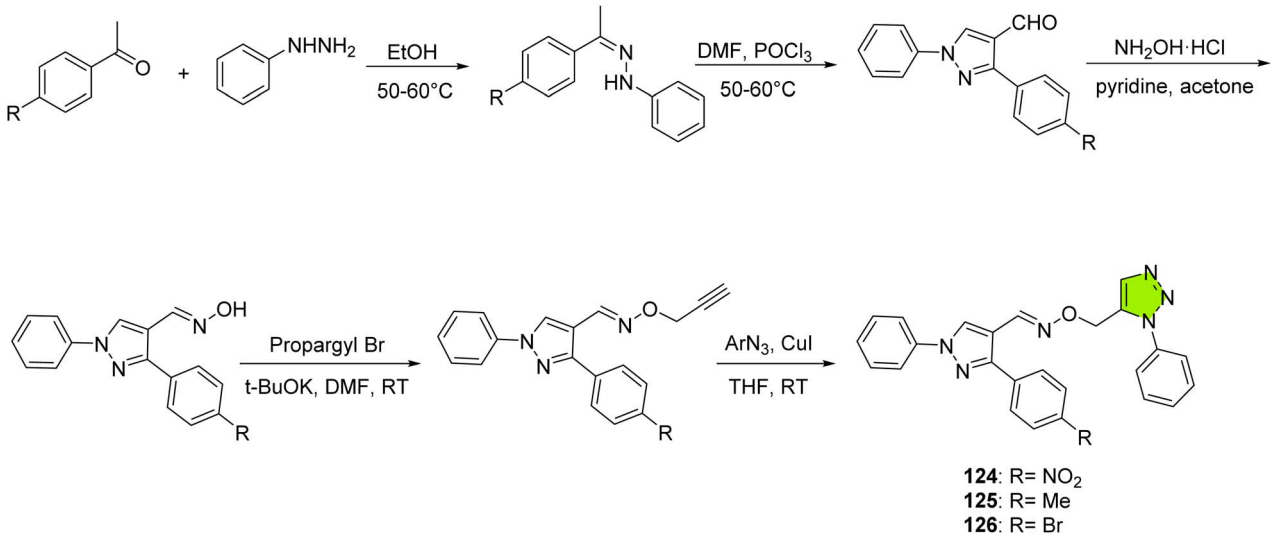

Scheme 58 Synthesis of 1,2,3-triazole hybrids **124–126**.

HeLa lines (Scheme 58).[123] The **124** analogue exhibited IC_{50} values of 8.21 ± 0.18 μM (MCF-7), 10.18 ± 0.53 μM (IMR-32), and 11.06 ± 1.22 μM (HeLa), with minimal toxicity toward HEK293 cells (IC_{50} > 89 μM). Binding energy calculations placed **124** at −11.54 kcal mol^{-1} in EGFR's active site, where it formed four hydrogen bonds (including Lys721 and Phe699) and multiple π-interactions (Leu834, Val702). Compounds **125** and **126** also demonstrated sub-20 μM cytotoxicity and engaged Lys721 and Thr766, underscoring the pyrazole–triazole scaffold's versatility.

Another series of triazoles was prepared by Guttikonda, afforded in good to very good yields of 65–85% (Scheme 59), which are generally acceptable for small-molecule synthesis, though some steps may benefit from optimization. Following evaluation in MCF-7, MDA-MB-231, and HeLa cells,[124] compounds **127** and **128** achieved IC_{50} values of 1.82 μM and 1.90 μM in MCF-7—comparable to doxorubicin (1.07 μM)—while **129**, **130**, and **131** showed ≤2.85 μM potency in MDA-MB-231 and HeLa. Docking against EGFR (−9.97 to −10.62 kcal mol^{-1}) revealed hydrogen bonds with Met769 for **127**, **129** and **130**, with **129** displaying the lowest inhibition constant (16.4 nM). All three exhibited IC_{50} values >100 μM in HEK-293, indicating high selectivity.

Guided by DFT and docking studies, El Azab *et al.* designed novel 1,2,3-triazole-containing hybrids, synthesized in good to very good yields of 75–85%, a reproducible range that supports further development. They tested them in HepG-2, HCT-116, and MCF-7 cells.[125] Their top compound, **132** (4-aminophenyl) (Scheme 60), yielded IC_{50} values of 12.22, 14.16, and 14.64 μM, respectively—on par with doxorubicin. Docking against EGFR (PDB: 1XKK) produced a binding energy of −17.01 kcal mol^{-1}, forming hydrogen bonds to Thr854 (*via* water), Met793, and Cys797, mirroring lapatinib's interactions. SAR analysis confirmed electron-donating *para*-substituents enhanced cytotoxicity.

Another validated target in cancer therapy is tubulin polymerization, essential for mitotic spindle formation and cell division.[126] Coupling EGFR inhibition with tubulin disruption offers a synergistic strategy to enhance antiproliferative effects. Shaheen *et al.* synthesized triazole hybrids that co-inhibit EGFR, mTOR, and tubulin polymerization, afforded in good to very good yields of 69–89% (Scheme 61)[127] indicating reliable methodology with minor variation across analogues. Lead compounds **133** and **134** exhibited GI_{50} values of 0.00169–0.0459 nM and 0.00192–0.0464 nM across colorectal, melanoma, and breast cancer panels, while sparing FHC cells (IC_{50} =

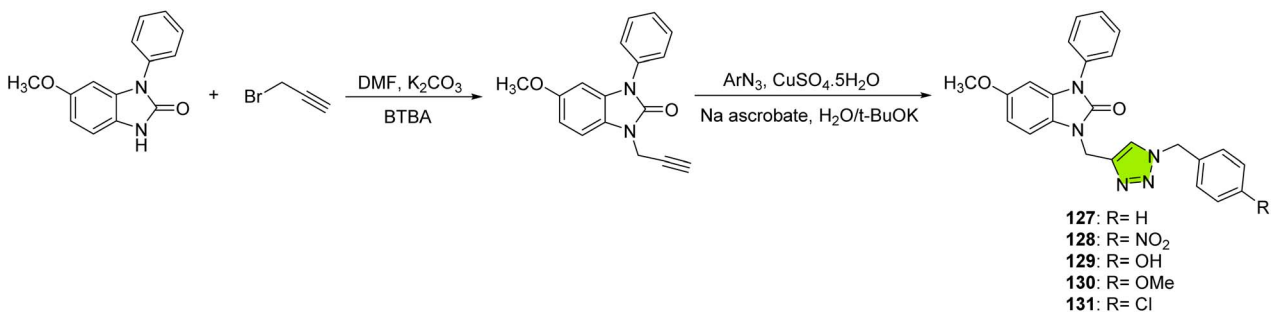

Scheme 59 Synthesis of 1,2,3-triazole hybrids **127–131**.

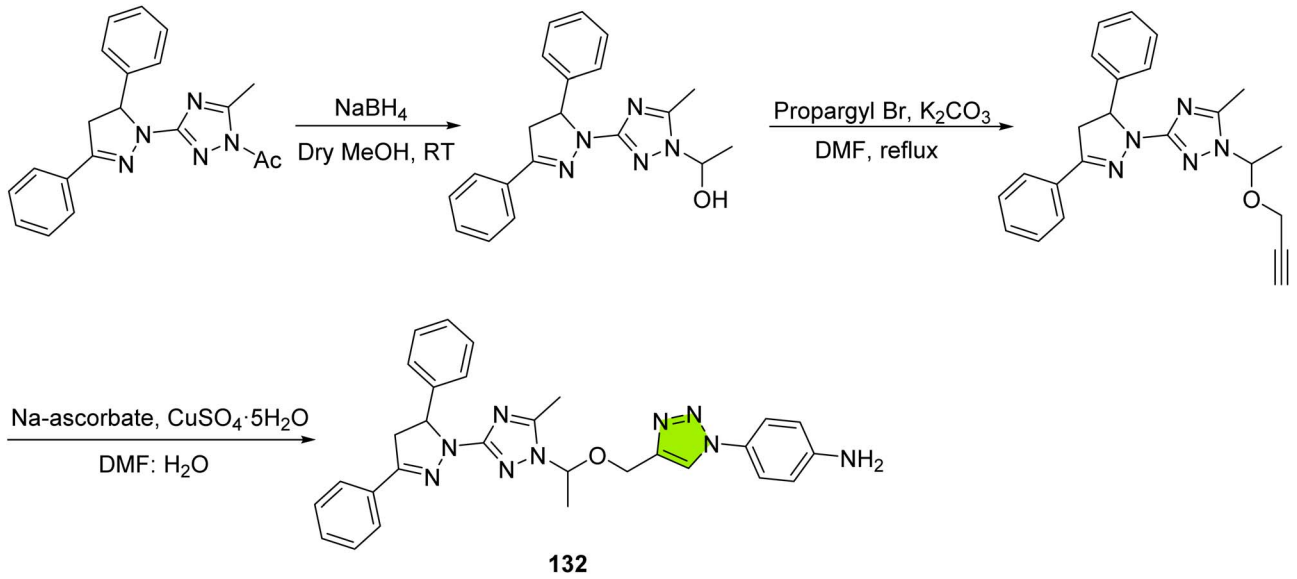

Scheme 60 Synthesis of 1,2,3-triazole hybrid **132**.

36.9–43.4 μg mL^{-1}). Both induced G_1/S arrest and apoptosis in HCT-116, upregulated Bax and caspase-9, and reduced Bcl-2. EGFR inhibition (IC_{50} = 0.155 μg mL^{-1} for **134**; 0.639 μg mL^{-1} for **133**) and tubulin blockade (IC_{50} = 2.705–7.339 μg mL^{-1}) were confirmed by docking (−7.70 to −8.03 kcal mol^{-1}) at respective ATP and colchicine sites. *In silico* toxicity predictions further reinforced their safety, with both compounds being non-mutagenic, non-carcinogenic, and non-irritant, showing no tumorigenic alerts, while maintaining high human intestinal absorption (>90%) and strong plasma protein binding. Their favorable drug scores, exceeding reference erlotinib, highlight their promise as selective, low-toxicity anticancer leads.

6. EGFR targeting profiles of key triazole hybrids based on molecular docking

To better understand the molecular targeting profiles of representative 1,2,3-triazole EGFR inhibitors, we analyzed docking data for representative 1,2,3-triazole EGFR inhibitors. Across all compounds the classic EGFR pharmacophore was maintained: namely, hinge-region hydrogen bonds (typically to Met769 in EGFR), plus contacts with nearby residues such as Lys721, Thr766 and Asp831, and extensive hydrophobic pocket occupation. For instance, a quinazolinone–triazole hybrid (compound **4**) accepts a hydrogen bond from Met769 (2.34 Å) and uses its sugar hydroxyls to H-bond Asp831. In general, the triazole ring often contributes polar anchors: previous reports note that "the triazole N formed a hydrogen bond with a lysine residue (Lys721) in the active site". Here we highlight specific compounds to illustrate these conserved motifs and the additional stabilizing interactions enabled by the triazole linker.

For example, compound **5** (a triazole-linked quinazoline) exemplifies canonical hinge binding. Its quinazoline N1 forms a strong H-bond to Met769 (3.13 Å) and the triazole N2 hydrogen-bonds to Lys721 (3.04 Å), anchoring the ligand at the ATP site. Compound **5**'s halogen substituent also engages Gln767 and its aromatic rings make π-alkyl contacts with Leu694, Leu820 and Cys751, while a π-sulfur interaction with Met742 further stabilizes binding. Compound **7**, a methoxyphenoxy-triazole quinazolinone, similarly H-bonds its quinazolinone N3 to Met769 (2.51 Å). Its triazole then forms a π-anion electrostatic contact with Asp831 (3.44 Å) and an additional H-bond to Lys721 (1.96 Å). These polar interactions are complemented by π-alkyl hydrophobics to Leu694, Ala719 and Leu768. Together these examples show how triazole hybrids recapitulate approved EGFR inhibitors' pharmacophore

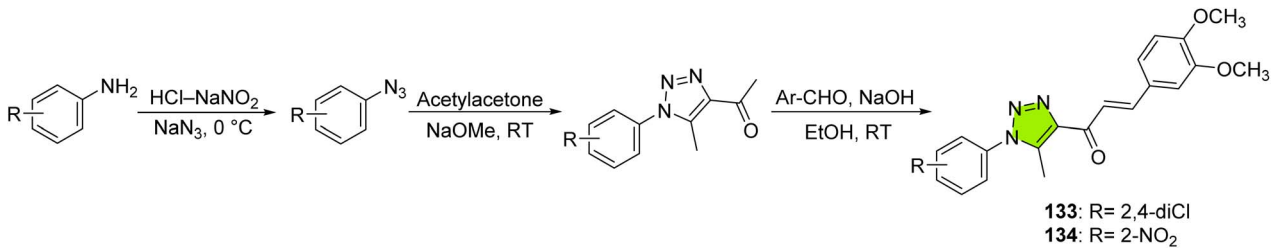

Scheme 61 Synthesis of 1,2,3-triazole hybrids **133–134**.

(Met769 hinge bond, Lys721 contact) while appending substituents (*e.g.* a methoxyphenoxy group in compound **7**) that occupy adjacent hydrophobic pockets.

Other scaffolds in the series reinforce this pattern. Compound **4**, a quinazolinone–triazole glycoside, fitted exceptionally in the EGFR cleft. Its 4-carbonyl accepts a hydrogen bond from Met769, and the glycoside OH's donate two H-bonds to Asp831. This dual anchoring is rare among non-covalent EGFR ligands. Compound **10**, an indole–triazole hybrid, showed four H-bonds with Lys721, Glu738 and Met769, anchoring both the hinge and nearby pocket. It also makes two ionic contacts with Asp831, and – importantly – its fluorine atoms form a halogen bond to Gln767, adding a directional stabilizing interaction. Altogether, these interactions (Lys721/Met769 H-bonds plus Asp831 anchoring and halogen bonding) explain compound **10**'s superior docking score. Such multifunctional binding – hinge bonds plus polar and halogen contacts – aligns with known EGFR ligand pharmacophores.

Some triazole hybrids exploit the non-covalent Cys773 "back-pocket" residue. Compound **12** (a 3-acetyl analog) forms key H-bonds with Met769 and with Cys773 (dual N···O contacts at 2.40, 2.95 Å), while also engaging Lys721 and Thr766 *via* hydrophobic contacts. This network overlaps with doxorubicin's anchoring at Met769/Ala719 (EGFR reference), underscoring the grip on the hinge area. Likewise, compounds **60** and **61** each form a strong Met769 hinge bond; compound **61**'s fluoro-phenyl also creates a halogen bond that further stabilizes the complex. Both compounds engage Cys773 (compound **60** through π-donor bonding, compound **61** indirectly *via* water), plus extensive hydrophobic contacts to Leu694, Val702, Ala719 and Leu820. In contrast, compound **65** relies on Lys721 as the hinge anchor: it forms a single but strong H-bond to Lys721 (1.97 Å), giving it the best docking score in its series. Thus, triazole inhibitors can anchor either at the classic Met769 hinge or alternatively at Lys721/Cys773, with both modes yielding high-affinity binding.

Several compounds highlight advantages like solvent-mediated binding and dual-target potential. Compound **3** (a dioxy-quinazoline triazole) formed two hydrogen bonds in EGFR: directly to Met769 and to Thr766 *via* structural water. This water-bridged H-bond to Thr766 (analogous to the EGFR "gatekeeper" pocket) illustrates how the triazole can mediate interactions beyond the hinge. Compound **19** showed an especially rich profile: its quinazoline core H-bonds to Met769 and to Cys773, and crucially, water molecules mediate H-bonds to Lys721, Thr766 and Asp831. MD simulations confirmed that Met769, Cys773 and Lys721 remain stably engaged throughout a 300 ns trajectory, underscoring these residues as the binding hotspots. By comparison, compound **1** (a quinazoline–triazole) not only mimics erlotinib with two Met769 H-bonds, but also docks strongly to BRAF^V600E. In BRAF it establishes π-H interactions with Lys483 and Val471 (and a triazole-Ser535 contact), rationalizing its cross-kinase activity. This dual-target example highlights how the 1,2,3-triazole linker can enable multi-kinase engagement without losing EGFR potency.

Finally, some hybrids adopt alternative binding modes. Compound **50** uniquely eschews the hinge: it binds EGFR *via* H-bonds to Cys773 and Asp776, an amide-π stack with Phe771, and a sulfur-π contact to Met742. In this pose Met769 is untouched, yet the ligand is secured deep in the pocket by these interactions (supported by extensive hydrophobics to Val702, Ala719, *etc.*). Such an alternate binding profile – distinct from erlotinib's hinge-centered mode – suggests that triazole hybrids can occupy non-classical pockets, which may help overcome resistance mutations at the hinge.

In summary, the docking profiles of diverse triazole hybrids consistently feature the expected EGFR pharmacophore: hinge-region hydrogen bonds (Met769 or Lys721), interactions with the gatekeeper/activation loop residues (Thr766, Asp831, Cys773), and complementary hydrophobic contacts. Water-bridged hydrogen bonding (as in compounds **3** and **19**) and halogen bonding (as in compounds **10** and **61**) further enhance affinity.

7. ADME-pharmacokinetic evaluation of triazole-based EGFR inhibitors

Across diverse scaffold classes, the *in silico* ADME and pharmacokinetic profiles of representative 1,2,3-triazole-based EGFR inhibitors demonstrate broad alignment with the physicochemical and safety characteristics expected of orally developable anticancer agents. These computational assessments provide a rational basis for interpreting the potent enzymatic and cellular activities reported throughout the review. Within the quinazoline class, the xylopyranosylated analogue **4** is particularly illustrative. It retained submicromolar EGFR inhibitory activity while satisfying Lipinski's criteria and exhibiting favorable solubility and polarity. Crucially, it was predicted to lack hERG channel inhibition and to exhibit negligible blood–brain barrier (BBB) penetration, supporting its suitability for peripheral, kinase-targeted therapeutic applications.

In the chromene/coumarin series, sugar- and benzimidazole-conjugated derivatives such as **19–21** demonstrated robust EGFR inhibition while maintaining compliance with Lipinski and Veber filters. These compounds were associated with high predicted intestinal absorption and an absence of hepatotoxicity and cardiotoxicity alerts. In particular, compounds **20** and **21** showed a low probability of BBB penetration, supporting their potential as systemically acting anticancer agents with minimal central nervous system (CNS) exposure. Among pyridine- and pyrimidine-based hybrids, several low-micromolar to submicromolar inhibitors (*e.g.*, **23–26**) exhibited physicochemical features consistent with oral bioavailability. The thiazolidinone-linked analogue **27** stood out for combining potent EGFR inhibition with predicted P-glycoprotein non-substrate behavior and restricted BBB penetration, indicating potential for favorable systemic exposure without CNS-related adverse effects.

Quinoline–triazole hybrids, exemplified by **37** and **39**, exhibited potent kinase inhibition within a lipophilicity and polarity range compatible with oral drug candidates. Compound **37** achieved an EGFR IC_{50} of 0.14 μM while fully

satisfying drug-likeness criteria. Compound **39** similarly demonstrated no violations of Lipinski's rules and was predicted to have low BBB permeability, supporting its pharmacokinetic suitability for selective antiproliferative activity. The benzimidazole–triazole derivatives **41** and **42** combined nanomolar EGFR inhibition with predicted oral bioavailability and absence of major toxicity risks. Their favorable profiles, including projected selectivity toward cancer cells, reinforce their candidacy for further development. Indole-based triazoles, including **45** and **46**, offered a comparable balance between efficacy and drug-likeness. These compounds remained within acceptable physicochemical bounds (*e.g.*, moderate log *P*, TPSA), exhibited low-to-moderate hERG liability, and demonstrated permeability characteristics consistent with oral absorption.

Oxindole and isatin hybrids provided further examples of dual-target inhibitors exhibiting favorable developability. Compound **52**, in particular, combined nanomolar inhibition of both EGFR and PARP-1 with compliance to Lipinski's rule and low predicted BBB permeability. Compound **53**, also favorably positioned in physicochemical space, was characterized by selective cytotoxicity and low off-target liability. The imidazole-linked series, especially compounds **62–65**, demonstrated broad compliance with drug-likeness rules, favorable intestinal absorption, and limited BBB access. Their balanced lipophilicity ($\log P \approx 1$–3) and mid-range TPSA values further support their oral viability.

Oxadiazole–triazole conjugates such as **66–68** combined dual inhibition of EGFR and VEGFR-2 in the low-nanomolar range with classical medicinal chemistry attributes, including moderate lipophilicity ($\log P \approx 2$–3), TPSA $\approx$ 100 Å^2, and full compliance with Lipinski's criteria. Related analogues **69–71** mirrored these profiles, suggesting scaffold-level consistency. Thiadiazine-based hybrids (**75–77**) achieved submicromolar EGFR inhibition while exhibiting acceptable aqueous solubility and minimal hERG risk, supporting their inclusion among orally tractable leads.

Natural product-inspired scaffolds provided additional pharmacokinetically promising designs. The carvacrol-derived compound **78** combined strong EGFR affinity with predicted high oral bioavailability and a non-mutagenic profile. Similarly, the thymol-based analogue **79** satisfied standard drug-likeness parameters and showed excellent predicted intestinal absorption. Schiff base and thiosemicarbazone hybrids (**80–82**) also aligned well with drug-like physicochemical space. Compound **80**, in particular, paired potent EGFR inhibition with favorable ADME attributes and negligible predicted BBB penetration, supporting peripheral restriction.

Finally, drug-derived triazole hybrids extended this developability into translational territory. Gefitinib–triazole conjugates (**83** & **84**) and erlotinib derivative **88** combined improved kinase potency with excellent predicted absorption and low CNS exposure. Additionally, metronidazole-based analogues **92** and **93** maintained acceptable physicochemical profiles and low-micromolar antiproliferative activity, further validating the utility of triazole-based modifications for enhancing pharmacokinetic properties.

Collectively, these data—spanning quinazoline, chromene, pyridine/pyrimidine, quinoline, benzimidazole, indole, oxindole/isatin, imidazole, oxadiazole, and thiadiazine hybrids, as well as natural-product, Schiff base, and clinically derived scaffolds—underscore the pharmacokinetic versatility of the 1,2,3-triazole motif. This moiety can be rationally incorporated to maintain or enhance EGFR-targeted efficacy while conferring key developability features such as high intestinal absorption, rule-of-five compliance, low hERG and mutagenicity risk, and, when desirable, peripherally restricted distribution. This integrated pharmacokinetic perspective reinforces the clinical potential of triazole-bearing EGFR inhibitors and directly addresses the reviewer's request by linking structural class to drug-likeness and *in silico* PK properties.

8. Structure–activity relationship

8.1. Triazole as hinge-binding enhancer

The 1,2,3-triazole moiety facilitates EGFR affinity *via* hydrogen bonding (often with Met793 or Lys721) and π-stacking with aromatic residues. Its incorporation at C-6 or C-7 positions of kinase-recognized scaffolds (*e.g.*, quinazoline, quinoline, pyrimidine) enhances orientation within the ATP pocket and frequently improves cellular activity.

8.2. Substitution on triazole-linked phenyl rings tunes cytotoxicity

Electron-withdrawing groups (*e.g.*, 4-chloro, 4-nitro, CF_3) on triazole-linked aryl rings significantly increase antiproliferative potency and enzymatic inhibition. For instance, dichlorophenyl- or trifluoromethyl-substituted hybrids often reached IC_{50} values <0.5 μM in EGFR enzyme assays and <5 μM in MCF-7 or A549 cells.

8.3. Flexible *vs.* rigid linkers between core and triazole

Methylene and ethylene linkers afford flexibility, improving kinase pocket accommodation and cellular uptake. However, rigid linkers (*e.g.*, barbituric acid or oxadiazole) can improve selectivity and binding affinity if sterically well-oriented, especially in dual EGFR/VEGFR-2 inhibitors.

8.4. Sugar conjugation boosts solubility and selectivity

Glycosylation (*e.g.*, D-glucose or glucopyranosyl moieties) on triazole-bearing hybrids significantly enhanced water solubility, membrane permeability, and cancer selectivity. Glucosylated triazole-pyrimidines and quinazolines showed IC_{50} values of 0.16–0.31 μM for EGFR and reduced toxicity against normal WI-38 fibroblasts.

8.5. Halogen tuning enhances selectivity and binding stability

Halogenated phenyl groups (*e.g.*, Cl, F, I) improved binding energy and docking stability *via* halogen-π and hydrophobic interactions. Uracil-coumarin hybrids with iodine (compound

22) showed lower RMSD and better EGFR docking profiles than erlotinib.

9. Nitrosamine risk considerations in the synthesis of 1,2,3-triazole-based EGFR inhibitors

Given the increasing regulatory emphasis on nitrosamine control, and considering the prevalence of 1,2,3-triazole hybrids and associated heterocycles (*e.g.*, quinazoline, coumarin, pyrimidine, quinoline, benzimidazole, indole, oxindole, imidazole, oxadiazole, thiadiazine) in the EGFR inhibitor literature, a brief risk assessment of potential *N*-nitrosamine formation during synthetic steps is warranted.

Nitrosamines (R_2N–NO) are classified as probable human carcinogens,[128] and their formation typically arises from the reaction of secondary or tertiary amines with nitrosating species such as nitrous acid (HNO_2), particularly under mildly acidic conditions (optimal pH ~3–4). Regulatory agencies including the EMA, FDA, and ICH now mandate proactive evaluation of nitrosamine drug substance-related impurities (NDSRIs) during development and commercial manufacturing, even in the absence of observed contamination. Acceptable daily intake (AI) thresholds for many nitrosamines are extremely low—26.5 ng per day (FDA) and 18 ng per day (EMA)[129,130] for cohort-of-concern compounds—placing a premium on early route design and risk mitigation.

While the Cu(I)-catalyzed azide–alkyne cycloaddition ("click chemistry") used to generate 1,4-disubstituted 1,2,3-triazoles does not itself employ nitrosating reagents, the precursor steps often do. Notably, diazotization of anilines ($NaNO_2$/HCl) to form aryl azides is a commonly used strategy in triazole-based EGFR inhibitor synthesis. These reactions introduce nitrosating conditions and can leave residual nitrite,[131] which, if not properly purged, may interact with amines present in the substrate, intermediates, solvents (*e.g.*, dimethylamine-containing DMF), or excipients to generate nitrosamines such as NDMA or NDEA.[132]

In the case of 1,2,3-triazole-EGFR inhibitor hybrids, the risk of nitrosamine formation is route-dependent, not scaffold-intrinsic. The triazole ring itself contains no N–H group and is chemically stable. However, the azide installation step—often required for the "click" reaction—poses a recurring concern. Several synthetic pathways reported in the literature utilize diazotization/azidation protocols that could introduce nitrite. If the triazole-bearing molecule also contains morpholine, piperazine, or dialkylamino side chains, as seen in many quinazoline– or benzimidazole–triazole hybrids, the structural conditions for NDSRI formation become plausible.

Scaffold-specific insights are also relevant:

- Quinazoline, quinoline, pyridine, and pyrimidine scaffolds, which lack secondary amine N–H groups, are inherently low-risk. However, appended side chains or synthetic intermediates bearing nitrosatable nitrogen atoms should be carefully evaluated.
- Benzimidazole, indole, imidazole, oxindole, and isatin scaffolds do contain N–H groups, but classical *N*-nitrosamine formation is uncommon due to aromatic stabilization and low nucleophilicity. Nevertheless, these systems may undergo rearrangements under nitrosative conditions, especially in the presence of NOx, necessitating caution.
- Coumarins, oxadiazoles, and thiadiazines, which lack nitrogen-based functionalities capable of nitrosation, are intrinsically safe with respect to classical R_2N–NO formation, provided their synthetic routes avoid exogenous amines and nitrosating agents.

Regulatory guidance (*e.g.*, ICH M7, FDA RAIL, EMA Q&A) recommends the following best practices during development of triazole-EGFR inhibitors:

- Prefer nitrite-free azide synthesis routes (*e.g.*, halide → azide) when possible.
- If diazotization is used, strictly control pH, temperature, and avoid the co-presence of secondary amines.
- Rigorously purge nitrite residues prior to exposure to amine-containing steps.
- Employ validated LC-HRMS methods to detect potential nitrosamines at low ng per day levels, guided by structural alerts and CPCA-based potency categorization.

Despite the fact that none of the reviewed EGFR-targeted triazole hybrids report detected nitrosamine impurities, adherence to these control strategies ensures synthetic robustness and regulatory compliance. Future reports should transparently document whether diazotization was used, what amine-bearing functionalities were present, and how nitrosation risks were mitigated or excluded.

10. Impurity profiling and analytical validation for 1,2,3-triazole hybrids

When designing new 1,2,3-triazole hybrids, the impurity profiles of the synthetic routes are only inconsistently addressed in the medicinal chemistry literature. Most reports confirm compound integrity by NMR, HRMS, or HPLC purity (>95%), but systematic impurity profiling—particularly of residual copper or minor byproducts—is seldom performed. Dedicated process-oriented studies demonstrate that such profiling is feasible: ICP-MS has quantified copper in CuAAC products at levels as low as ≤1 ppm with heterogeneous catalysts, 14–20 ppm in continuous-flow reactions, and 15 ppm after targeted sulfide washes, all comfortably below ICH Q3D Class 3 thresholds. Yet, these careful analyses remain the exception rather than the rule, and medicinal chemistry reports on triazole-EGFR hybrids generally stop short of quantifying or validating impurity controls.

Organic impurities and side reactions provide a further layer of concern. Excess or unreacted alkyne and azide starting materials are not always reported, and under more forcing conditions, oxidative alkyne homocoupling can generate significant byproducts, as shown by Ali *et al.*[133] with 43% dimerization of propargyl ethers. In typical SAR studies, such impurities are not actively investigated, and NMR alone may

overlook species present at <5%. More advanced tools such as LC-MS, GC-MS, or ion chromatography—capable of identifying low-level organic impurities, nitrite residues, or unreacted azides—are rarely applied. This suggests that, while "purity" is often declared, a complete impurity profile is usually not established when new triazole hybrids are reported.

The quality of the experimental methods available for impurity profiling, however, is high when they are employed. ICP-MS and ICP-OES provide ppb–ppm sensitivity for elemental copper, ion chromatography can detect residual nitrite and azide at ppm levels, and validated LC-MS/MS or GC-MS/MS methods (USP ⟨1469⟩) reliably quantify nitrosamines and mutagenic species down to the low-ppb range. Regulatory frameworks such as ICH Q2(R2), Q3D(R2), and Q14 outline how these methods should be validated and applied. The limitation lies not in the adequacy of the analytical platforms—which are robust, sensitive, and regulatory-accepted—but rather in their inconsistent adoption in medicinal chemistry practice. Future development of 1,2,3-triazole hybrids would benefit from systematically incorporating such validated impurity assessments into routine characterization, ensuring both scientific rigor and compliance with evolving regulatory expectations.

11. Future directions

Future research on 1,2,3-triazole EGFR inhibitors must evolve from proof-of-concept cytotoxicity studies toward clinically actionable drug candidates. Several concrete opportunities stand out.

11.1. Advancing promising scaffolds to *in vivo* validation

Quinazoline–triazole hybrids and oxadiazole–triazole conjugates have repeatedly demonstrated sub-nanomolar EGFR inhibition and strong apoptosis induction *in vitro*. Yet, most reports stop at docking and 2D cell assays. Moving these leads into xenograft or patient-derived models is an urgent next step to confirm therapeutic relevance.

11.2. Resistance-directed design

Only a handful of triazole derivatives have been tested against clinically important resistant mutants (*e.g.*, EGFR^L858R/T790M, EGFR^C797S). Expanding structure-based optimization against these variants, possibly using irreversible or covalent triazole linkers, will directly address one of the greatest clinical challenges.

11.3. Rational polypharmacology with translational focus

While dual EGFR/VEGFR-2 or EGFR/BRAF hybrids have shown promise, careful balance between efficacy and off-target toxicity is still lacking. Future efforts should systematically explore triazole hybrids that couple EGFR inhibition with epigenetic modulators (*e.g.*, HDAC, BET inhibitors) or immuno-oncology targets, supported by mechanistic pathway assays.

11.4. Emerging modalities

Incorporating triazoles into PROTAC-based EGFR degraders is an attractive paradigm, but the field is still nascent. Early triazole-containing degraders should be optimized for linker length, ternary complex stability, and selective degradation of mutant EGFR isoforms. Similarly, covalent triazole conjugates targeting non-classical cysteine residues could open new allosteric opportunities.

11.5. Drug-likeness and delivery

Solubility and pharmacokinetics remain bottlenecks. Beyond standard medicinal chemistry, formulation approaches—nanoparticle encapsulation, triazole-based prodrugs, or antibody–drug conjugates—should be explored to improve tumor selectivity and systemic stability.

11.6. AI-driven design

The increasing availability of EGFR mutant crystal structures and machine-learning models enables prediction of triazole substitutions with higher precision. Coupling AI-guided SAR exploration with rapid click-chemistry synthesis could accelerate discovery pipelines dramatically.

Conclusion

1,2,3-Triazole-based hybrids have proven to be highly versatile scaffolds in the development of EGFR inhibitors, combining ease of synthesis, chemical stability, and the capacity to form productive interactions within the kinase active site. When integrated into privileged scaffolds such as quinazolines, coumarins, pyrimidines, quinolines, benzimidazoles, indoles, oxindoles, and oxadiazoles, these hybrids have delivered potent EGFR inhibition, strong antiproliferative effects, and, in many cases, the ability to selectively target cancer cells over normal ones. Importantly, several triazole derivatives have demonstrated activity against resistant EGFR mutants, and some have shown encouraging dual-target effects on kinases like VEGFR-2 or BRAF, opening avenues for multi-pathway modulation. Looking ahead, future progress will depend on advancing the most promising scaffolds beyond *in vitro* assays into *in vivo* models to confirm their therapeutic relevance, and on prioritizing resistance-directed design to address clinically challenging mutations such as T790M and C797S. Expanding the scope of triazole hybrids into allosteric inhibitors and degraders offers a particularly promising route, as these strategies may bypass classical resistance mechanisms. At the same time, continued efforts to improve solubility, metabolic stability, and pharmacokinetics—through structural optimization, prodrug design, or modern delivery systems—will be essential for translation into clinical settings. In this way, the integration of medicinal chemistry, structural biology, and pharmacology can ensure that triazole hybrids advance from potent experimental agents to viable candidates for next-generation EGFR-targeted therapies.

Author contributions

Hussam Elddin Nabeih Khasawneh: conceptualization, writing – original draft, supervision, project administration; Hesham M. Hassan: writing – original draft, methodology, visualization, funding acquisition; Amal Ali Alharbi: data curation, writing – review & editing; Wesam Taher Almagharbeh: investigation, data curation, writing – review & editing; Raed Fanoukh Aboqader Al-Aouadi: investigation, resources; Kirandeep Kaur: formal analysis, validation; Ramya Maranan: data curation, writing – review & editing; Hadeer M. Farhan: methodology, validation, writing – original draft; Hamada Hashem: software, visualization, writing – review & editing; Mariam M. Hassan: software, visualization, writing – review & editing; Stefan Bräse: supervision, conceptualization, writing – review & editing; Ahmed Al-Emam: writing – original draft, methodology, visualization, funding acquisition.

Conflicts of interest

There are no conflicts to declare.

Data availability

No primary research results, software or code have been included and no new data were generated or analysed as part of this review.

Supplementary information is available. See DOI: https://doi.org/10.1039/d5ra03819g.

Funding

The authors declare that financial support was received for the research and/or publication of this article. This study was funded by Deanship of Research and Graduate Studies at King Khalid University through a Large Research Project under grant number RGP2/373/46.

Acknowledgements

The authors extend their appreciation to the Deanship of Research and Graduate Studies at King Khalid University for funding this work through Large Research Project under grant number RGP2/373/46.

References

1 Cancer Facts & Figures 2025Available online: https://www.cancer.org/research/cancer-facts-statistics/all-cancer-facts-figures/2025-cancer-facts-figures.html (accessed on 22 May 2025).
2 S. Sigismund, D. Avanzato and L. Lanzetti, Emerging Functions of the EGFR in Cancer, *Mol. Oncol.*, 2018, **12**, 3–20, DOI: 10.1002/1878-0261.12155.
3 M. L. Uribe, I. Marrocco and Y. Yarden, EGFR in Cancer: Signaling Mechanisms, Drugs, and Acquired Resistance, *Cancers*, 2021, **13**, 2748, DOI: 10.3390/cancers13112748.
4 G. Bethune, D. Bethune, N. Ridgway and Z. Xu, Epidermal Growth Factor Receptor (EGFR) in Lung Cancer: An Overview and Update, *J. Thorac. Dis.*, 2010, **2**, 48–51.
5 A. A. Hashmi, S. Naz, S. K. Hashmi, M. Irfan, Z. F. Hussain, E. Y. Khan, H. Asif and N. Faridi, Epidermal Growth Factor Receptor (EGFR) Overexpression in Triple-Negative Breast Cancer: Association with Clinicopathologic Features and Prognostic Parameters, *Surg. Exp. Pathol.*, 2019, **2**, 6, DOI: 10.1186/s42047-018-0029-0.
6 S. Nair, J. A. Bonner and M. Bredel, EGFR Mutations in Head and Neck Squamous Cell Carcinoma, *Int. J. Mol. Sci.*, 2022, **23**, 3818, DOI: 10.3390/ijms23073818.
7 R. I. Nicholson, J. M. W. Gee and M. E. Harper, EGFR and Cancer Prognosis, *Eur. J. Cancer*, 2001, **37**, 9–15, DOI: 10.1016/S0959-8049(01)00231-3.
8 A. Kanbour, F. Salih, W. Abualainin, M. Abdelrazek, L. Szabados, I. Al-Bozom and N. E. Omar, Leptomeningeal Metastatic L858R EGFR-Mutant Lung Cancer: Prompt Response to Osimertinib in the Absence of T790M-Mutation and Effective Subsequent Pulsed Erlotinib, *OncoTargets Ther.*, 2022, **15**, 659–667, DOI: 10.2147/OTT.S336012.
9 C. Xu, L. Lei, W. Wang, L. Lin, Y. Zhu, H. Wang, L. Miao, L. Wang, W. Zhuang, M. Fang, *et al.*, Molecular Characteristics and Clinical Outcomes of EGFR Exon 19 C-Helix Deletion in Non-Small Cell Lung Cancer and Response to EGFR TKIs, *Transl. Oncol.*, 2020, **13**, 100791, DOI: 10.1016/j.tranon.2020.100791.
10 L. H. Al-Wahaibi, A. M. Elshamsy, T. F. S. Ali, B. G. M. Youssif, S. Bräse, M. Abdel-Aziz and N. A. El-Koussi, Design and Synthesis of New Dihydropyrimidine Derivatives with a Cytotoxic Effect as Dual EGFR/VEGFR-2 Inhibitors, *ACS Omega*, 2024, **9**, 34358–34369, DOI: 10.1021/acsomega.4c01361.
11 N. Karachaliou, M. Fernandez-Bruno, J. W. P. Bracht and R. Rosell, EGFR First- and Second-Generation TKIs—There Is Still Place for Them in EGFR-Mutant NSCLC Patients, *Transl. Cancer Res.*, 2019, **8**, S23–S47, DOI: 10.21037/tcr.2018.10.06.
12 R. Shah and J. F. Lester, Tyrosine Kinase Inhibitors for the Treatment of EGFR Mutation-Positive Non–Small-Cell Lung Cancer: A Clash of the Generations, *Clin. Lung Cancer*, 2020, **21**, e216–e228, DOI: 10.1016/j.cllc.2019.12.003.
13 H. A. Yu, M. E. Arcila, M. D. Hellmann, M. G. Kris, M. Ladanyi and G. J. Riely, Poor Response to Erlotinib in Patients with Tumors Containing Baseline EGFR T790M Mutations Found by Routine Clinical Molecular Testing, *Ann. Oncol.*, 2014, **25**, 423–428, DOI: 10.1093/annonc/mdt573.
14 B. Ricciuti, G. Metro, M. Brambilla, V. Ludovini, S. Baglivo, A. Siggillino, E. Prosperi and R. Chiari, Acquired Resistance to Afatinib Due to T790M-Positive Squamous Progression in EGFR-Mutant Adenosquamous Lung Carcinoma, *J. Thorac. Oncol.*, 2018, **13**, e9–e12, DOI: 10.1016/j.jtho.2017.08.025.
15 Y. Yang, Q. Liu, L. Cao, W. Sun, X. Gu, B. Liu, N. Xiao, F. Teng, X. Li, M. Chen, *et al.*, Osimertinib versus Afatinib in Patients with T790M-Positive, Non-Small-Cell Lung

Cancer and Multiple Central Nervous System Metastases after Failure of Initial EGFR-TKI Treatment, *BMC Pulm. Med.*, 2021, **21**, 172, DOI: 10.1186/s12890-021-01539-x.

16 Y. Li, T. Mao, J. Wang, H. Zheng, Z. Hu, P. Cao, S. Yang, L. Zhu, S. Guo, X. Zhao, *et al.*, Toward the next Generation EGFR Inhibitors: An Overview of Osimertinib Resistance Mediated by EGFR Mutations in Non-Small Cell Lung Cancer, *Cell Commun. Signaling*, 2023, **21**, 71, DOI: 10.1186/s12964-023-01082-8.

17 J. Szczepański, D. Khylyuk, A. Korga-Plewko, M. Michalczuk, S. Mańdziuk, M. Iwan and N. Trotsko, Rhodanine-Piperazine Hybrids as Potential VEGFR, EGFR, and HER2 Targeting Anti-Breast Cancer Agents, *Int. J. Mol. Sci.*, 2024, **25**, 12401, DOI: 10.3390/ijms252212401.

18 L. H. Al-Wahaibi, A. M. Elshamsy, T. F. S. Ali, B. G. M. Youssif, S. Bräse, M. Abdel-Aziz and N. A. El-Koussi, Design, Synthesis, in Silico Studies, and Apoptotic Antiproliferative Activity of Novel Thiazole-2-Acetamide Derivatives as Tubulin Polymerization Inhibitors, *Front. Chem.*, 2025, **13**, 1565699, DOI: 10.3389/fchem.2025.1565699.

19 A. H. Mohamed, A. A. Aly, M. B. Alshammari, A. Ahmad, B. A. A. Balboul, D. A. Ghareeb, M. E. Abdelaziz and E. J. El-Agroudy, New Thiazolo-Quinolone Hybrids as EGFR and/or PI3K Inhibitors and as Apoptosis Inducers via Modulating Bax/Bcl-2/P53 Cascade, *Monatsh. Chem.*, 2024, **155**, 1131–1143, DOI: 10.1007/s00706-024-03259-4.

20 S. Bräse, C. Gil, K. Knepper and V. Zimmermann, Organic Azides: An Exploding Diversity of a Unique Class of Compounds, *Angew. Chem., Int. Ed.*, 2005, **44**, 5188–5240, DOI: 10.1002/anie.200400657.

21 N. Belskaya, J. Subbotina and S. Lesogorova, Synthesis of 2*H*-1,2,3-Triazoles, in *Chemistry of 1,2,3-Triazoles*, ed. W. Dehaen and V. A. Bakulev, Springer International Publishing, Cham, 2015, pp. 51–116 ISBN 978-3-319-07962-2.

22 D. Lengerli, K. Ibis, Y. Nural and E. Banoglu, The 1,2,3-Triazole "All-in-One" Ring System in Drug Discovery: A Good Bioisostere, a Good Pharmacophore, a Good Linker, and a Versatile Synthetic Tool, *Expert Opin. Drug Discovery*, 2022, **17**, 1209–1236, DOI: 10.1080/17460441.2022.2129613.

23 M. M. Matin, P. Matin, M. R. Rahman, T. Ben Hadda, F. A. Almalki, S. Mahmud, M. M. Ghoneim, M. Alruwaily and S. Alshehri, Triazoles and Their Derivatives: Chemistry, Synthesis, and Therapeutic Applications, *Front. Mol. Biosci.*, 2022, **9**, 864286, DOI: 10.3389/fmolb.2022.864286.

24 E. Bonandi, M. S. Christodoulou, G. Fumagalli, D. Perdicchia, G. Rastelli and D. Passarella, The 1,2,3-Triazole Ring as a Bioisostere in Medicinal Chemistry, *Drug Discovery Today*, 2017, **22**, 1572–1581, DOI: 10.1016/j.drudis.2017.05.014.

25 K. Bozorov, J. Zhao and H. A. Aisa, 1,2,3-Triazole-Containing Hybrids as Leads in Medicinal Chemistry: A Recent Overview, *Bioorg. Med. Chem.*, 2019, **27**, 3511–3531, DOI: 10.1016/j.bmc.2019.07.005.

26 B. Zhang, Comprehensive Review on the Anti-Bacterial Activity of 1,2,3-Triazole Hybrids, *Eur. J. Med. Chem.*, 2019, **168**, 357–372, DOI: 10.1016/j.ejmech.2019.02.055.

27 N. Agouram, 1,2,3-Triazole Derivatives as Antiviral Agents, *Med. Chem. Res.*, 2023, **32**, 2458–2472, DOI: 10.1007/s00044-023-03154-3.

28 S. M. Abdul Rahman, J. S. Bhatti, S. Thareja and V. Monga, Current Development of 1,2,3-Triazole Derived Potential Antimalarial Scaffolds: Structure- Activity Relationship (SAR) and Bioactive Compounds, *Eur. J. Med. Chem.*, 2023, **259**, 115699, DOI: 10.1016/j.ejmech.2023.115699.

29 S. N. Sirakanyan, D. Spinelli, A. Petrou, A. Geronikaki, V. G. Kartsev, E. K. Hakobyan, H. A. Yegoryan, L. Zuppiroli, R. Zuppiroli, A. G. Ayvazyan, *et al.*, New Bicyclic Pyridine-Based Hybrids Linked to the 1,2,3-Triazole Unit: Synthesis via Click Reaction and Evaluation of Neurotropic Activity and Molecular Docking, *Molecules*, 2023, **28**, 921, DOI: 10.3390/molecules28030921.

30 H. H. H. Hashem, Design, Synthesis, and Molecular Docking of Novel Urea Linked 1,2,3-Triazole-Benzenesulfonamide Hybrid as Potential Carbonic Anhydrase Inhibitors, *J. Adv. Biomed. Pharm. Sci.*, 2024, **7**, 53–59, DOI: 10.21608/jabps.2023.243204.1206.

31 H. H. H. Mohammed, A. A. Abd El-Hafeez, K. Ebeid, A. I. Mekkawy, M. A. S. Abourehab, E. I. Wafa, S. O. Alhaj-Suliman, A. K. Salem, P. Ghosh, G. E. A. Abuo-Rahma, *et al.*, New 1,2,3-Triazole Linked Ciprofloxacin-Chalcones Induce DNA Damage by Inhibiting Human Topoisomerase I& II and Tubulin Polymerization, *J. Enzyme Inhib. Med. Chem.*, 2022, **37**, 1346–1363, DOI: 10.1080/14756366.2022.2072308.

32 C. M. Perry and A. Markham, Piperacillin/Tazobactam, *Drugs*, 1999, **57**, 805–843, DOI: 10.2165/00003495-199957050-00017.

33 A. Dokala and S. S. Thakur, Extracellular Region of Epidermal Growth Factor Receptor: A Potential Target for Anti-EGFR Drug Discovery, *Oncogene*, 2017, **36**, 2337–2344, DOI: 10.1038/onc.2016.393.

34 C. H. Heldin, Dimerization of Cell Surface Receptors in Signal Transduction, *Cell*, 1995, **80**, 213–223, DOI: 10.1016/0092-8674(95)90404-2.

35 K. Sato, T. Nagao, T. Iwasaki, Y. Nishihira and Y. Fukami, Src-Dependent Phosphorylation of the EGF Receptor Tyr-845 Mediates Stat-P21waf1 Pathway in A431 Cells, *Genes Cells*, 2003, **8**, 995–1003, DOI: 10.1046/j.1356-9597.2003.00691.x.

36 T. M. Brand, M. Iida, C. Li and D. L. Wheeler, The Nuclear Epidermal Growth Factor Receptor Signaling Network and Its Role in Cancer, *Discov. Med.*, 2011, **12**, 419–432.

37 J. Martinez-Useros and J. Garcia-Foncillas, The Challenge of Blocking a Wider Family Members of EGFR against Head and Neck Squamous Cell Carcinomas, *Oral Oncol.*, 2015, **51**, 423–430, DOI: 10.1016/j.oraloncology.2015.02.092.

38 A. Gazdar, Activating and Resistance Mutations of EGFR in Non-Small-Cell Lung Cancer: Role in Clinical Response to EGFR Tyrosine Kinase Inhibitors, *Oncogene*, 2009, **28**, S24–S31, DOI: 10.1038/onc.2009.198.

39 J.-C. Soria, T. S. Mok, F. Cappuzzo and P. A. Jänne, EGFR-Mutated Oncogene-Addicted Non-Small Cell Lung Cancer: Current Trends and Future Prospects, *Cancer Treat. Rev.*, 2012, **38**, 416–430, DOI: **10.1016/j.ctrv.2011.10.003**.

40 D. Westover, J. Zugazagoitia, B. C. Cho, C. M. Lovly and L. Paz-Ares, Mechanisms of Acquired Resistance to First- and Second-Generation EGFR Tyrosine Kinase Inhibitors, *Ann. Oncol.*, 2018, **29**, i10–i19, DOI: **10.1093/annonc/mdx703**.

41 J.-C. Soria, Y. Ohe, J. Vansteenkiste, T. Reungwetwattana, B. Chewaskulyong, K. H. Lee, A. Dechaphunkul, F. Imamura, N. Nogami, T. Kurata, *et al.*, Osimertinib in Untreated EGFR-Mutated Advanced Non-Small-Cell Lung Cancer, *N. Engl. J. Med.*, 2018, **378**, 113–125, DOI: **10.1056/NEJMoa1713137**.

42 C. E. McCoach and A. Jimeno, Osimertinib, a Third-Generation Tyrosine Kinase Inhibitor Targeting Non-Small Cell Lung Cancer with EGFR T790M Mutations, *Drugs Today*, 2016, **52**, 561–568, DOI: **10.1358/dot.2016.52.10.2541343**.

43 M. H. Kim, S. M. Lim, K. Lee, R. A. Soo and B. C. Cho, Can We Prevent Resistance to Osimertinib? Combination or Sequential, *J. Thorac. Oncol.*, 2018, **13**, 877–879, DOI: **10.1016/j.jtho.2018.05.012**.

44 T. Amelia, R. E. Kartasasmita, T. Ohwada and D. H. Tjahjono, Structural Insight and Development of EGFR Tyrosine Kinase Inhibitors, *Molecules*, 2022, **27**, 819, DOI: **10.3390/molecules27030819**.

45 C.-H. Yun, T. J. Boggon, Y. Li, M. S. Woo, H. Greulich, M. Meyerson and M. J. Eck, Structures of Lung Cancer-Derived EGFR Mutants and Inhibitor Complexes: Mechanism of Activation and Insights into Differential Inhibitor Sensitivity, *Cancer Cell*, 2007, **11**, 217–227, DOI: **10.1016/j.ccr.2006.12.017**.

46 N. Shaban, D. Kamashev, A. Emelianova and A. Buzdin, Targeted Inhibitors of EGFR: Structure, Biology, Biomarkers, and Clinical Applications, *Cells*, 2024, **13**, 47, DOI: **10.3390/cells13010047**.

47 J. D. Moyer, E. G. Barbacci, K. K. Iwata, L. Arnold, B. Boman, A. Cunningham, C. DiOrio, J. Doty, M. J. Morin, M. P. Moyer, *et al.*, Induction of Apoptosis and Cell Cycle Arrest by CP-358,774, an Inhibitor of Epidermal Growth Factor Receptor Tyrosine Kinase, *Cancer Res.*, 1997, **57**, 4838–4848.

48 P. Thirumurugan, D. Matosiuk and K. Jozwiak, Click Chemistry for Drug Development and Diverse Chemical–Biology Applications, *Chem. Rev.*, 2013, **113**, 4905–4979, DOI: **10.1021/cr200409f**.

49 S. G. Agalave, S. R. Maujan and V. S. Pore, Click Chemistry: 1,2,3-Triazoles as Pharmacophores, *Chem.–Asian J.*, 2011, **6**, 2696–2718, DOI: **10.1002/asia.201100432**.

50 *Privileged Scaffolds in Medicinal Chemistry: Design, Synthesis, Evaluation*, ed. S. Bräse, The Royal Society of Chemistry, 2015, ISBN 978-1-78262-030-3.

51 A. Aljuhani, M. S. Nafie, N. R. Albujuq, M. Alsehli, S. K. Bardaweel, K. M. Darwish, S. Y. Alraqa, M. R. Aouad and N. Rezki, Discovery of New Benzothiazole-1,2,3-Triazole Hybrid-Based Hydrazone/Thiosemicarbazone Derivatives as Potent EGFR Inhibitors with Cytotoxicity against Cancer, *RSC Adv.*, 2025, **15**, 3570–3591, DOI: **10.1039/D4RA07540D**.

52 A. A. Y. Ahmed, A. F. Mohammed, Z. M. Almarhoon, S. Bräse and B. G. M. Youssif, Design, Synthesis, and Apoptotic Antiproliferative Action of New Benzimidazole/1,2,3-Triazole Hybrids as EGFR Inhibitors, *Front. Chem.*, 2025, **12**, 1541846, DOI: **10.3389/fchem.2024.1541846**.

53 R. D. Busto, E. Haas, T. Madhavan, K. Burch, F. Cox, E. Fisher, E. Quinn and D. Pohlod, In Vitro and Clinical Studies of Cefatrizine, a New Semisynthetic Cephalosporin, *Antimicrob. Agents Chemother.*, 1976, **9**, 397–405, DOI: **10.1128/aac.9.3.397**.

54 I. K. Sharawat, P. K. Panda, P. Panda and L. Dawman, Efficacy and Safety of Rufinamide as Adjunctive Therapy in Patients with Lennox Gastaut Syndrome: A Systematic Review and Meta-Analysis, *Seizure*, 2021, **91**, 296–307, DOI: **10.1016/j.seizure.2021.07.004**.

55 S. H. Preskorn, Comparative Pharmacology of the 3 Marketed Dual Orexin Antagonists-Daridorexant, Lemborexant, and Suvorexant: Part 1: Pharmacokinetic Profiles, *J. Psychiatry Pract.*, 2022, **28**, 478–480, DOI: **10.1097/PRA.0000000000000672**.

56 P. Wei, X. Wang, Q. Fu and B. Cao, Progress in the Clinical Effects and Adverse Reactions of Ticagrelor, *Thromb. J.*, 2024, **22**, 8, DOI: **10.1186/s12959-023-00559-3**.

57 R. A. Joss, R. L. Galeazzi, A. K. Bischoff and K. W. Brunner, Alizapride, a New Substituted Benzamide, as an Antiemetic during Cancer Chemotherapy, *Eur. J. Clin. Pharmacol.*, 1985, **27**, 721–725, DOI: **10.1007/BF00547056**.

58 X. Si, J. Wang, Y. Cheng, J. Shi, L. Cui, H. Zhang, Y. Huang, W. Liu, L. Chen, J. Zhu, *et al.*, A Phase III, Randomized, Double-Blind, Controlled Trial of Carboxyamidotriazole plus Chemotherapy for the Treatment of Advanced Non-Small Cell Lung Cancer, *Ther. Adv. Med. Oncol.*, 2020, **12**, 1758835920965849, DOI: **10.1177/1758835920965849**.

59 D. J. Brooks, S. Papapetropoulos, F. Vandenhende, D. Tomic, P. He, A. Coppell and G. O'Neill, An Open-Label, Positron Emission Tomography Study to Assess Adenosine A2A Brain Receptor Occupancy of Vipadenant (BIIB014) at Steady-State Levels in Healthy Male Volunteers, *Clin. Neuropharmacol.*, 2010, **33**, 55–60, DOI: **10.1097/WNF.0b013e3181d137d2**.

60 J. Nagasawa, A. Mizokami, K. Koshida, S. Yoshida, K. Naito and M. Namiki, Novel HER2 Selective Tyrosine Kinase Inhibitor, TAK-165, Inhibits Bladder, Kidney and Androgen-Independent Prostate Cancer in Vitro and in Vivo, *Int. J. Urol.*, 2006, **13**, 587–592, DOI: **10.1111/j.1442-2042.2006.01342.x**.

61 K. Beckermann, B. Rini, N. Haas, D. George and E. Jonasch, Phase 1b/2 Trial of Ipilimumab, Nivolumab, and Ciforadenant (INC) (Adenosine A2a Receptor Antagonist) in First-Line Advanced Renal Cell Carcinoma, *Oncologist*, 2023, **28**, S13–S14, DOI: **10.1093/oncolo/oyad216.022**.

62 A. Şandor, I. Ionuţ, G. Marc, I. Oniga, D. Eniu and O. Oniga, Structure–Activity Relationship Studies Based on

Quinazoline Derivatives as EGFR Kinase Inhibitors (2017–Present), *Pharmaceuticals (Basel)*, 2023, **16**, 534, DOI: 10.3390/ph16040534.

63 A. M. Mohamed, O. M. F. Abou-Ghadir, Y. A. Mostafa, Z. M. Almarhoon, S. Bräse and B. G. M. Youssif, Design, Synthesis, and Antiproliferative Activity of New 1,2,3-Triazole/Quinazoline-4-One Hybrids as Dual EGFR/BRAFV600E Inhibitors, *RSC Adv.*, 2024, **14**, 38403–38415, DOI: 10.1039/D4RA06694D.

64 C. Ding, S. Chen, C. Zhang, G. Hu, W. Zhang, L. Li, Y. Z. Chen, C. Tan and Y. Jiang, Synthesis and Investigation of Novel 6-(1,2,3-Triazol-4-Yl)-4-Aminoquinazolin Derivatives Possessing Hydroxamic Acid Moiety for Cancer Therapy, *Bioorg. Med. Chem.*, 2017, **25**, 27–37, DOI: 10.1016/j.bmc.2016.10.006.

65 G. Le-Nhat-Thuy, T. V. Dinh, H. Pham-The, H. Nguyen Quang, N. Nguyen Thi, T. A. Dang Thi, P. Hoang Thi, T. A. Le Thi, H. T. Nguyen, P. Nguyen Thanh, *et al.*, Design, Synthesis and Evaluation of Novel Hybrids between 4-Anilinoquinazolines and Substituted Triazoles as Potent Cytotoxic Agents, *Bioorg. Med. Chem. Lett.*, 2018, **28**, 3741–3747, DOI: 10.1016/j.bmcl.2018.10.016.

66 A. A.-H. Abdel-Rahman, M. N. El-Bayaa, A. Sobhy, E. M. El-Ganzoury, E. S. Nossier, H. M. Awad and W. A. El-Sayed, Novel Quinazolin-4-One Based Derivatives Bearing 1,2,3-Triazole and Glycoside Moieties as Potential Cytotoxic Agents through Dual EGFR and VEGFR-2 Inhibitory Activity, *Sci. Rep.*, 2024, **14**, 24980, DOI: 10.1038/s41598-024-73171-8.

67 B. Banerji, K. Chandrasekhar, K. Sreenath, S. Roy, S. Nag and K. D. Saha, Synthesis of Triazole-Substituted Quinazoline Hybrids for Anticancer Activity and a Lead Compound as the EGFR Blocker and ROS Inducer Agent, *ACS Omega*, 2018, **3**, 16134–16142, DOI: 10.1021/acsomega.8b01960.

68 J. Song, S. Jang, J. W. Lee, D. Jung, S. Lee and K. H. Min, Click Chemistry for Improvement in Selectivity of Quinazoline-Based Kinase Inhibitors for Mutant Epidermal Growth Factor Receptors, *Bioorg. Med. Chem. Lett.*, 2019, **29**, 477–480, DOI: 10.1016/j.bmcl.2018.12.020.

69 M. Safavi, A. Ashtari, F. Khalili, S. S. Mirfazli, M. Saeedi, S. K. Ardestani, P. Rashidi Ranjbar, M. Barazandeh Tehrani, B. Larijani and M. Mahdavi, Novel Quinazolin-4(3*H*)-One Linked to 1,2,3-Triazoles: Synthesis and Anticancer Activity, *Chem. Biol. Drug Des.*, 2018, **92**, 1373–1381, DOI: 10.1111/cbdd.13203.

70 N. F. M. El Hamaky, A. Hamdi, W. A. Bayoumi, A. A. Elgazar and M. N. A. Nasr, Novel Quinazolin-2-Yl 1,2,3-Triazole Hybrids as Promising Multi-Target Anticancer Agents: Design, Synthesis, and Molecular Docking Study, *Bioorg. Chem.*, 2024, **148**, 107437, DOI: 10.1016/j.bioorg.2024.107437.

71 C.-I. Lee, C.-B. Liao, C.-S. Chen, F.-Y. Cheng, Y.-H. Chung, Y.-C. Wang, S.-Y. Ciou, W.-Y. Hsueh, T.-H. Lo, G.-R. Huang, *et al.*, Design and Synthesis of 4-Anilinoquinazolines as Raf Kinase Inhibitors. Part 1. Selective B-Raf/B-RafV600E and Potent EGFR/VEGFR2 Inhibitory 4-(3-Hydroxyanilino)-6-(1*H*-1,2,3-Triazol-4-Yl) Quinazolines, *Bioorg. Chem.*, 2021, **109**, 104715, DOI: 10.1016/j.bioorg.2021.104715.

72 A. Hajlaoui, S. Chortani, M. Morjen, H. Lazrag, Z. Kibou, N. Choukchou-braham, N. Srairi-Abid, N. Marrakchi, H. B. Jannet and A. Romdhane, Novel 1,2,3-Triazole Linked Chromene Hybrids: Microwave-Assisted Synthesis, Cytotoxic Activity, α-Amylase Inhibitory Potential, Molecular Docking Analysis, and In-Silico ADMET Profiling, *Chem. Afr.*, 2024, **7**, 3129–3148, DOI: 10.1007/s42250-024-01024-y.

73 Y. Hemasri, A. K. Bojja, V. Thumma and S. Panga, Synthesis of Novel Chromene/[1,2,3]Triazole Hybrid Derivatives: Cytotoxicity/Molecular Docking Studies, *AJC*, 2023, **35**, 2256–2264, DOI: 10.14233/ajchem.2023.28242.

74 K. Vidya, Synthesis and Biological Evaluation of Chromene-1,3,4-Oxadiazole Based 1,2,3-Triazoles: EGFR-Targeting Anticancer Agents, *Russ. J. Bioorg. Chem.*, 2023, **49**, 1328–1336, DOI: 10.1134/S1068162023060134.

75 D. T. Nguyen, S. H. Do, T. H. Le, T. H. Nguyen, M. H. Nguyen, T. N. B. Vu, T. T. H. Pham, N. T. Vu, T. K. V. Hoàng and T. K. G. Nguyen, Synthesis and Antiproliferative Activity of 1*H*-1,2,3-Triazole-4*H*-Chromene-D-Glucose Hybrid Compounds with Dual Inhibitory Activity against EGFR/VEGFR-2 and Molecular Docking Studies, *New J. Chem.*, 2022, **46**, 23179–23197, DOI: 10.1039/D2NJ04373D.

76 N. M. Kumar, S. K. Nukala, N. S. Thirukovela, R. Sreerama, E. R. Sucharitha, P. Kamarajugadda and S. Narsimha, Ramachary–Bressy–Wang [3+2]Cycloaddition Reaction: Synthesis of Fully Decorated 1,2,3-Triazoles as Potent Anticancer and EGFR Inhibitors, *J. Mol. Struct.*, 2022, **1262**, 132975, DOI: 10.1016/j.molstruc.2022.132975.

77 M. Sanduja, J. Gupta, R. Rawat, U. Singh and S. M. Verma, Designing, Molecular Docking, and Dynamics Simulations Studies of 1,2,3-Triazole Clamped Uracil-Coumarin Hybrids against EGFR Tyrosine Kinase, *J. Appl. Pharm. Sci.*, 2020, **10**, 001–011, DOI: 10.7324/JAPS.2020.103001.

78 E. H. Eltamany, S. M. Shaban, A. T. A. Boraei, E. M. A. Gad and M. S. Nafie, Synthesis of Novel Cyanopyridine Compounds as Potential EGFR Inhibitors Targeting A549 and PC3 Cancer Cell Lines: *In Vitro, In Vivo* and ADME Pharmacokinetics Studies, *J. Mol. Struct.*, 2024, **1306**, 137906, DOI: 10.1016/j.molstruc.2024.137906.

79 A. M. Elshamsy, T. F. S. Ali, M. Osman and N. A. El-Koussi, Recent Progress in Biological Activities of Dihydropyrimidine Derivatives: An Updated Mini-Review, *J. Adv. Biomed. Pharm. Sci.*, 2023, **6**, 114–123, DOI: 10.21608/jabps.2023.198467.1183.

80 R. Sreerama, N. M. Kumar, S. K. Nukala, E. R. Sucharitha, H. R. Babu and S. Narsimha, Synthesis and Biological Evaluation of Novel 1,2,3-Triazole Based Pyrido[4,3-d] Pyrimidines as Potent Anticancer and EGFR Inhibitors, *Russ. J. Gen. Chem.*, 2021, **91**, 2515–2521, DOI: 10.1134/S1070363221120227.

81 S. R. Bandi, R. Kapavarapu, R. Palabindela, M. Azam, K. Min and S. Narsimha, Synthesis of Novel Pyrido[2,3-*d*]

Pyrimidine-Thiazolidine-1,2,3-Triazoles: Potent EGFR Targeting Anticancer Agents, *J. Mol. Struct.*, 2023, **1294**, 136451, DOI: **10.1016/j.molstruc.2023.136451**.

82 B. C. Narasimhachar, A. Ravish, N. M. Beeraka, B. C. Pookunoth, S. Basappa, D. Vishwanath, K. S. Rangappa, O. Nagaraja, M. Madegowda, P. G. Chandrashekara, *et al.*, Development of Novel Pyrimidine-Thio-Triazoles Targeting EGFR in Breast Cancer Cells *via* One-Pot Copper-Catalyzed 1,3-Dipolar Cycloaddition, *Results Chem.*, 2025, **14**, 102150, DOI: **10.1016/j.rechem.2025.102150**.

83 N. D. Thanh, D. S. Hai, L. Thi Huyen, N. T. K. Giang, N. T. Thu Ha, D. T. Tung, C. Thi Le, H. T. K. Van and V. N. Toan, Synthesis and *in vitro* Anticancer Activity of 4*H*-Pyrano[2,3-*d*]pyrimidine-1*H*-1,2,3-Triazole Hybrid Compounds Bearing D-Glucose Moiety with Dual EGFR/HER2 Inhibitory Activity and Induced Fit Docking Study, *J. Mol. Struct.*, 2023, **1271**, 133932, DOI: **10.1016/j.molstruc.2022.133932**.

84 N. S. A. Al-Sahaly, S. Alghannay, K. Aouadi, M. N. El-Bayaa, F. M. Alminderej, S. M. Gomha, H. H. Elganzory and W. A. El-Sayed, Synthesis, Molecular Docking and Anticancer Activity of New Substituted Pyridine-1,2,3-Triazole Hybrid N-Glycosides Via Click Chemistry, *Egypt. J. Chem.*, 2024, **67**, 1221–1233, DOI: **10.21608/ejchem.2024.326738.10597**.

85 S. Lavunuri, R. Venkata Nadh, D. Banothu and S. Kumar Rapeti, Synthesis of Quinoline Fused 1,2,3-Triazole Derivatives *via* Continuous CuAAC and CH Arylation; Anti-Breast Cancer, Anti-EGFR and HER2 Activities, Computational Studies, *Tetrahedron Lett.*, 2024, **150**, 155282, DOI: **10.1016/j.tetlet.2024.155282**.

86 A. Mamidala, K. Bokkala, N. S. Thirukovela, N. Sirassu, S. Bandari and S. K. Nukala, Synthesis of Quinoline-Morpholine-Coupled 1,2,3-Triazole Hybrids as In Vitro EGFR Inhibitors, *ChemistrySelect*, 2022, **7**, e202203763, DOI: **10.1002/slct.202203763**.

87 A. Mamidala, N. S. Thirukovela, A. K. Bapuram, K. Bokkala and S. K. Nukala, Synthesis of Some New Barbituric Acid Linked Quinoline-1,2,3-Triazole Hybrids as Dual EGFR/VEGFR-2 Inhibitors, *Russ. J. Gen. Chem.*, 2024, **94**, 1399–1411, DOI: **10.1134/S1070363224060173**.

88 E. M. El-Sheref, S. Bräse, H. N. Tawfeek, F. A. Alasmary and B. G. M. Youssif, Synthesis, Antioxidant and Antiproliferative Actions of 4-(1,2,3-Triazol-1-Yl)Quinolin-2(1*H*)-Ones as Multi-Target Inhibitors, *Int. J. Mol. Sci.*, 2023, **24**, 13300, DOI: **10.3390/ijms241713300**.

89 P. Pinnoju, S. Kudikala, M. Scandakashi, M. Ramesh and S. Madderla, In Vitro Antibreast Cancer and Anti-EGFR Studies of Some Novel Benzimidazole-Piperazine Containing 1,2,3-Triazoles, *Russ. J. Bioorg. Chem.*, 2024, **50**, 1724–1734, DOI: **10.1134/S106816202405025X**.

90 R. Barothu, N. B. Chilakala, S. Etnoori, D. Ayodhya and P. Kokku, Design, Synthesis, Anticancer, Antimicrobial and Molecular Docking Studies of Substituted 2-[2,4-Bis-(1-Phenyl-1*H*-[1,2,3]Triazol-4-Ylmethoxy)Phenyl]-1*H*-Benzoimidazole Derivatives, *AJC*, 2024, **36**, 2921–2930, DOI: **10.14233/ajchem.2024.32819**.

91 J. M. R. Velidandla and S. K. Koppula, Synthesis of Indole-1,3,4-Oxadiazole Based Sulfonyl 1,2,3-Triazoles as Potent Anticancer and EGFR Inhibitors, *Russ. J. Bioorg. Chem.*, 2023, **49**, 1337–1345, DOI: **10.1134/S1068162023060146**.

92 N. Perike, P. K. Edigi, G. Nirmala, V. Thumma, S. Bujji and P. S. Naikal, Synthesis, Anticancer Activity and Molecular Docking Studies of Hybrid Molecules Containing Indole-Thiazolidinedione-Triazole Moieties, *ChemistrySelect*, 2022, **7**, e202203778, DOI: **10.1002/slct.202203778**.

93 M. S. Nafie, M. Ali, M. A. Alwehaibi, A. A. Alayyaf, M. K. Al-Muhanna, N. S. Almuqati, A. A. Alghamdi, M. Haukka, S. S. Tariq, Z. Ul-Haq, *et al.*, Potent EGFR/PARP-1 Inhibition by Spirooxindole-Triazole Hybrids for Targeted Liver Cancer Therapy, *RSC Adv.*, 2025, **15**, 58–74, DOI: **10.1039/D4RA05966B**.

94 A. Das, G. Greco, S. Kumar, E. Catanzaro, R. Morigi, A. Locatelli, D. Schols, H. Alici, H. Tahtaci, F. Ravindran, *et al.*, Synthesis, in Vitro Cytotoxicity, Molecular Docking and ADME Study of Some Indolin-2-One Linked 1,2,3-Triazole Derivatives, *Comput. Biol. Chem.*, 2022, **97**, 107641, DOI: **10.1016/j.compbiolchem.2022.107641**.

95 S. Ghosh, T. A. Ramarao, P. K. Samanta, A. Jha, P. Satpati and A. Sen, Triazole Based Isatin Derivatives as Potential Inhibitor of Key Cancer Promoting Kinases- Insight from Electronic Structure, Docking and Molecular Dynamics Simulations, *J. Mol. Graphics Modell.*, 2021, **107**, 107944, DOI: **10.1016/j.jmgm.2021.107944**.

96 S. Alluru, B. B. V. Sailaja and A. Pal, Synthesis and Anticancer Evaluation of New 1*H*-Naphtho[2,3-*d*]Imidazole-4,9-Dione-1,2,3 Triazole Hybrids, *RJC*, 2023, **16**, 519–526, DOI: **10.31788/RJC.2023.1618187**.

97 S. Johnpasha, R. Palabindela, M. Azam, R. Kapavarapu, V. Nasipireddy, S. I. Al-Resayes and S. Narsimha, Synthesis and Anti-Breast Cancer Evaluation of Fused Imidazole-Imidazo[1,2-*c*][1,2,3]Triazoles: PEG-400 Mediated One-Pot Reaction under Ultrasonic Irradiation, *J. Mol. Struct.*, 2024, **1312**, 138440, DOI: **10.1016/j.molstruc.2024.138440**.

98 R. Samala, S. K. Nukala, R. Manchal, V. R. Nagavelli and S. Narsimha, Synthesis and Biological Evaluation of Coumarine-Imidazo[1,2-c][1,2,3]Triazoles: PEG-400 Mediated One-Pot Reaction under Ultrasonic Irradiation, *J. Mol. Struct.*, 2023, **1290**, 135944, DOI: **10.1016/j.molstruc.2023.135944**.

99 M. A. Mahmoud, A. F. Mohammed, O. I. A. Salem, T. M. Almutairi, S. Bräse and B. G. M. Youssif, Design, Synthesis, and Apoptotic Antiproliferative Action of New 1,2,3-Triazole/1,2,4-Oxadiazole Hybrids as Dual EGFR/VEGFR-2 Inhibitors, *J. Enzyme Inhib. Med. Chem.*, 2024, **39**, 2305856, DOI: **10.1080/14756366.2024.2305856**.

100 M. S. Ayoup, I. Shawki, H. Abdel-Hamid, D. A. Ghareeb, A. Masoud, M. F. Harras, M. El-Atawy, N. S. Alharbi and M. M. F. Ismail, Targeting EGFR/PI3K/AKT/mTOR Signaling in Lung and Colon Cancers: Synthesis, Antitumor Evaluation of New 1,2,4-Oxdiazoles Tethered

1,2,3-Triazoles, *RSC Adv.*, 2024, **14**, 16713–16726, DOI: 10.1039/D4RA02222J.

101 M. A. Mahmoud, A. F. Mohammed, O. I. A. Salem, H. A. M. Gomaa and B. G. M. Youssif, New 1,3,4-Oxadiazoles Linked with the 1,2,3-Triazole Moiety as Antiproliferative Agents Targeting the EGFR Tyrosine Kinase, *Arch. Pharm. (Weinheim)*, 2022, **355**, e2200009, DOI: 10.1002/ardp.202200009.

102 P. Telukuntla, M. Chandrakanth, P. G. Amrutha, N. M. Thomas, R. Gondru, K. R. Valluru and J. Banothu, 1,2,3-Triazole – [1,2,4]Triazolo[3,4-*b*][1,3,4]Thiadiazine Hybrids: A Switch for Improvement of Antibreast Cancer Activity Targeting Epidermal Growth Factor Receptor, *Tetrahedron Lett.*, 2024, **146**, 155180, DOI: 10.1016/j.tetlet.2024.155180.

103 S. Chirra, R. Gondru, M. Manne, M. Azam, S. I. Al-Resayes, R. Manchal and S. Narsimha, Synthesis of [1,2,4]Triazolo [3,4-b][1,3,4]Thiadiazine-1,2,3-Triazoles as Potent EGFR Targeting Anti-Breast Cancer Agents, *J. Mol. Struct.*, 2024, **1306**, 137803, DOI: 10.1016/j.molstruc.2024.137803.

104 M. Enneiymy and A. El Aissouq, Carvacrol-Derived 1,2,3-Triazole Hybrids: Synthesis, Computational Insights, and Targeted Inhibition of EGFR, BRAF V600E, and Tubulin Enzymes, *J. Fluoresc.*, 2025, DOI: 10.1007/s10895-025-04232-y.

105 Y. Riadi, M. H. Geesi, A. Oubella and M. Y. A. Itto, Synthesis, spectroscopic analysis, molecular docking and DFT study of novel 1,2,3-triazole derivatives incorporating paramethoxythymol and salicylaldehyde moieties, *J. Mol. Struct.*, 2024, **1318**, 139251, DOI: 10.1016/j.molstruc.2024.139251.

106 N. A. Nawareg, A. S. A. Yassen, E. M. Husseiny, M. A. A. El-Sayed and H. A. Elshihawy, Exploring 1,2,3-Triazole-Schiff's Base Hybrids as Innovative EGFR Inhibitors for the Treatment of Breast Cancer: In Vitro and in Silico Study, *Bioorg. Chem.*, 2025, **155**, 108106, DOI: 10.1016/j.bioorg.2024.108106.

107 A. Aljuhani, M. S. Nafie, N. R. Albujuq, M. Alsehli, S. K. Bardaweel, K. M. Darwish, S. Y. Alraqa, M. R. Aouad and N. Rezki, Discovery of New Benzothiazole-1,2,3-Triazole Hybrid-Based Hydrazone/Thiosemicarbazone Derivatives as Potent EGFR Inhibitors with Cytotoxicity against Cancer, *RSC Adv.*, 2025, **15**, 3570–3591, DOI: 10.1039/d4ra07540d.

108 E. Gao, Y. Wang, G.-L. Fan, G. Xu, Z.-Y. Wu, Z.-J. Liu, J.-C. Liu, L.-F. Mao, X. Hou and S. Li, Discovery of Gefitinib-1,2,3-Triazole Derivatives against Lung Cancer via Inducing Apoptosis and Inhibiting the Colony Formation, *Sci. Rep.*, 2024, **14**, 9223, DOI: 10.1038/s41598-024-60000-1.

109 P. Deng, G. Sun, J. Zhao, K. Yao, M. Yuan, L. Peng and L. Mao, Synthesis and Antitumor Activity of Erlotinib Derivatives Linked With 1,2,3-Triazole, *Front. Pharmacol.*, 2022, **12**, 793905, DOI: 10.3389/fphar.2021.793905.

110 P. Biegański, M. Godel, C. Riganti, D. F. Kawano, J. Kopecka and K. Kowalski, Click Ferrocenyl-Erlotinib Conjugates Active against Erlotinib-Resistant Non-Small Cell Lung Cancer Cells in Vitro, *Bioorg. Chem.*, 2022, **119**, 105514, DOI: 10.1016/j.bioorg.2021.105514.

111 H. H. Alsayad, A. A. A. Alibeg and Z. K. Oleiwi, Molecular Docking, Synthesis, Characterization, and Preliminary Cytotoxic Study of Novel 1, 2, 3-Triazole-Linked Metronidazole Derivatives, *Adv. J. Chem., Sect. A*, 2024, **7**, 797–809, DOI: 10.48309/ajca.2024.464130.1570.

112 H. Şenol, A. G. Ağgül, S. Atasoy and N. U. Güzeldemirci, Synthesis, Characterization, Molecular Docking and *in Vitro* Anti-Cancer Activity Studies of New and Highly Selective 1,2,3-Triazole Substituted 4-Hydroxybenzohyrdazide Derivatives, *J. Mol. Struct.*, 2023, **1283**, 135247, DOI: 10.1016/j.molstruc.2023.135247.

113 N. Rezki, M. A. Almehmadi, S. Ihmaid, A. M. Shehata, A. M. Omar, H. E. A. Ahmed and M. R. Aouad, Novel Scaffold Hopping of Potent Benzothiazole and Isatin Analogues Linked to 1,2,3-Triazole Fragment That Mimic Quinazoline Epidermal Growth Factor Receptor Inhibitors: Synthesis, Antitumor and Mechanistic Analyses, *Bioorg. Chem.*, 2020, **103**, 104133, DOI: 10.1016/j.bioorg.2020.104133.

114 S. Chaidam, N. Saehlim, K. Suksen, A. Chairoungdua and R. Saeeng, Design, Synthesis, Evaluation and Molecular Docking Studies of 1,6-Bis-Triazole-Linked α-Galactoside Derivatives as Potential Anticancer Agents, *ChemistrySelect*, 2021, **6**, 8052–8057, DOI: 10.1002/slct.202102288.

115 W. A. A. Fadaly, M. T. M. Nemr, T. H. Zidan, F. E. A. Mohamed, M. M. Abdelhakeem, N. N. Abu Jayab, H. A. Omar and K. R. A. Abdellatif, New 1,2,3-Triazole/1,2,4-Triazole Hybrids Linked to Oxime Moiety as Nitric Oxide Donor Selective COX-2, Aromatase, B-RAFV600E and EGFR Inhibitors Celecoxib Analogs: Design, Synthesis, Anti-Inflammatory/Anti-Proliferative Activities, Apoptosis and Molecular Modeling Study, *J. Enzyme Inhib. Med. Chem.*, 2023, **38**, 2290461, DOI: 10.1080/14756366.2023.2290461.

116 M. A. Mahmoud, A. F. Mohammed, O. I. A. Salem, S. M. Rabea and B. G. M. Youssif, Design, Synthesis, and Antiproliferative Properties of New 1,2,3-Triazole-Carboximidamide Derivatives as Dual EGFR/VEGFR-2 Inhibitors, *J. Mol. Struct.*, 2023, **1282**, 135165, DOI: 10.1016/j.molstruc.2023.135165.

117 M. T.-E. Maghraby, O. I. A. Salem, B. G. M. Youssif and M. M. Sheha, Design, Synthesis, and Modelling Study of New 1,2,3-Triazole/Chalcone Hybrids with Antiproliferative Action as Epidermal Growth Factor Receptor Inhibitors, *Chem. Biol. Drug Des.*, 2023, **101**, 749–759, DOI: 10.1111/cbdd.14178.

118 T. R. Deshmukh, A. P. Sarkate, D. K. Lokwani, S. V. Tiwari, R. Azad and B. B. Shingate, New Amide Linked Dimeric 1,2,3-Triazoles Bearing Aryloxy Scaffolds as a Potent Antiproliferative Agents and EGFR Tyrosine Kinase Phosphorylation Inhibitors, *Bioorg. Med. Chem. Lett.*, 2019, **29**, 126618, DOI: 10.1016/j.bmcl.2019.08.022.

119 F. Acheampong, T. Ostlund, E. Hedge, J. Laddusaw, F. Alotaibi, Y. A. M. M. Elshaier and F. Halaweish,

Triazole-Estradiol Analogs Induce Apoptosis and Inhibit EGFR and Its Downstream Pathways in Triple Negative Breast Cancer, *Molecules*, 2025, **30**, 605, DOI: 10.3390/molecules30030605.

120 M. K. Vanga, R. Bhukya, V. Thumma, S. S. S. S. S. Ambadipudi, V. L. Nayak, S. B. Andugulapati and V. Manga, Design and Synthesis of Meldrum's Acid Based 7-Azaindole Anchored 1,2,3-Triazole Hybrids as Anticancer Agents, *RSC Med. Chem.*, 2024, **15**, 1709–1721, DOI: 10.1039/D4MD00015C.

121 D. J. Boruah, D. Kathirvelan, K. Bora, R. A. Maurya and P. Yuvaraj, Efficient and Environmentally Friendly Synthesis of 1,2,3-Triazole Derivatives *via* [3 + 2] Cycloaddition and Their Potential as Lung Cancer Inhibitors: An in Silico Study, *Results Chem.*, 2023, **5**, 100903, DOI: 10.1016/j.rechem.2023.100903.

122 U. Boda, V. Guguloth, S. Mood and H. Guguloth, Copper(I)-Catalyzed Regioselective Synthesis of 1,2,3-Triazole–Phthalazine-1,4-Dione Hybrids, and Their Anticancer and Molecular Docking Studies, *Russ. J. Org. Chem.*, 2023, **59**, 1064–1070, DOI: 10.1134/S1070428023060143.

123 K. Swapna, K. Deepthi, Ch. Sivudu, N. Kotilingaiah, B. Srinu and J. Sandhya, Design and Synthesis of Novel Pyrazole-Based 1,2,3-Triazole Hybrids with Potent Cytotoxic Activity as Selective EGFR Kinase Inhibitors, *Russ. J. Org. Chem.*, 2024, **60**, 2430–2438, DOI: 10.1134/S1070428024120170.

124 M. Guttikonda, Synthesis, Spectral Analysis and in Vitro Anticancer Activity of 1,2,3 Triazole Derivatives and Their Molecular Docking Studies, *Indian J. Chem.*, 2024, **63**, 286–292, DOI: 10.56042/ijc.v63i3.6682.

125 I. H. El Azab, H. S. El-Sheshtawy, R. B. Bakr and N. A. A. Elkanzi, New 1,2,3-Triazole-Containing Hybrids as Antitumor Candidates: Design, Click Reaction Synthesis, DFT Calculations, and Molecular Docking Study, *Molecules*, 2021, **26**, 708, DOI: 10.3390/molecules26030708.

126 H. Hashem, A. Hassan, W. M. Abdelmagid, A. G. K. Habib, M. A. A. Abdel-Aal, A. M. Elshamsy, A. El Zawily, I. T. Radwan, S. Bräse, A. S. Abdel-Samea, *et al.*, Synthesis of New Thiazole-Privileged Chalcones as Tubulin Polymerization Inhibitors with Potential Anticancer Activities, *Pharmaceuticals*, 2024, **17**, 1154, DOI: 10.3390/ph17091154.

127 M. A. Shaheen, K. M. Darwish, S. M. Kishk, M. A.-A. El-Sayed and I. Salama, Development of 1,2,3-Triazole Hybrids as Multi-Faced Anticancer Agents Co-Targeting EGFR/mTOR Pathway and Tubulin Depolymerization, *Bioorg. Chem.*, 2025, **156**, 108153, DOI: 10.1016/j.bioorg.2025.108153.

128 H. P. R. Vikram, T. P. Kumar, G. Kumar, N. M. Beeraka, R. Deka, S. M. Suhail, S. Jat, N. Bannimath, G. Padmanabhan, R. S. Chandan, *et al.*, Nitrosamines Crisis in Pharmaceuticals – Insights on Toxicological Implications, Root Causes and Risk Assessment: A Systematic Review, *J. Pharm. Anal.*, 2024, **14**, 100919, DOI: 10.1016/j.jpha.2023.12.009.

129 Research, C. for D. E., *CDER Nitrosamine Impurity Acceptable Intake Limits*, FDA, 2025.

130 Research, C. for D. E. and Control of Nitrosamine Impurities in Human DrugsAvailable online: https://www.fda.gov/regulatory-information/search-fda-guidance-documents/control-nitrosamine-impurities-human-drugs (accessed on 5 September 2025).

131 W. Wichitnithad, S. Nantaphol, K. Noppakhunsomboon and P. Rojsitthisak, An Update on the Current Status and Prospects of Nitrosation Pathways and Possible Root Causes of Nitrosamine Formation in Various Pharmaceuticals, *Saudi Pharm. J.*, 2023, **31**, 295–311, DOI: 10.1016/j.jsps.2022.12.010.

132 W. Wichitnithad, S. Nantaphol, K. Noppakhunsomboon and P. Rojsitthisak, An Update on the Current Status and Prospects of Nitrosation Pathways and Possible Root Causes of Nitrosamine Formation in Various Pharmaceuticals, *Saudi Pharm. J.*, 2023, **31**, 295–311, DOI: 10.1016/j.jsps.2022.12.010.

133 T. H. Ali, T. Heidelberg, R. S. D. Hussen and H. A. Tajuddin, Unexpected Reactions of Terminal Alkynes in Targeted "Click Chemistry" Coppercatalyzed Azide-alkyne Cycloadditions, *Curr. Org. Synth.*, 2019, **16**, 1143–1148, DOI: 10.2174/1570179416666191105152714.